Pneumatic-modulation comprehensive two-dimensional gas chromatography for environmental analysis

by

Paul McAllan Harvey

A thesis submitted in fulfilment of the requirements for the degree of

Doctor of Philosophy

UNIVERSITY OF TASMANIA

Submitted 17 April 2012

Dedication

For my family.

Julie Louise Harvey, dearest friend, lifetime companion and immensely dedicated mother of our two beautiful girls, Claire Louise M^{c}Allan Harvey and Ada May Charlotte Harvey

Declarations

This thesis contains no material which has been accepted for a degree or diploma by the University or any other institution, except by way of background information and duly acknowledged in the thesis, and to the best of the my knowledge and belief no material previously published or written by another person except where due acknowledgement is made in the text of the thesis, nor does the thesis contain any material that infringes copyright.

Paul Harvey

17 April 2012

The publishers of the papers comprising Chapters 3 to 4 and Appendix 2 hold the copyright for that content, and access to the material should be sought from the respective journals. The remaining non published content of the thesis may be made available for loan and limited copying and communication in accordance with the Copyright Act 1968.

Paul Harvey

17 April 2012

Statement of Co-Authorship

The following people and institutions contributed to the publication of the work undertaken as part of this thesis:

"Design considerations for pulsed-flow comprehensive two dimensional gas chromatography: dynamic flow model approach"
PM Harvey (80%), RA Shellie (15%), PR Haddad (5%)

"Factors affecting peak shape in comprehensive two-dimensional gas chromatography with non-focusing modulation" *PM Harvey (80%), RA Shellie (20%)*

"Data reduction in comprehensive two-dimensional gas chromatography for rapid and repeatable automated data analysis" *PM Harvey (80%), RA Shellie (20%)*

Details of the Authors roles:
PM Harvey and RA Shellie contributed to the ideas, their formalisation and development. All authors assisted with refinement and presentation.

We the undersigned agree with the above stated "proportion of work undertaken" for each of the above published (or submitted) peer-reviewed manuscripts contributing to this thesis:

Signed: _____ _____

RA Shellie
Supervisor
School of Chemistry
University of Tasmania

GW Dicinoski
Head of School
School of Chemistry
University of Tasmania

Date:_____

Acknowledgements

For the preparation of this thesis I offer my sincere thanks to the community of helpers I have been lucky enough to have surrounding me. First and foremost my supervisor, Rob Shellie, has discussed many ideas, given me enough space to follow leads in the laboratory and then persisted with the editing of this document in all its glorious and inglorious forms. Thanks also go to Paul Haddad and Ian Snape who, as co supervisors, have set up the teams and environments that allowed this work to progress. The balance between allowing relatively free reign to research ideas, working behind the scenes (at the University of Tasmania and the Australian Antarctic Division) and insightful guidance to thesis writing is much appreciated.

To my fellow University of Tasmania PhD students – all the chats and the supportive push towards PhD completion has been invaluable. The team in the PARC laboratory, especially Boon and Naama, were great to have around. While cafe lunches and social drinks at the bar have been too few my (mostly) younger PhD colleagues have been fabulous. When Claire and Ada made an appearance at the School of Chemistry they were always welcomed, became the centre of attention and were watched over by a fabulous bunch. Greg Hince, the Raymonds, Ursula and a host of others also played this role at the Australian Antarctic Division. In particular Greg played a major role in this PhD journey, a role which was an honour to have received.

The greater community of University and Antarctic Division staff, Yogis, Yoginis, my extended family and friends from the Tarremah Steiner School are all praised for your fortitude, diverse assistance and encouragement throughout this process.

List of Abbreviations and Definitions

Definitions

^{1}D	First separation column in a GCxGC system
^{2}D	Second separation column in a GCxGC system
1D	A single dimension of data or a single separation column
2D	Two Dimensional
n-C_6	Straight chain alkane with 6 carbons (or alternative number)
σ	Standard deviation of a Gaussian distribution
w_b	width of base of a chromatographic peak using $w_b = 4\,\sigma$

Abbreviations

AAD	Australian Antarctic Division
C1, C2….	A parent structure alkylated with 1 carbon atom, 2 carbon atoms…
DMBP	Dimethyl Biphenyl
DMN	Dimethyl Naphthalenes
DMP	Dimethyl Phenanthrene
EBP	Ethyl Biphenyl
EC	Equivalent Carbon
ECL	Effective Chain Lengths
EP	Ethyl Phenanthrene
EPA	Environmental Protection Agency
FAME	Fatty Acid Methyl Ester
FID	Flame Ionisation Detector
GRAM	Generalised Rank Annihilation Method
GC	Gas Chromatography
GC-FID	Gas Chromatography Flame Ionisation Detection
GC-MS	Gas Chromatography Mass Spectrometry

GCxGC	Comprehensive Two-Dimensional Gas Chromatography
GCxGC-FID	GCxGC Flame Ionisation Detection
GCxGC-MS	GCxGC Mass Spectrometry
HEM	Hexane Extractable Material
HPLC	High Performance Liquid Chromatography
LMCS	Longitudinally Modulating Cryogenic System
MDS	Multidimensional Scaling
mg /kg	Concentration unit. Soil sample mass is evaluated on the basis of soil mass after drying at 105 °C.
MN	Methyl Naphthalene
1-MN	1-Methyl Naphthalene
2-MN	2-Methyl Naphthalene
MS	Mass Spectrometry
m/z	Mass to Charge ratio
MBP	Methyl Biphenyl
MDPM	Methyl Diphenyl Methane
MP	Methyl Phenanthrene
NAPL	Non Aqueous Phase Liquid
NEPC	National Environment Protection Council
NEPM	Australian National Environmental Protection Measure
NOM	Natural Organic Matter
PAH	Poly Aromatic Hydrocarbon
PFM	Pulsed Flow Modulation
PHC	Petroleum Hydrocarbon
PID	Photo Ionisation Detector (field device for volatile PHC detection)
PIONA	Paraffins, Isoparaffins, Olefins, Naphthenes, and Aromatics
pwhh	peak width at half height (2.355 σ)
ppm	part per million, equivalent to mg /kg. Soil sample mass is evaluated on the basis of soil mass after drying at 105 °C.
SAB	Special Antarctic Blend diesel
SIM	Selected Ion Monitoring (during GC-MS data acquisition)

SCCM	Standard cubic centimetres per minute gas flow. Standard conditions used in this work are 20 ºC and 101.325 kPa
TeMN	Tetramethyl Naphthalenes
TMBP	Trimethyl Biphenyl
TMN	Trimethyl Naphthalenes
TOF-MS	Time of Flight Mass Spectrometry
TPAH	Total Poly Aromatic Hydrocarbon
TPH	Total Petroleum Hydrocarbons
TPHCWG	Total Petroleum Hydrocarbons Criteria Working Group
TRNCC	Texas Natural Resource Conservation Commission
UCM	Unresolved Complex Mixture
US EPA	United States Environmental Protection Agency

List of outcomes

Peer reviewed publications and manuscripts in review

P.M. Harvey, R.A. Shellie, P.R. Haddad, (2010). "Design considerations for pulsed-flow comprehensive two dimensional gas chromatography: dynamic flow model approach". Journal of Chromatographic Science, **48**(4): Special Issue, 245-250.

P.M. Harvey, R.A. Shellie, (2011). "Factors affecting peak shape in comprehensive two-dimensional gas chromatography with non-focusing modulation", Journal of Chromatography A, **1218**, 3153-3158.

P.M. Harvey, R.A. Shellie, (2012). "Data reduction in comprehensive two-dimensional gas chromatography for rapid and repeatable automated data analysis". Analytical Chemistry. **84**(15), 6501-6507.

Australian Antarctic Division outcomes

Report: 2010 assessment and report on remediation activities at Macquarie Island and AAD laboratory installation for GC-FID and GCxGC-FID at Macquarie Island.

Selected oral presentations of research outcomes

P.M. Harvey. "Pneumatic modulation GCxGC". Final PhD seminar, School of Chemistry, University of Tasmania, Hobart, Tasmania, Australia, Aug 2010

Selected poster presentations at conferences

P.M. Harvey, R.A. Shellie. "Design considerations for GCxGC with Pulsed Flow Modulation (PFM): dynamic flow model approach". 6th International symposium on GCxGC. Portland, USA, 16-17 May 2009

Abstract

Environmental petroleum hydrocarbon (PHC) monitoring is a major challenge. Analytical methods must be robust; operate with minimal user intervention; be suitable for remote field operation; and furnish analytical data that allows the different mechanisms of PHC environmental fate to be investigated. PHC are amenable to analysis by comprehensive two-dimensional gas chromatography (GCxGC). However, conventional GCxGC instrumentation relies on bulky thermal modulation systems. Thus alternative approaches based on fluidic modulation were investigated to determine their suitability for environmental PHC monitoring.

First, a dynamic flow model, which maps carrier gas pressure and flow rate through the first-dimension separation column, the modulator sample loop, and the second-dimension column(s) in a fluidic modulation GCxGC system is described. The dynamic flow model assists design of a pneumatic modulation ensemble and leads to rapid determination of pneumatic conditions, timing parameters, and the dimensions of the separation columns and connecting tubing used to construct the GCxGC system. Three significant innovations are introduced, that were all uncovered by using the dynamic flow model, viz. i) a "symmetric flow path" modulator improved baseline stability, ii) appropriate selection of flow restrictors in the first dimension column assembly provides a generally more stable and robust system, and iii) these restrictors increase the modulation period flexibility of the GCxGC system.

Next, a model was developed that permitted a systematic investigation of peak shape in fluidic modulation. In the case of a non-focusing modulator for comprehensive

two-dimensional gas chromatography, the systematic distortions induced when the modulator loads the second-dimension column give rise to a characteristic peak shape. Depending on the operating conditions this systematic distortion can be the dominant component of the second-dimension elution profiles. Understanding the factors that cause different peak shape observations provides a rugged approach to method development. It is shown that low flow ratio can lead to significant peak skewing and increasing the flow ratio reduces the magnitude of peak skewing. Validation of the peak shape model is made by comparison with experimental data.

Finally GCxGC methodology was developed and applied to analysis of PHC contaminated soil. GCxGC results met or exceeded, the standards set by regulators and environmental scientists. Fluidic modulation approaches provided excellent sensitivity and permitted detailed monitoring of key PHC transport and degradation pathways, including evaporation, dissolution, and biodegradation.

Table of Contents

1 Introduction and Literature Review

1.1 Petroleum hydrocarbon analysis and fuel spills assessment

Since the use and exploration for fossil fuels became widespread the analysis of petroleum hydrocarbons (PHCs) has been an important area of chemical analysis [1-3]. With increased environmental awareness building in society over many decades the analysis of samples from fuel spills, monitoring of clean-up operations and investigation into the fate of fuel spilt into the environment has been an expanding area. Towards this end the analyst must choose a suitable extraction method, clean-up method of the extract before instrumental analysis, appropriate instrumentation and instrument conditions. Specific environmental analysis tasks including determination of: PHCs, pesticides, dioxins, polychlorinated biphenyls, all have dedicated methods. Certified reference materials are available to support these methods in many cases. A variety of laboratory accreditation options exist and inter laboratory comparisons are frequently run with a wide range of analysis tasks.

Despite reviews [1,4], extensive interest in forensic analysis [3,5] and widespread commercial analysis no universal approach exists for PHC spill analysis. This is, in part, due to the enormous range of PHCs themselves. Products range through different grades of crude oil to tightly specified materials such as Jet-A1 fuel. The lack of a standard analytical approach is also partly due to the wide variety of circumstances that characterise a PHC spill. A final factor may well be the difficulty of achieving the

necessary consensus across the many parties interested in a PHC spill. The setting and circumstance of fuel spill analysis can vary from large crude oil spills (which include the 1989 Exxon Valdez oil tanker disaster in Alaska, the 2010 Gulf of Mexico leaking undersea well, or the 1990 Gulf War oil spill) to minor spills or the tracking of minor fuel spill components that are the last remnants of an earlier spill.

In an effort to address the wide range of contaminated site cleanup requirements in the United States (and the concurrent analytical tasks) The Total Petroleum Hydrocarbons Criteria Working Group (TPHCWG) was convened in 1993. The stated goal of the group was "*To develop scientifically defensible information for establishing soil cleanup levels that are protective of human health at petroleum contaminated sites"* [6]. The output of the TPHCWG (1998-1999) was a 5 volume set of documents [7-11]. This serves as an excellent source of information for PHC analysis as well as setting the analysis results form a contaminated site against the stated human health criteria.

1.1.1 Legislation related to fuel spills

The issue of how to regulate contaminated site remediation (and any subsequent redevelopment) has proved a difficult area for policy makers. The variability of the type of contamination, difficulty in assessing the longevity and impact of this contamination, the possibility of future analysis altering previous perceptions and the vexing question of "what is a 'safe' level" for a given contaminant are all important parts in this overall problem across any contaminated site. The actual development and review of policy in the area of contaminated sites has itself received academic interest from a range of perspectives [12-14]. In general terms risk based assessment is used as a criteria for clean-up which requires inputs of both bioavailability / bioaccessibility of the

contaminants, impact on the local area from these accessible components and some consideration of local area use. Obviously, an important breeding area for local species will receive different attention compared to an area considered to be a minor migration route for these species. This is analogous to a pre-school play ground receiving greater attention than a car park that services local schools etc.

In an Australian context the National Environment Protection Council (NEPC) has produced the "Guideline on the Investigation levels for soil and groundwater" [15]. This guideline specifies 6 different health investigation levels ranging from a 'standard residential' category, which includes preschools, to a 'commercial / Industrial' category. Most volatile contaminants do not have a specific investigation level as models for exposure are being determined for an Australian context. Guidance is given for PHCs in the range "$>n$-C_{16} to n-C_{35} Aromatics" and "$>n$-C_{16} to n-C_{35} Aliphatics". In the case of the 'standard residential' category these are 90 and 5600 mg/kg respectively. These levels were set as described in "Guideline on Health-Based Investigation Levels" [16]. In this document the extensive work of the TPHCWG has been reappraised with additional modeling. It should be pointed out that presence of

'*indicator chemicals which are carcinogenic substances. This generally includes substances such as benzene and polycyclic aromatic hydrocarbons'*

requires the use of other, specific, health based investigation levels. Presumably the presence of biologically active alkylated PAHs in the "$>n$-C_{16} to n-C_{35} Aromatics" range account for the investigation level of these compounds being some 62 times lower than the aliphatic hydrocarbons in the same range. These compounds, while being different from the parent PAHs and existing as a huge range of isomers and homologues, account

for much larger proportion of fuel than the actual parent PAHs. As closely related analogues they should be regarded as potential, if unproven, carcinogens.

1.1.2 Investigations into fuel spill fate in the environment

Clean-up targets at PHC spills are set by the legal bodies with jurisdiction over the affected area. These clean-up targets are often set over broad hydrocarbon ranges like *n*-C_8- *n*-C_{36}, with reference made to a technical description of how this range is determined for a PHC sample. These clean-up targets may be contained in legislation or determined by site specific criteria. The scientific investigation of fate and environmental impact of a particular spill is a more general question. The terms "*fate*" and "*impact*" of a PHC spill are themselves hard to define precisely since different fuel components interact with the environment via different mechanisms and subsequently lead to different outcomes for the assorted species that are present at the spill site. As such the analysis requirements for samples forming the basis of these investigations are different to the question of "is measured fuel in the sample at or below the clean-up target".

The 1989 Exxon Valdez crude oil spill in Prince William Sound, Alaska is an example of a major environmental fuel spill. A considerable body of literature exists about this spill and its subsequent fate. In the last 21 years 361 papers, across a wide range of journals, specifically use the term "Exxon Valdez" in the title alone[1] [17-26]. Initially the clean-up activities and many of the early papers dealt with effects from the sheer bulk of fuel in the environment [20]. As clean-up progressed natural biodegradation, as a significant (or dominant) oil reduction mechanism became better understood after trials and detailed analysis of field samples. Biodegradation was

[1]Papers found by a web of science search. The 10 most highly cited papers are in the reference section.

facilitated by the addition of treatments that were aimed at supplying nitrogen and phosphorus, the availability of which was identified as the limiting factors for biodegradation at oil affected areas of coastline [27].

After clean-up operations were ceased (at the end of the 1991 northern hemisphere summer) the on-going monitoring task became more focused on either subsurface oil trapped at beaches or spill residues contained within local wildlife, such as mussels [28]. Currently, subsurface oil remnants are found at beach sites that were both heavily contaminated and protected from wave action [29,30]. Even at these sites fuel weathering has generally been extensive with analysis of persistent biomarkers, especially PAHs being used as the main technique to identify components from the Exxon Valdez crude oil spill [31]. Alternative biomarkers used to identify and track the spill include polycyclic aliphatic components such as terpanes and steranes which persist longer than the acyclic *n*-alkanes and isoprenoids [32,33]. Across the Gulf of Alaska other PAH sources (such as natural seeps etc.) have been identified with recent interest and lively debate about the bioavailability of these different PAH sources appearing in the literature [34-36].

A key point when attempting a long term scientific monitoring program, compared to assessing a particular sample against a threshold value, is the progression from measuring total PHC signals in a specified elution range to the assessment of specific markers. These specific biomarkers are chosen partly by their ability to point towards different environmental fates and partly by the ability to actually measure them at low concentrations in the environment. In the Exxon Valdez example the specific markers

most commonly employed are PAHs including various methylated analogues found in the original crude oil that was spilt [37].

1.2 Gas Chromatography

Gas Chromatography (GC) is one of the most commonly employed chemical analysis techniques since its development in the 1950s. By the early 1960's GC was well advanced with much of the literature addressing analysis topics still relevant today [38-42]. Nowadays the ready availability of commercial instrumentation, the large body of published methods and numerous reviews on particular aspects of the technique are all available to users of the technique. This body of literature is extensive with more than 27,000 papers specifically using "Gas Chromatography" in the title alone. Despite the ability of capillary GC columns to resolve many hundreds of discrete compounds, certain types of complex samples still present an insurmountable challenge to conventional GC methods.

Complex samples such as PHCs typically contain numerous different classes of compounds and a proliferation of similar components within each class. Selecting an appropriate GC stationary phase, or adjusting analysis conditions, can usually separate a particularly important analyte from compounds known to interfere with this target analyte. In the case of a truly complex sample the sheer number of co-elution problems will, at some stage, prevent the desired separation from being achieved. Selective detection, especially with mass spectrometry (MS), can greatly assist with the separation of analytes from interferences although problems still remain. PHCs are typical examples of complex samples that remain problematic even with the best available GC methods and detection hardware. In an environmental context total petroleum hydrocarbons (TPH)

analysis (within set hydrocarbon ranges) and the analysis of specific PHC marker compounds are two distinct tasks undertaken for different reasons.

The technique most commonly employed for detailed PHC analysis is GC-MS, following the addition of deuterium labelled internal standards and the application of sample fractionation prior to GC-MS analysis [43]. An alternative rapid screening liquid chromatography method has been reported for use with Exxon Valdez oil spill samples [44]. This method was tailored towards detecting the total two- and three-ring PAH content in the samples (but lacked the compound specific data obtained from GC-MS analysis). The screening technique was also seen as way of identifying a reduced number of samples that needed analysis by the "*prohibitively expensive and excessively time-consuming*" GC-MS technique, an important point when thousands of samples were available for analysis.

1.2.1 FID detection

A key point, when attempting to assess short term fuel spill fate or carry out a long term scientific monitoring program (compared to assessing a particular sample against a threshold value) is the progression to measuring specific fuel markers and identifiers in addition to measuring total PHCs in a given sample. With flame ionisation detector (FID) detection the response of the detector is, for most compound types, proportional to the amount of carbon entering the detector in the sampling period of the detector [45-48]. This aspect of the FID is very beneficial when an analyst is required to report TPH in a sample in the ranges specified by an overseeing legal body. Unfortunately the destructive and non-selective nature of the flame in the detector results in the acquisition of no structural information about compound(s) entering the FID in the sampling period. With

this in mind the GC-FID methods employed are often measuring extracted organics that are able to pass through the GC column with the method conditions. Methods such as US EPA 1664 uses gravimetric detection and specifically sets out to measure organic matter, such as oil and grease, and any TPH components that make up the hexane extractable material (HEM). In an environmental sample with GC-FID detection any extracted natural organic matter (NOM) that passes through the GC column will be included in the reported TPH value.

It is the lack of specificity that limits FID detection in the tracking of fuel spill component fate. Only specific fuel compounds that are significantly more concentrated than other PHC components can be estimated. This usually limits FID identification to the *n*-alkanes and a few isoprenoid markers. As a PHC mixture typically contains many 100-1000's of compounds the smaller components appear as an unresolved complex mixture (UCM) of components which are eluted as a broad hump from the GC column. Extensive pre-fractionation with normal phase silica gel preparative chromatography can separate various classes of compounds (i.e. aliphatics, alkylated-aromatics, PAHs etc). Even after this lengthy step is taken FID detection will still be limited to the peaks larger than the UCM that is in that fraction.

Each separated fraction contains more and more isomers of compounds, as molecular weight within the fraction increases so an unresolved mass of peaks at higher molecular weight is inevitable. The compounds most amenable to detection with this approach are the first examples of the compounds in that class. Naphthalene and the two different methyl naphthalene isomers may well be measured correctly by this approach. *n*-Butyl naphthalene and its 87 different structural isomers are, however, likely to present

as an extremely challenging mass of peaks – an UCM. It should be noted that the term UCM is descriptive. A "resolved to UCM" ratio is a measure dependent on both the analysis method and personal choice during data interpretation. As such it is not a measure based on SI units and will inevitably pose problems when a quantitative measure of this is requested.

1.2.2 MS detection

With MS detection, the selectivity of the MS arises from unique fragment ions being able to be observed even when a range of components are eluted from the GC column into the mass analyser. As such the MS permits the analyst to identify compounds with MS fragments that are unique, or appear against a relatively low background. As with analysis by sample fractionation and subsequent GC-FID detection the compounds most amenable to detection are the first examples of the compounds in a given class.

Isobaric interferences, often from regioisomers of target compounds, can preclude unique detection of specific compounds by MS methods. In the case of fuel analysis this effectively means that parent PAH compounds and the early alkyl analogues can be detected uniquely but overlap by different isomers will limit this. A partial solution to this is to measure the summed response of the combined isomer set. Table 1 lists the 39 PAH analytes chosen for analysis by Page *et al*. in their assessment of the Exxon Valdez oil spill [49]. Various fused polycyclic aliphatics in fuel also produce unique ions as the fused rings remain intact giving unique high mass fragments. For this reason various hopanes, steranes, terpanes, adamantanes and diamonoids etc. are all used (to various extents) as biomarkers in fuel analysis.

Compound quantification following MS is quite different to FID detection as the MS detector does not respond equally to compounds. Higher PAH and PAH derivatives tend to easily produce high molecular mass ions, especially compared to aliphatic compounds. For this reason a standard of the compound to be measured is usually required although an isomer is often substituted for detector calibration. MS calibration must be performed regularly because contamination within the MS and slow degradation of the ionisation source causes considerable drift, both in the total ion current response and, in some cases, the relative ratios of fragment ions. Analysis of environmental samples after limited clean-up exacerbates MS contamination and requires more frequent instrument maintenance [50]. The calibration problem becomes more acute when calibration standards are not available for a target compound class being considered or when TPH measurements are required. Typically full scan MS spectra are summed when such TPH measures are required with the assumption that the overall fuel response will be the same as that of a standard fuel.

With MS detection the detector sampling speed can be a limiting factor, especially when slower scanning MS instruments are used to collect complete mass spectra across a wide mass range. As GC approaches produce narrower chromatographic peaks, instrument manufactures have responded by producing MS detectors that are capable of faster data acquisition. This data acquisition can be in either full scan or selected MS fragment ion(s). The increasing popularity of time of flight mass spectrometry (TOF-MS) may well be largely due to the fundamental design being well suited to fast acquisition of full mass-range MS data.

Table 1. Listing of the 39 PAH analytes measured in assessment of the Exxon Valdez fuel spill. In this work and reference the designations C1, C2, C3, and C4 correspond to the sum of all resolved isomers having one, two, three or four methyl groups. [a] U.S. EPA priority pollutant. From D.S. Page, P.D. Boehm, W.A. Stubblefield, K.R. Parker, E.S. Gilfillan, J.M. Neff, A.W. Maki, Environmental Toxicology and Chemistry 21 (2002) 1438 [49].

Naphthalene[a]	Anthracene[a]	Chrysene
C1 naphthalenes	C1 phenanthrenes/anthracenes	C1 chrysene
C2 naphthalenes	C2 phenanthrenes/anthracenes	C2 chrysene
C3 naphthalenes	C3 phenanthrenes/anthracenes	C3 chrysene
C4 naphthalenes	C4 phenanthrenes/anthracenes	C4 chrysene
Biphenyl	Dibenzothiophene	Benzo[b]fluoranthene[a]
Acenaphthylene[a]	C1 dibenzothiophenes	Benzo[k]fluoranthene[a]
Acenaphthene[a]	C2 dibenzothiophenes	Benzo[e]pyrene
Fluorene[a]	C3 dibenzothiophenes	Benzo[a]pyrene[a]
C1 fluorenes	Fluoranthene[a]	Perylene
C2 fluorenes	Pyrene[a]	Indeno[1,2,3-c,d]pyrene[a]
C3 fluorenes	C1 fluoranthenes/pyrenes	Dibenz[a,h]anthracene[a]
Phenanthrene[a]	Benzo[*a*]anthrancene[a]	Benzo[*g,h,l*]perylene[a]

1.3 Comprehensive two-dimensional gas chromatography

The challenges presented by complex samples led to the development of techniques that, without the tedium of manual fraction collection and re-injection, sequentially couple two GC separations. Each of these GC separations has a different selectivity and the GC columns are coupled in such a way as to essentially preserve the separation achieved on each GC column. When all the components from the first GC column are sampled and rapidly analysed on the second GC column the technique is comprehensive two-dimensional gas chromatography (GCxGC). This mode of the technique is the topic of this thesis as it gives an analysis result that includes all the PHC components in a sample taken from a fuel spill site in an environmentally sensitive setting. This is an essential requirement when total environmental impact is being investigated and when legalisation requires the estimate of a TPH value.

GCxGC started in 1991 within the research group of Phillips [51]. The technique was subsequently applied to PHC samples with the separation of over 6000 components in a kerosene sample published in 1993 [52]. The key piece of equipment is the part that couples the columns together while preserving the separation of each. This is called the modulator and is the only additional piece of hardware when the GCxGC instrument is compared to a conventional GC using a single column. The introduction of pneumatic modulators are especially relevant as it allows this modulator to be physically small, robust, easily added to a conventional GC and be run with, at worst, a small increase in carrier gas usage [53,54]. With this development any site, remote or otherwise, that is running a GC method could potentially use a GCxGC method with minimal change to the required hardware, spare part inventory or ongoing consumables. Switching between

pneumatic modulation GCxGC methods and normal GC methods is simply a matter of changing some capillary column connections.

Despite the lengthy period that the GCxGC technique has existed, development and uptake has been at a slower rate when compared to the fast expansion of competing GC-MS instrumentation and methods in the same time [55]. The extra information and specificity from the mass spectrometer allow for both improved identification of unknown compounds and selective detection of analytes, especially those with unique high mass fragments. This extra information is very useful when compared to the usual detector for hydrocarbon analysis, the FID. While the uptake of GCxGC instrumentation and methods has been slower than GC-MS, the field has evolved considerably. This environmental application appears to be particularly well suited to the strengths of pneumatic modulation GCxGC. Environmentally important information can be obtained on site to facilitate monitoring of fuel spill fate and the effectiveness of clean up operations. The field of GCxGC has been reviewed several times [4,55-65].

As noted in the review by Cortes *et al*. GCxGC research papers have moved, in general, towards more applications of existing technology and less on apparatus development [62]. This is especially true for papers using cryogenic modulation since this apparatus has had the largest amount of commercial development. The most recent modulation method, pneumatic modulation, is still mostly comprised of papers exploring the fundamentals and breadth of the technique as opposed to multiple applications with well refined apparatus and method choices.

1.4 Performance of modulators

The principles of modulator operation is discussed and compared in reviews [4,55-65] and in book chapters [66]. The purpose of the following review is to examine the performance aspects of the different modulator types. A direct and unbiased comparison of all the different modulator types is not available, nor likely given the wide range of types. Unfortunately the different acquisition methods and analytical method goals used by different researchers combine to make it difficult to directly compare performance from stated instrument outputs.

1.4.1 Thermal and cryogenic modulators.

Thermal modulation was pioneered by Phillips in the 1990's [51]. The commercialised 'thermal sweeper' arrangement involves containing the analytes eluting from the first-dimension (^{1}D) column in a short, thick film capillary column then releasing the contained analytes onto the second-dimension (^{2}D) column with a thermal sweeper [64,67,68]. Cryogenic modulators condense analytes eluting from the ^{1}D on a cooled capillary column [63]. The condensed analytes are released onto the ^{2}D column by either exposure to the oven air or by using a dedicated heat source to rapidly heat the band which was cryogenically cooled. A significant point to note with cryogenic modulators is that modulation time can be altered without consideration of factors such as analyte breakthrough (although sampling the ^{1}D column needs to be frequent enough to preserve the important separations obtained on the ^{1}D column).

The time required for heat to pass from the capillary exterior to the trapped components has been numerically estimated to be in the order of 10 to 15 ms or less depending on capillary dimensions and the temperatures of the various components

[69,70]. This is in good agreement with an experimental study of the heating time constant, for compounds in the range of *n*-C_4 to *n*-C_{40}, in thermal modulation GCxGC [64]. The limiting width of a released band may well be from other contributions. In the case of the LMCS approach of Marriott *et al*. this may be the longitudinal movement of the cryogenic trap (estimated at approximately 20 ms) or governed by other factors [69,71]. Marriott and Kinghorn note that "*Peaks generated by the* [LMCS] *modulator itself may be as narrow as 20–50 ms*" [72]. When implementing thermal modulation across a range of oven temperatures (and other analysis conditions) careful attention needs to be paid to both cooling and heating dynamics to avoid a loss in overall separation performance [64,73]. This loss in performance is due to the presence of peaks which are either fronting, tailing, excessively broad (in either separation dimension) or appearing as multiple spots.

Observed peak width is an important performance measure, though this will vary significantly with system hardware, operation parameters and the retention factor of the compound in question. Peak width at 10% height for peaks released from the LMCS device have been shown to be as narrow as 84 ms for *n*-decane analysed at 130 ºC although peaks of width 50 ms were seen as possible [74]. A slow (120 min) temperature programmed analysis of a test mix containing 24 semi-volatile aromatic compounds gave peak widths at base of between 330 and 640 ms with a LMCS and between 330 and 690 ms for a nearly identical method employing a thermal sweeper [72]. Kallio *et al*. report width at base (using the definition of $w_b = 4\ \sigma$) for anthracene, fluoranthene, chrysene and dibenzo[a,h]anthracene in the range of 100 to 180 ms using a laboratory-made semi-rotating cryogenic modulator [75,76]. Table 2 shows a selection of observed ^{2}D peak

widths, method conditions relevant to the ^{2}D column and peak width in the standard format of standard deviation, σ.

Gaines et al. used a rotating thermal modulator assembly manufactured by Zoex Corp with resulting peaks that were "*typically 0.2 s duration*" in a GCxGC-FID analysis used for source identification of oil spills [77]. In a separate study Gaines and Frysinger used a cryogenic loop modulator for the analysis of *n*-alkane standards and then the Exxon Valdez cargo oil [64]. In the fuel analysis, all the non-polar alkanes in the range *n*-C_6 to *n*-C_{47} can all be eluted such that the ^{2}D peaks are symmetrical with a pwhh in the range of 50-70 ms. This corresponds to width at base (using the definition of $w_b = 4\ \sigma$) of 85 to 120 ms. The more retained aromatics in the fuel sample were reported to have a ^{2}D width at base in the range of 170 to 270 ms.

From this brief review of cryogenic modulation peak widths, during the GCxGC analysis of complex samples, it can be seen that a ^{2}D peak with a width at base of 85 - 100 ms is a good approximation for current best practice. Earlier GCxGC methods tended to have longer analysis times and corresponding longer width at base for these peaks. When cooling and heating dynamics are carefully optimised the release time, of cryogenically trapped analytes, may be in the order of 10~15 ms. If the trend towards faster chromatography continues, peaks may continue to become sharper and thus approach the current limit for release from current thermal modulators. Sharper peaks may become problematic with detectors limited in data acquisition rates of <200 Hz. Authors appear to universally report GCxGC peaks obtained with cryogenic modulators as being symmetrical (and presumably Gaussian in shape).

Table 2. Comparison of ^{2}D peak widths from different modulators under different operation conditions.

Reference	Modulator type	Stated performance and available ^{2}D operation conditions [calculated ^{2}D velocity from method notes]	Calculated peak σ in ms
[74]	LMCS	84 ms base peak widths (measured at 10% height). ^{2}D conditions 0.3 m x 0.050 mm i. d. x 0.05 µm BPX70, *n*-C_{10} modulated, oven at 130 ºC, Helium carrier gas velocity 70 cm/s.	20
[68]	Thermal sweeper	0.21 s wide at baseline. 2D conditions 0.14 m, 0.10 mm i.d. bare fused silica capillary, *n*-C_{12} modulated, oven at 50 ºC, Helium carrier gas velocity >30 cm/s.	52
[72]	LMCS	W_b 330-640 ms. ^{2}D conditions 0.8 m x 0.1 mm i.d. x 0.10 µm BPX50, Hydrogen carrier gas [0.62 ml/min at 40C, ^{2}D velocity 119 cm/s at 40 ºC start of method]	82-160
[72]	Thermal sweeper	W_b 330-690 ms. ^{2}D conditions 0.1 m x 0.1 mm i.d. uncoated deactivated capillary then 0.8 m x 0.1 mm i.d. x 0.10 µm BPX50, Hydrogen carrier gas [0.50 ml/min, ^{2}D velocity 98 cm/s at 40 ºC start of method]	82-172
[75,76]	semi-rotating cryogenic modulator	W_b 100-180 ms. ^{2}D conditions 0.5 m x 0.1 mm i.d. 0.10 µm BGB-1701, Helium carrier gas [0.91 ml/min, ^{2}D velocity 166 cm/s at 60 ºC reference temperature for the stated head pressure at this temperature]	25-45
[77]	rotating thermal modulator	Typically 0.2s duration. ^{2}D conditions 0.20 m x 0.1 mm i.d. deactivated capillary then 1.0 m x 0.1 mm i.d. 0.14 µm Phase 007-CW, Hydrogen carrier gas 0.50 ml/min, [^{2}D velocity 98 cm/s at 50 ºC start of method]	~50
[64]	rotating thermal modulator	fwhh 50-70 ms for aliphatics, fwhh 100-160 ms for more retained aromatics. ^{2}D conditions 1.0 m x 0.1 mm i.d. deactivated capillary then 1.0 m x 0.1 mm i.d. 0.1 µm BPX-50 with a 0.5 m x 0.1 mm i.d deactivated transfer column, Hydrogen carrier gas 0.40 ml/min, [^{2}D velocity 67 cm/s at 30 ºC start of method]	21-30, aliphatics 42-68, aromatics

1.4.2 Valve modulation with the valve in the chromatographic path

Valve-based modulation relies on a specialised multiport mechanical valve located at the end of the ^{1}D separation column. The valve is actuated rapidly by electrical drives with the timing of actuation controlled electronically. The key feature of the multiport valve is that it controls both where ^{1}D outlet flow is directed and simultaneously determines what is entering the start of the ^{2}D separation column. A high flow of ^{2}D mobile phase is normally directed to the start of the ^{2}D column. The ^{1}D flow is periodically directed onto the head of the ^{2}D column when the multiport valve is actuated. During this short duration ^{2}D loading the ^{2}D mobile phase is directed to waste. When the valve returns to the initial position the ^{2}D mobile phase again enters the ^{2}D separation column while the outlet flow from the ^{1}D column is sent to waste [78] Alternatively valve geometries have been employed such that a portion of the ^{1}D column effluent is physically trapped in a chamber within the valve assembly giving a relatively large ^{1}D sampling ability [79]. Rapid actuation of the valve moves the chamber containing these components to the load position for the ^{2}D column and this material is loaded onto the ^{2}D column by the rerouted high flow ^{2}D mobile phase. Depending on the valve geometry and operation parameters all the material from the ^{1}D column can be passed to the ^{2}D column, an arrangement that results in comprehensive two-dimensional chromatographic separations. Alternatively, only a portion of material from the ^{1}D column is contained within the valve sampling chamber while the remainder passes to a waste line, an arrangement that gives multiple heart-cuts from the ^{1}D column [79]. As the proportion of material allowed to pass to the waste line is reduced the distinction between the two technologies becomes less and less important in terms of the separation of

components achieved. Despite this it is necessary to account for effects caused by incomplete sampling from such a valve arrangement [80]. Valve operation is generally sufficiently fast that consideration of what happens as the valve is in transition between the two valve positions is not critical (or even required) when evaluating overall performance. Valve modulation is an effective modulation method for both two-dimensional GC and two-dimensional liquid chromatography [81,82].

Valve-based modulators are non-focusing (with respect to the analyte concentration (mol/mol) in the mobile phase), a distinct difference from the cryogenic focusing employed in thermal GCxGC modulators. As the band of material from the ^{1}D column held within the valve sampling chamber becomes larger the loading time of this band onto the ^{2}D column increases. Consequently longer modulation cycles (with other system parameters held constant) lead to broader peaks emerging from the ^{2}D separation column but only when this loading time becomes a significant contributor to total band broadening [83]. The simple and effective solution to this problem is to only allow a small portion of the ^{1}D column to be loaded onto the ^{2}D column with the venting of other components. While this operation can have a positive outcome on the separation of target compounds, partial sampling of the ^{1}D column causes complications in terms of quantification of analytes. Changes in the elution time of the ^{1}D peak maximum relative to valve timing leads to different proportions of the ^{1}D peak being sent to waste [80].

The valve modulation approach to GCxGC has numerous recent papers in the scientific literature [65,84-87]. Extremely fast valve operation has enabled research into fast and ultra fast GC analysis and even multidimensional GC involving 3 GC columns and 2 valve based modulators, (called GC^{3} methods). With valve modulators it is usual to

direct a significant portion of the ^{1}D column effluent to waste and inject "typically….*~5-10%*" of effluent to the ^{2}D column [84]. This can, however, by varied so that 80% [79] or even 100% [84] of the ^{1}D effluent is directed onto the ^{2}D column and then to the detector.

Most of the valve modulation GCxGC work has avoided the use of extremely high oven temperatures (and therefore valve temperatures) as valve integrity and lifetime are seen as being compromised in this environment. A temperature limit of 175 ºC is typically reported [88]. Additionally, the thermal degradation of analytes within these high temperature valve components is an area of concern as is the cost of such valves. Despite the 175 ºC limit to the valve sections containing O-rings, placement of these temperature sensitive components outside the oven while locating the sampling loops etc inside the oven valve has been shown to be effective for >6 months use with methods having oven temperatures up to 265 ºC [88].

A point that is receiving more attention, especially as GC and GCxGC methods target faster and faster chromatographic separations, is the role of band broadening and peak asymmetry / tailing from processes other than direct on-column broadening during chromatography [83]. Reid *et al*. note that "*More likely, the observed peak tailing in the present study was due to the difficulty in minimizing sources of extra-column band broadening such as dead volumes*" [89]. As the different modulation strategies and associated hardware progress through cycles of development and refinement it may well be that the different strategies reach different limits driven by these extra-column band broadening processes.

1.4.3 Pneumatic modulation using a valve that is not in the chromatographic path

A more recent development of particular relevance has been the introduction of pneumatic modulators [53,54]. These modulators include both differential and pulsed flow modulators (see sections 2.3.3 and 3.2 for apparatus schematics). A pneumatic GCxGC modulator requires neither the cryogen employed in thermal modulators nor a temperature cycled multiport valve that is in the flow path of analytes, as previous valve based modulators required. As such these modulators necessitate only a small increase in carrier gas usage and the only moving part is a robust valve, external to the oven and able to be placed in any convenient place that is in close proximity to the oven itself. In the case of using FID detection and hydrogen carrier gas the additional gas required for the rapid separation in the second dimension is saved by an equal reduction in hydrogen flow to the FID. This results in no net difference to hydrogen requirements when all the flow exiting the modulator is directed into the ^{2}D column.

In the pulsed flow mode of the technique (shown in Figure 8, section 3.2) the external valve normally directs a high flow rate of ^{2}D carrier gas directly to the head of the ^{2}D column while material emerging from the ^{1}D separation column enters a modulator fill tube between the ^{1}D and ^{2}D separation columns. When the external valve is actuated this high flow rate ^{2}D carrier gas is directed towards the end of the ^{1}D separation column and thus rapidly loads what is within the modulator fill tube onto the start of the ^{2}D separation column. This redirection of ^{2}D carrier gas also generates a considerable pressure pulse at the end of the ^{1}D column which temporarily stops ^{1}D column outlet flow by inducing a short term backflow at the end of the ^{1}D separation

column. The combination of rapidly loading the ^{2}D column while stopping the ^{1}D column outlet flow give rise to the pulsed flow modulation. The effect that backflow at the end of the ^{1}D separation column has on ^{1}D separation is difficult to determine. Switching off the modulator valve and comparing the results to a run with the valve on does not reveal the extent of this effect as it is confounded by ^{1}D flow changing when the valve is off (even if ^{2}D flow does not change significantly). A final consideration is the effect of valve switching causing rapid compression of the gas in the modulator sample loop. This compression may well lead to increased mixing of components in the sample loop as the flow profile is very different to the relatively slow and steady flows normally associated with chromatography. Valve modulators will have this problem to a certain extent so the effect may not be significant with appropriate capillary dimensions. Poliak and Amirav demonstrated a released pulse width in the order of 20 ms, from the modulator, may be obtained with high flow ratios (127 was the calculated flow ratio) and a low modulation time (2 s) [90]. Measurement of the released band at an FID, after passing through a 0.7 m x 0.25 mm i.d transfer line, gave a minimum peak width at half height of 18 ms, corresponding to a $w_b = 4\sigma = 31$ ms.

As a relatively new technique most reported methods using this pulsed flow modulation approach follow flow settings and timings similar to the first reported methods. Typically these methods have a total ^{2}D to ^{1}D flow ratio of 20-30 : 1. Excessive ^{2}D peak broadening, stemming from a large ^{2}D loading volume, is usually limited by having a short modulation period, typically 1.5 to 2 seconds.

The other variation of the technique, differential flow modulation, has received less attention in the literature – no doubt due to the increased complexity of construction. In

this technique, a flow diagram for which is shown in Figure 2, section 2.3.3, the external valve directs the high flow ^{2}D carrier gas into one of two fill tubes in the modulator. The majority of this ^{2}D carrier gas from the external valve constantly sweeps one of the fill tubes in the apparatus onto the start of the ^{2}D separation column. In conjunction to this a small percentage of the gas from the external valve follows an alternate route which directs all of the ^{1}D separation column outlet flow into the fill tube which is not being actively swept out. Actuation of the external valve reverses which fill tube is being swept out (thus loading material that had flowed into that fill tube onto the ^{2}D column) while directing the ^{1}D separation column outlet flow into the fill tube which is not being actively swept out.

Compared to the pulsed flow version of the apparatus, twice as many fittings are required. In addition, the required capillary dimensions and apparatus pressure settings for successful modulation are less well explored in the literature. The extra fittings will exacerbate problems associated with these fittings, namely dead volumes and peak tailing. As the apparatus exists with two distinct flow paths the apparatus will need to be built such that the flow through each flow path is matched or retention time of an analyte will vary depending on valve position. These drawbacks appear to have made the pulsed flow version of the apparatus more favourable. Despite this, the lack of modulator switching induced backflow at the outlet of the ^{1}D separation column is a distinct advantage compared to the pulsed flow modulator. In the future this may make the apparatus more attractive if the construction problems can be overcome. This would be especially true with very rapid modulation cycles as the pulsed flow method introduces a separate backflow event with modulation cycle.

In both the differential flow and the pulsed flow configurations the high ^{2}D flow and low ^{1}D flow is a clear change from optimal pneumatic conditions. Also the ability of detectors to function acceptably with high flows may limit the technique – especially when MS detection is required.

1.5 Data analysis in GCxGC

1.5.1 Class structure of analytes in GCxGC

One of the most powerful aspects of GCxGC analysis is the chemically ordered class structure of analytes as they appear in the 2D separation space. In the case of fuel analysis, where the relative amounts of different analyte classes are important parameters to quantify, this is a fundamental reason for carrying out the technique. This can be readily seen in the banded structure of the contoured GCxGC-FID plot shown in Figure 1. The analysis conditions, used in the acquisition of Figure 1, use the conventional column arrangement of non-polar ^{1}D separation column then a more polar ^{2}D column. The reversed class structure can be seen when the opposite arrangement of separation column polarities is used [91].

In Figure 1 the yellow lines are approximately lined up over the different major series of aliphatic components. The lowest of these series (i.e. earliest to elute from the ^{2}D separation column) are the branched, acyclic alkanes, including isoprenoids such as norpristane, pristine and phytane. Normal alkanes appear just above this series then the alicyclic alkanes (often called naphthanes in the petroleum industry and related

literature). These series include alkylated cyclohexanes and cyclopentanes as the major ring structures. *n*-Alky cyclohexanes are an important set of biomarkers frequently

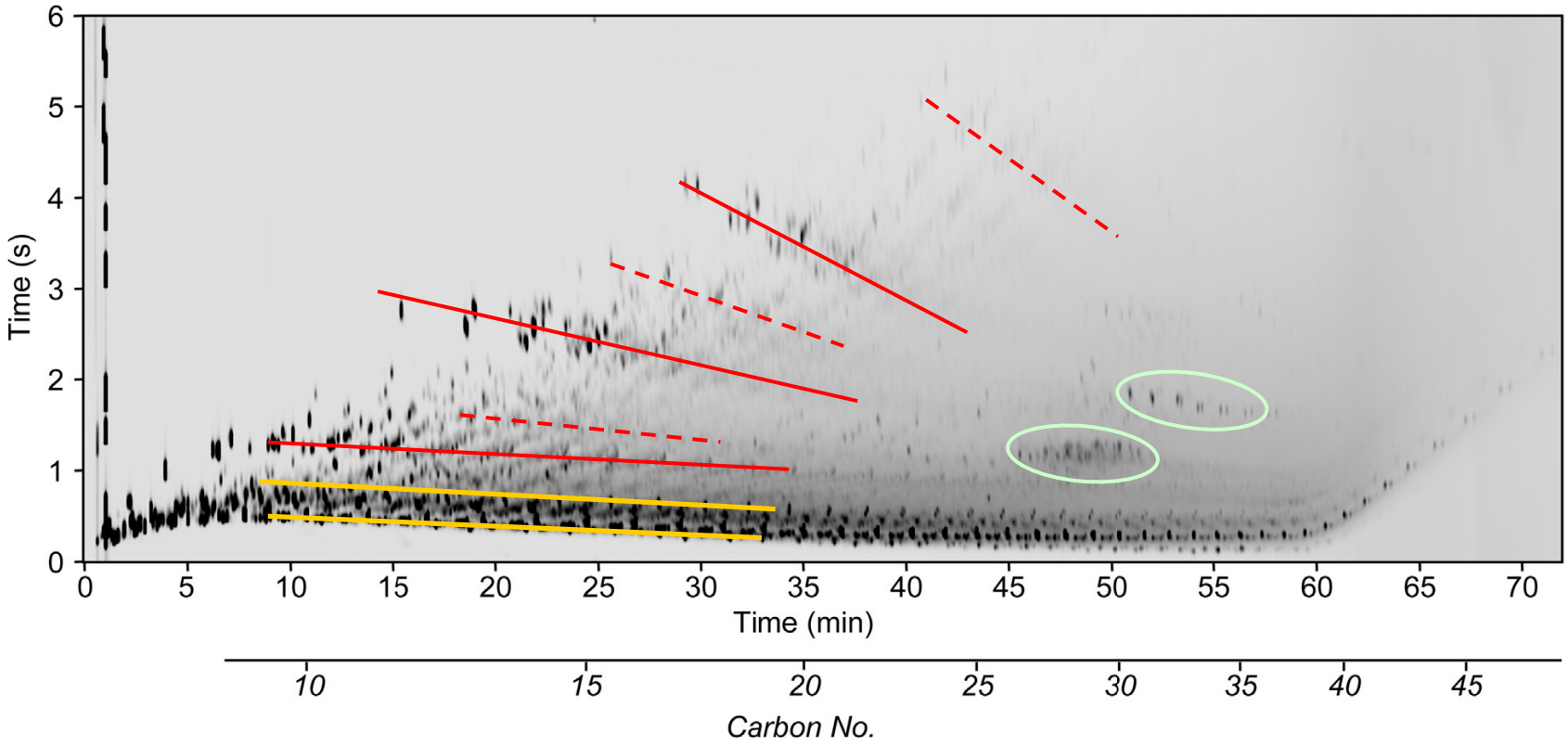

Figure 1 GCxGC-FID Analysis of Exxon Valdez crude oil, from R.B. Gaines, G.S. Frysinger, Journal of Separation Science 27 (2004) 380. The location of *n*-alkanes with specific carbon numbers are shown on the lower x-axis. The earliest eluting *n*-alkane is *n*-C7 and the latest eluting *n*-alkane is *n*-C47. Yellow bands are acyclic aliphatics (lower) and cyclo-alkanes (upper). Solid red bands are, from bottom to top, alkyl benzenes, alkyl naphthalenes and alkyl-anthracenes + phenanthrenes. See thesis text for other groupings

measured in fuel samples to judge geological maturity [92] or track biodegradation [3]. All these series have been identified with GCxGC methods.

Environmental analysis of these components (in PHC contaminated samples) is usually done to establish a fingerprint of the fuel to allow identification of the fuel spill source. Alternatively, these materials may be measured to give some information about the relative extent of biodegradation of a spilt fuel with known initial composition. As all the aliphatics have low aqueous solubility and limited toxicity (as deduced by dose response experiments) the environmental impact of these compounds is essentially caused by their action as a non aqueous phase liquid (NAPL) [93,94]. As this NAPL will retain the more environmentally active aromatic contaminants and mediate their transport and release it is still an important part of a fuel spill to consider. Other outcomes for the presence of a NAPL are derived from a fuel sheen (or thicker layer) on affected surfaces. Such a layer of fuel reduces the natural fluxes between air and/or water and the contaminated surface. The complete coverage of larger wildlife (such as birds and aquatic mammals) with a viscous crude oil NAPL is often presented in the media and is one of the most emotionally distressing images from a large spill in an environmentally sensitive area.

In commercial diesel fuels the combined aliphatic content is typically 70% ~ 85% of the total hydrocarbon content on a mass for mass basis [9]. While the crude oil shown in Figure 1 extends to ~*n*-C_{47}, vehicle diesels typically contain components of lower molecular mass (i.e. more volatile) than ~*n*-C_{28}. The molecular mass range in a diesel is subject to considerable variation due with winterised fuels containing lower amounts of the larger mass components that lead to waxing at low temperatures. Extreme examples

of this can be seen in Special Antarctic Blend (SAB) diesel which only has minor components above ~ *n*-C_{15} – *n*-C_{16} and a product specification of the "low temperature filtration point" of -38 ºC. Jet-A1 is another notable example of a highly refined product, with tightly control tested specifications, containing a high aliphatic content and components with a low boiling point distribution range.

The three bands in Figure 1 shown in the solid red lines correspond to the alkylated aromatics containing, from bottom to top, 1, 2 and 3 fused aromatic rings. These are the series whose parent aromatics are benzene, naphthalene and 'anthracene + phenanthrene'. Like the cyclohexanes, the *n*-alkylated benzenes (formula C_6H_5-C_nH_{2n+1}) form an observable set of compounds, often measured as fuel markers and available commercially. Apart from this easily defined set of compounds the complications of branched alkylations and the multiple locations (on the parent aromatic ring structure) of additional alkylations, make other alkylation series lower in abundance. In addition to this the branched alkylation series are more difficult to separate and reference materials are harder to obtain. This is particularly true for the more heavily alkylated naphthalenes, anthracenes and phenanthrenes etc. Companies, such as Chiron, offer a substantial library of compounds available as pure components, dilute solutions or as mixtures of assorted concentration [95]. In the case of two and three ring fused aromatics as the C1 and C2 alkylated isomers appear to be available as analytical standards but quantities for large dose response experiments may be prohibitively expensive. While reference materials with higher degrees of alkylation become increasingly difficult to obtain the ^{1}D and ^{2}D retention times of such compounds can be estimated on a GCxGC chromatogram without the standard in hand.

The dashed lines in Figure 1 show the positioning of other alkylated series from different parent aromatics. Parents such as biphenyl, acenaphthenes, acenaphthylenes, fluorenes, terphenyls, pyrenes, chrysenes and higher ring structures are all candidates for these classes. Indeed these parent PAHs (plus alkylated analogues and higher PAHs) are all found in the Exxon Valdez crude oil spill as shown in Table 1 (page 11). As can be seen by the decreased intensity of these higher mass alkyl PAH compounds, and increase in the number of isomers in a given alkylation group, specific compounds that can be targeted represent a smaller and smaller component of total alkyl PAH content. This is similar to separating and identifying every PHC compound with approximately <10 carbons in a PIONA analysis but uniquely separating and identifying a progressively smaller proportion of compounds as the number of carbon atoms in the molecule increases. In terms of extrapolation to total environmental impact of PHC compounds, measuring these smaller and smaller abundance markers, despite an increase in toxicity of these markers as mass increases, allows for the possibility of greater and greater extrapolation errors.

The final features indicated in Figure 1 are the ellipses around carbon numbers ~26 to ~31 and ~30 to ~36. These cover the majority of compounds that are contained within the hopane and sterane classes respectively. As the earliest eluting members of the hopanes are just within the volatility window of a non-winterised commercial diesel (applying the *n*-C_{28} cut off approximation) the concentrations of hopanes in commercial diesels will be, at most, very minor. Steranes will be correspondingly lower in abundance or absent. In the case of winterised fuels, and especially products like SAB, the hopane and sterane concentrations will be present in trace quantities. While measuring

biodegradation, evaporation and dissolution resistant marker hopanes and steranes is a well established practice, it should be restricted to spills that have significant concentrations of these components. Otherwise much analytical effort will be put into measuring incredibly minor (or absent) components not representative of the bulk fuel. Furthermore, any results will be easily confounded by very minor spill of a PHC source containing these components.

1.6 Project Aims

The aim of the project is to develop the fundamental understanding of pneumatic modulation GCxGC analysis and demonstrate this by delivering a pneumatic modulation GCxGC-FID package for remote site fuel spill analysis. The applied focus for the work was the environmental analysis of fuels for the AAD. In this context the analyte range is principally from diesel spills (*n*-C_9 to *n*-C_{28}), especially the main SAB components (*n*-C_9 to $\leq$ *n*-C_{20}). As lubricant range PHC components are often found in conjunction with these spills, aliphatics (and some related highly alkylated aromatics) are required to be eluted up to ~ *n*-C_{36}. The 2D separation of aliphatics and the different classes of PAH and alkylated PAH present in SAB diesel complete the analysis requirements for the Australian Antarctic Division (AAD). PAH and alkyl PAH compounds with more than 4 fused rings are of separate interest to AAD fuel spill analysis as the refined diesels used by the AAD contain these components in very low (or zero) concentrations.

The specific aims of the project can be divided into 2 broad themes: (1) fundamental development of the technique and (2) use of the technique for a PHC site assessment (such as the site assessments carried out by the AAD).

- Fundamental development of the technique

- Develop numerical flow models for the different pneumatic modulation apparatus geometries. This is to facilitate the prediction of successful operation conditions and the extent of flow deviations from a normal (steady state) chromatographic flow.
- Develop peak shape models for non-focusing modulators (such as pneumatic modulation GCxGC) so that the effect of modulator dimensions and flow conditions on peak shape can be assessed prior to modulator construction. This is required for the rapid development of a modulator that meets method requirements. The numerical model is to take a given set of apparatus operation conditions as well as chromatographic performance in each dimension and return an expected peak shape.
- Develop a set of apparatus dimensions and operation parameters that minimise potential bias from flow distortions at the detector

- PHC site assessment (such as the site assessments carried out by the AAD).
  - Build GCxGC-FID apparatus that demonstrates the above features while achieving a PHC separation useful for the environmental analysis
  - Show that a PHC contaminated site assessment with GCxGC-FID methods is viable. The GCxGC-FID methods will need to meet regulator requirements for data quality and lead to significantly better knowledge of PHC fate compared to regular, on-site GC-FID methods.
  - Develop robust apparatus for the above application that analyses entire site sample batches.

- Present some software tools so that non-specialist collaborators can receive a meaningful summary of GCxGC-FID analysed samples.
- In conjunction with the AAD analyse Macquarie island soil samples from the Fuel Farm PHC contaminated site as an applied demonstration of the capabilities outlined above.

In meeting these goals GCxGC-FID should become an attractive PHC site analysis method able to be deployed at any site capable of operating a GC-FID. Furthermore, the need for on-site specialist operator input and extensive on-going maintenance normally associated with GC-MS methods will be avoided. The ability to automate aspects of data presentation and interpretation (with software tools) will allow on-site users to obtain meaningful site information with a minimum of effort and prior training. In these ways it is anticipated that environmental site assessment information will be maximised while minimising the valuable on-site time taken to get that information.

2 General Experimental, Calibration and Baseline Correction

2.1 Reagents

2.1.1 Gases and solvents

Hydrogen carrier gas was used from either cylinders or laboratory gas generators. Cylinders were either high purity or ultra high purity (BOC, Derwent Park, Australia). Generators were branded either Parker-Balston (Parker-Hannafin, Cleveland USA) or Domnick-Hunter (Parker-Hannafin, Cleveland, USA). Helium was used from either high purity or Ultra high purity cylinders (BOC). Nitrogen was used from either cylinders or laboratory gas generators. Cylinders were either high purity or Ultra high purity (BOC). The nitrogen generator was from Domnick-Hunter. Air was used from either cylinders or laboratory gas lines or laboratory scale instrument grade air generator from Domnick-Hunter. Cylinders were either instrument grade or 'zero air' grade from BOC.

Ethene used for column dead time determination was from a C.P. grade cylinder from BOC. Butane used for retention time determination was from a 150 g purified butane gas can (Dick Smith Electronics, Melbourne). Hexane was nanograde 95 % *n*-hexane (Mallinckrodt Baker Chemicals, Phillipsburg, USA).

All solvents used for sample extraction and standard preparation (excluding acetone) were 'nanograde' from Mallinckrodt. Acetone (Scharlau, Barcelona, Spain) was 'GC residue analysis' grade (P/N AC03084000) and was used as the extraction solvent for samples from the AAD permeable reactive barrier installation.

2.1.2 Internal standard mixture for low level GCxGC TPH calibration.

A list of internal standards is provided in Table 3. This set of internal standards was added to diesel standards and the test mix WC5. It was used for trials with the differential flow modulator described in Table 6 during tests on modulator performance, baseline correction methodology and limit of detection determination. Limit of detection trials employed low concentrations of diesel with a compound range from *n*-C_9 to ~*n*-C_{28} rather than the narrower compound distribution found in SAB.

Table 3. GCxGC internal standard compounds, selected properties and concentrations.

Name	MW	% Carbon by mass	Mass added, mg	Compound concentration in the hexane spike solution, mg/mL
1-bromo-4-fluoro-benzene	174.998	41.2%	864.6	1.729
Cyclooctane	112.214	85.6%	636.3	1.273
1,2-dichloro benzene	147.004	49.0%	230.3	0.4606
d_{22}-decane	164.420	73.1%	288.1	0.5762
p-Terphenyl	230.309	93.9%	29.2	0.0585
2,2'Dimethyl-1,1'-Binaphthalene	282.384	93.6%	89.4	0.179
d_{50}-tetracosane	388.969	74.1%	124.4	0.2488
1-Bromoeicosane	361.444	66.5%	634.9	1.270
1-Bromodocosane	389.498	67.8%	382.1	0.7642

2.1.3 Internal standard mixture used with Macquarie Island soil extracts.

The set of internal standards shown in Table 4 was added to the soil samples extracted at Macquarie Island. The same internal standard solution was used to make the TPH standards prepared at the same time as Macquarie Island soil samples were extracted. To each sample and to each TPH standard 500 µL of the stock solution was added.

Table 4. GCxGC internal standard compounds, selected properties and concentrations.

Name	MW	% Carbon by mass	Mass added, mg	Compound concentration in the hexane spike solution, mg/mL
Fluoroheptane	118.194	71.1%	249.6	0.0624
d_{10}-Ethylbenzene	116.229	82.7%	199.2	0.0498
Cyclooctane	112.214	85.6%	999.0	0.2498
d_{10}-Anthracene	188.295	89.3%	103.6	0.0259
Bromoeicosane	361.444	66.5%	1000.3	0.2501

2.1.4 Marker compounds and fuel standards

Retention times of specific compounds were determined by injection of a marker mixture. Marker mixtures obtained commercially were the 'TRPH Standard' 500 µg/mL each in hexane, (Ultra Scientific, Kingstown, RI, USA) and 'EPH Matrix spike Standard' (Supelco, Bellefonte). Alternatively marker mixtures were prepared by dilution of the required reference compound in hexane. Reference compounds were obtained from Sigma-Aldrich in the highest available purity and used without further purification.

A 200 L drum of SAB (from 2003 refuelling operations) was obtained and stored in the flammable bunker at AAD head office as a reference standard. All diesel standards came from a 4 L metal drum of diesel obtained at Kingston, Tasmania, 2003. For ongoing

retention time calibration the 'WC5' in-house standard was used. The WC5 standard contained a mixture of 5.01 g SAB, 19.99 g diesel and 1.00 g 'night light' candle wax (Coles, Kingston, Tasmania). The addition of *n*-C_8, *n*-C_9, *n*-C_{10}, *n*-C_{20}, *n*-C_{24}, *n*-C_{28}, *n*-C_{32}, *n*-C_{35} and *n*-C_{36} modified the marker mix to allow easier identification of these particular *n*-alkanes. These *n*-alkanes feature in hydrocarbon ranges required to be quantified [8]. A fuel standard containing enhanced concentrations of diesel range aromatics and depleted concentrations of aliphatics was obtained by separating the ~80% of the aliphatics from 5 mL of diesel with preparative chromatography on silica with hexane [96].

2.2 Procedures

Soil sample extraction and GC analysis procedures are based to a large extent on the work of the TPHCWG and the reference analytical method published by this group [96]. The principal modification to the TPHCWG was the replacement of the extraction solvent pentane with hexane. This modification was required to facilitate the safe transport and storage of both bulk solvent and sample extracts between the University of Tasmania (Sandy Bay), the AAD head office (Kingston) or the AAD research station at Macquarie Island. As no fuel range components of molecular mass less than *n*-C_8 are present in the SAB and diesel fuels being investigated this change introduced no co-elution problems. Safety problems with the shipping and storage of sample extracts in volatile solvents were greatly reduced by this change to hexane.

GCxGC-FID analysis was carried out on the Macquarie Island soil sample extracts in 2009 after they were shipped back from Macquarie Island. Between initial on-site GC-FID analysis and all subsequent analysis extracts were stored at -20 °C or -18 °C.

2.2.1 Standard preparation

All standards were prepared gravimetrically and diluted with the same solvent batch that was used for sample extraction. A minimum of 100 mg of pure fuel component or reference fuel was weighed when the available quantities permitted this. Serial dilutions were carried out gravimetrically. For readily available compounds, solutions and fuel standards a minimum of 200 mg of a stock solution or dilution was weighed out when diluting a higher concentration stock.

Portions of the SAB and diesel reference fuels were taken to each analysis location to ensure identical composition during preparation of the standards. Comparison, on a single GC-FID instrument after return shipping, between standards prepared at the three different locations indicated no detectable change in fuel composition.

2.2.2 Sample extraction and GC-FID analysis at Macquarie Island

Samples were excavated from the Macquarie Island Fuel Farm in the Austral 2006-07 summer and the 2007-08 summer with the assistance of the AAD bioremediation team. Soil sample excavation and site documentation procedures were carried out in accordance with the methods outlined in the papers [97] and reports [98] of the AAD Bioremediation team. Determination of a TPH estimate with a photo ionisation detector (PID) (MiniRAE “lite”, Envco – Environmental Equipment) was carried out in the 2007-08 summer by the AAD bioremediation team using documented methods [97,99]. Hydrocarbons were extracted from a 10 g sub-sample of homogenised wet soil by tumbling overnight with a mixture of 10 mL of deionised water, 10 mL of hexane, and 1 mL of hexane spiked with Internal standard mixture described earlier (Table 4). Samples were then centrifuged for 10 min at a relative centrifugal force of 208 g using a Haraeus

3SR Plus centrifuge (Thermo Scientific). Following removal of the hexane extract, soil remaining in the vial was dried at 105 °C for 24 hours and the dry mass recorded.

Extracts were analysed for TPH by GC-FID (Agilent 6890N with a split/splitless injector) and an auto-sampler (Agilent 7683 ALS). Separation was achieved using an SGE BP1 column (35 m x 0.22 mm ID, 0.25 µm film thickness). 1 µL of extract was injected (1:15 pulsed split) at 310 °C and 207 kPa of helium carrier gas. After 1.3 minutes, the carrier gas pressure was adjusted to maintain constant flow at 1.3 mL/min for the duration of the oven program. The oven temperature program was 50 °C (hold 3 min) 50 °C - 320 °C (18 °C/min), 320 °C (hold 12 min). Detector temperature was 340 °C.

TPH concentrations were determined using a calibration curve, generated from standard solutions of SAB, and standard diesel. TPH was measured using the ratio of the total detector response of all hydrocarbons to the internal standard 1-bromoeicosane peak response.

2.2.3 Method and Instrument quality control procedures.

GC apparatus was stabilised by the analysis of 2 solvent blanks prior to the analysis of any unknown site samples. Following this, retention time marker mixtures were analysed with an additional blank just prior to sample analysis. The main analysis sequence itself consisted of groups of 6 to 8 samples, one randomly selected sample repeat (from a sample analysed earlier in the sequence), 1-2 ongoing standards then a solvent blank. Sample to sample carry over from the injection system was tested for in the solvent blank following a high TPH standard. The high standards typically had a fuel concentration equivalent to that expected for a 10 g soil sample with 12000 mg/kg TPH.

The ongoing standards included the TPH standards (with a concentration range expected to bracket the samples being analysed) or repeat analysis of the retention marker mixtures. Solvent blanks were injected a maximum of 5 times before a new solvent blank vial was selected. At the conclusion of the analysis sequence the full range of standards were again analysed with additional solvent blanks unless the next sample batch was ready for immediate analysis.

2.2.4 GC-MS methods

GC-MS analysis was carried out with Dr Noel Davies at the University of Tasmania in 2010. Extracts were analysed with a Varian 3800 GC with 1177 injector, CP-8400 autosampler and 1200 triple quad MS. Separation was achieved using an SGE BPX-5 column (25 m x 0.25 mm ID, 0.25µm film thickness). 2 µL of extract was injected (60:1 split) at 280 °C. The helium carrier gas pressure was adjusted to maintain a constant flow at 1.2 mL/min. The oven temperature program was started at 40 °C (held for 5 min) and increased to 310 °C at 7 °C/min then held at 310 °C for 7 min. The transfer line to the MS was heated to 290 °C and the MS source was heated to 220 °C. MS data acquisition was started at 3.62 min and ended at 50.63 min.

All samples were analysed twice, initially with full scan MS detection (scanning from 35 to 350 m/z at 4 Hz, constant gain of 1300 V) then with selected ion detection. In analyses with selected ion detection 3 time segments with different selected ions were used. MS detector autogain was used in each of the segments. Segment 1 was from 3.62 to 17.02 min and used the following ions: 57, 83, 91, 98, 105, 112, 119, 128, 133 and 147 m/z. Segment 2 was from 17.03 to 25.01 min and used the following ions: 57, 83, 91, 105, 119, 133, 142, 147, 156, 170, 182, 184 and 198 m/z Segment 3 was from 25.02 to

50.63 min and used the following ions: 57, 83, 135, 137, 178, 184, 188, 192, 198, 202, 206 and 220 m/z. Standards analysed with GC-MS methods included the TPH calibration standards prepared at Macquarie Island as well as the EPH, TRPH and WC5 standards. These standards, as well as duplicate injections of the standards, were interspersed into the analysis sequence containing the samples.

2.3 Instrumentation

2.3.1 GC and GCxGC

All GCxGC separations were performed using an Agilent 6890N gas chromatograph. The instrument was fitted with a FID, split/splitless injector, a three-channel auxiliary electronic pressure controller (Agilent Kit G1570–60720) and autosampler (Agilent model 7683) [100]. Data were collected (200 Hz) using Agilent MSD Chemstation software. A standard capillary jet was used in the column - FID interface. FID flow rates were maintained within the recommended range of 24-60 ml/min hydrogen, 200-600 ml/min air and 10-60 ml/min nitrogen (make-up) with a hydrogen-to-air ratio maintained between 0.08:1 and 0.12:1 [101].

Modulator gas was supplied from one of the 3 auxiliary electronic pressure control lines. This gas was piped to the modulator valve via stainless steel parts and 1.2 m x 6.35 mm diameter stainless steel tubing (Swagelok). The additional electronic pressure control lines were also plumbed to this 1.2 m x 6.35 mm tubing allowing modulator valve feed pressure to be measured and electronically recorded with Chemstation software.

2.3.2 GCxGC apparatus and conditions for Chapter 3 and 4

Separation columns were obtained from SGE (Ringwood, Australia). Press fit capillary unions and glass lined mini unions were obtained from SGE [102,103]. Microvolume tee and cross connectors with fused silica adapters were obtained from Valco (Houston, USA). Methyl deactivated capillary columns were obtained from either SGE or Restek (Bellefonte, USA). Sulfinert® deactivated 1/16" o.d, x 0.010" i.d. stainless steel tubing was obtained from Restek with cutting, cleaning and bending following recommended procedures [104].

For the Pulsed Flow Modulation (PFM) GCxGC-FID apparatus the first dimension column used in all analyses was a 15 m × 0.22 mm I.D. column from SGE Analytical Science (Ringwood, Australia) with a 0.25 µm film thickness BP-1 (100% polydimethylsiloxane) stationary phase. The second dimension column was a 5 m × 0.25 mm I.D. column from SGE Analytical Science with 0.25 µm film thickness HT-8 (8% phenyl (equivalent) polycarborane-siloxane) stationary phase. The PFM modulation device was constructed using Valco capillary column unions (tee- and cross-unions) (Grace Davison Discovery Sciences, Rowville, Australia) a three-way switching valve (Parker Hannifin, Castle Hill, Australia) and 0.25 mm i.d. fused silica capillary tubing (Restek, Bellefonte, USA) according to the tubing dimensions reported in Chapter 3 (section 3.4).

The three-way switching valve (part number 091-0094-900) was from Parker Hannifin (Castle Hill, Australia). Actuation of this three-way valve was controlled using a purpose-built digital timer (Scielex, Kingston, Australia). Agilent MSD Chemstation software was used to signal the digital timer to commence modulation at a precise time to

minimise run-to-run retention time variability. Valco tee-unions or cross-unions (Grace Davison Discovery Sciences, Rowville, Australia) were used to construct the modulator. The temperature program used for the 3 s modulation separation of SAB was 40 °C (hold 4 min), 40 °C – 230 °C (6 °C /min). The temperature program used for the 9 s modulation separation of SAB was 40 °C (hold 15 min), 40 °C – 220 °C (1 °C /min), 220 °C (hold 5 min). A 1.0 µL split injection of neat SAB was performed using a split ratio of 300:1. Hydrogen carrier gas was used for all analyses. FID detector temperature was 300 °C.

The apparatus dimensions are the same as detailed above except for the addition of a 5 m × 0.25 mm i.d. deactivated fused silica capillary tubing split vent line. The temperature program used for the analysis was 40 ºC (hold 2.5 min), 40 °C – 252 °C (8 ºC / min), 252 ºC (hold 5 min). FID detector temperature was 300 °C.

2.3.3 GCxGC-FID instrumentation used in Chapters 5 and 6.

Two different differential flow modulators were built and extensively tested. A generic flow and apparatus diagram is shown in Figure 2 with the dimensions of the two different apparatus tabulated in Table 5 and Table 6. In each case the tees at P1, P3 and P5 were Swagelok 1/16" stainless steel micro volume tees for chromatography. Tees at P2 and P4 were normal Swagelok 1/16" stainless steel tees. Swagelok 2 part ferrules were used to connect all 1/16" stainless steel tubing into the tees. Tee P1 was directly connected to tees P2 and P4. The fragile 220 µm o.d. fused silica restrictors (which carry flows F3 and F4) are housed entirely within the stainless steel 'triple tee' arrangement P2-P1-P4 in a manner similar to that used by Poliak *et al*. in the construction of a PFM [105]. In order to make a gas tight connection with the stainless steel tees and fused silica

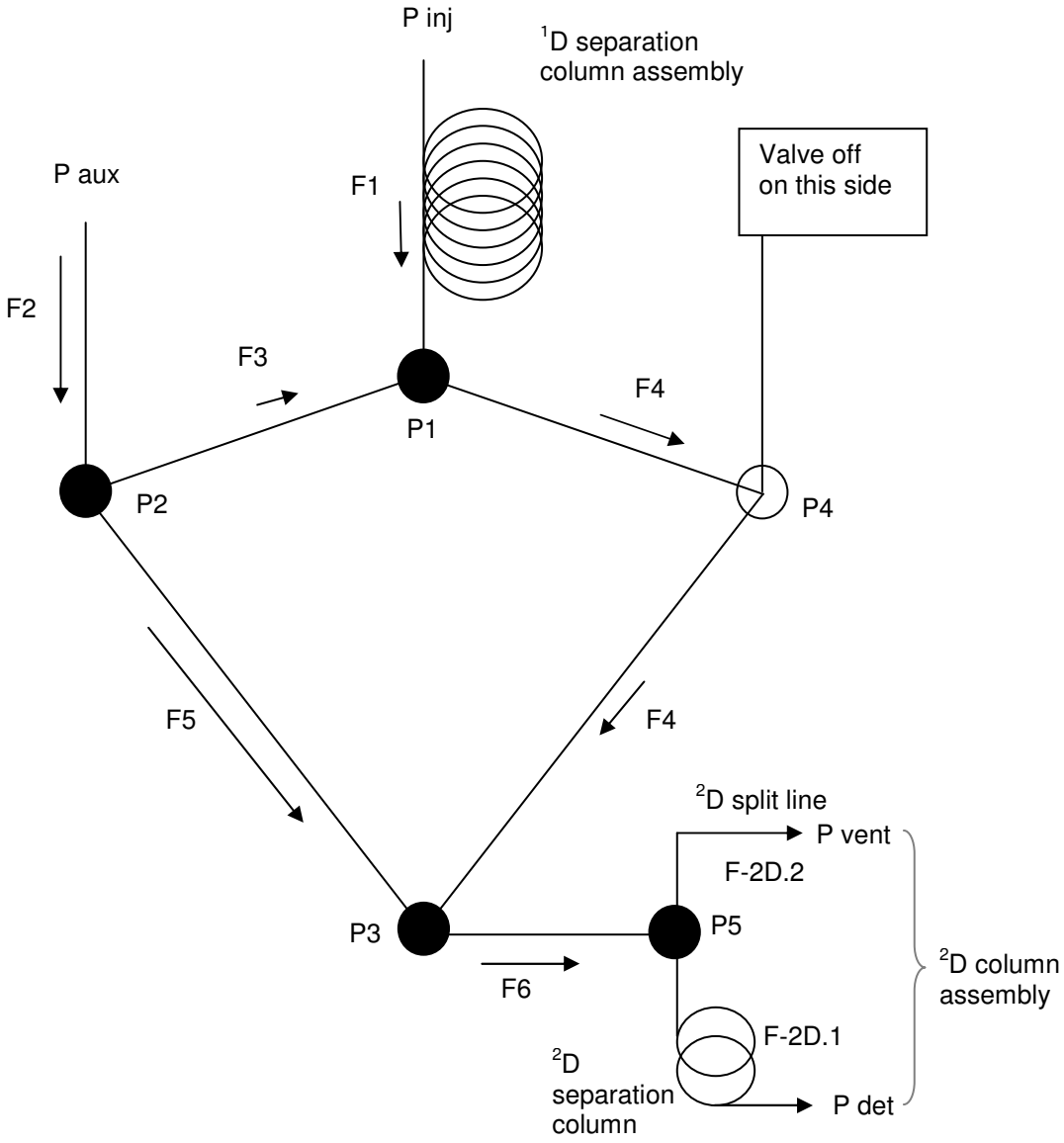

Figure 2. Flow and pressure identification in a stylized differential flow pneumatic GCx**GC modulator.**

Table 5. Differential flow pneumatic modulator, separation column dimensions and modulator timing– Macquarie Island sample apparatus. GCxGC method pressures programmed to maintain ^{1}D and ^{2}D flows

Part	Flow (Figure 2)	Dimensions
^{1}D assembly	F1, ~0.25 ml/min hydrogen	1.00 m x 0.075 mm i.d. methyl-deactivated followed by 12 m x 0.22 mm i.d. x 0.25 μm BP-1
Restrictors	F3 & F4	40 mm x 0.05 mm i.d. x 0.220 mm o.d. methyl-deactivated
Fill tubes	F5 & F4	S.S. 0.500 m x 0.25 mm i.d x 1/16" o.d.
^{2}D (no split vent line)	F6, ~15 ml/min hydrogen	4.8 m x 0.25 mm i.d. x 0.25 μm HT-8
Tube to start of fill tube from valve	F2	S.S. 0.500 m x 0.25 mm i.d x 1/16" o.d.
The external valve controlling the modulation switched flows every 3.600 s		

Table 6. Differential flow pneumatic modulator and separation column dimensions – Apparatus trials. GCxGC method pressures programmed to maintain ^{1}D and ^{2}D flows.

Part	Flow (Figure 2)	Dimensions
^{1}D assembly	F1, ~0.33 ml/min hydrogen	12 m x 0.15 mm i.d. x 0.25 μm BP-1
Restrictors	F3 & F4	41.3 mm x 0.05 mm i.d. x 0.220 mm o.d. methyl-deactivated
Fill tubes	F5 & F4	Restek S.S. 0.480 m x 0.25 mm i.d x 1/16" o.d. sulfinert
Tube to ^{2}D splitter	F6~24 ml/min hydrogen	Restek S.S. 0.040 m x 0.25 mm i.d x 1/16" o.d. sulfinert
^{2}D, separation column	F-2D.1 ~8 OR ~16 ml/min hydrogen depending on split	4.8 m x 0.25 mm i.d. x 0.25 μm HT-8
^{2}D, split line	F-2D.2	0.503 m x 0.17 mm i.d. methyl deactivated **OR** 1.24 m x 0.17 mm i.d. methyl deactivated
Tube to start of fill tube from valve	F2	S.S. 0.305 m x 0.25 mm i.d x 1/16" o.d.

restrictors. Agilent capillary column connection graphite ferrules were sanded down to make customised ferrules that fitted into available space.

For the GCxGC-FID analysis of Macquarie Island samples extracts (discussed in Chapters 5 and 6) the apparatus described in Table 5 was used. For these samples and associated standards 4 µL of extract was injected (1:16 split) at 340 °C. The carrier gas pressure was programmed to maintain a constant ^{1}D flow of 0.25 mL/min and a constant ^{2}D flow of 14.75 mL/min for the duration of the oven program. The oven temperature program was 40 °C (hold 4 min) 40 °C – 360 °C (7 °C /min), 360 °C (hold 3.5 min). FID detector temperature was 350 °C.

2.3.4 Other laboratory apparatus

Gas flow rates were determined with an 'Alltech Digital flow check-HR' from Grace Davidson (Epping, Victoria, Australia). Leaks at capillary unions were identified with an 'Alltech Helium Leak Detector', Grace Davidson. This leak detector was sensitive towards both hydrogen and helium leaks. Leaks checking took place prior to and following each sequence of samples analysed on the GC apparatus.

2.4 Numerical tools for GC-FID and GCxGC-FID data analysis

After data acquisition all GCxGC-FID and GC-MS data was exported and analysed with Matlab 2007a. This package was used to display all data, divide the GCxGC chromatograms into the bins and sum all the responses in the bins (as discussed in section 6.2). Binned data was passed to the package "R 2.12.0" (The R Project for statistical computing), for MDS analysis. MDS plotting parameters and the stress value were passed back to Matlab for subsequent plotting in Matlab.

2.4.1 GCxGC maximum searching algorithm.

A maxima searching algorithm was developed in Matlab 2007a. This algorithm examined data from the reshaped (rasterized) GCxGC-FID chromatogram and then "*performs*[s] *detection in both dimensions simultaneously*" [66]. This is suggested as the more powerful approach for GCxGC data [66], but is different to the 'blob' detection algorithm outlined of Reichenbach which is adapted from data processing literature. In the particular algorithm used in this thesis a rectangular portion of data is extracted about the particular GCxGC data point of interest. This rectangular extracted region is within ± x data points (inclusive) on the ^{2}D axis and within ± y modulations on the ^{1}D axis. Typically x = 5 or 10 while y = 1 or 2. When x = 5 and y = 1 the extracted region contained 11x3 data points (giving a window of ± 1 modulation and ± 25 ms in the second dimension).

A local maximum was identified if the point of interest was the maximum in the extracted region and greater than a preset absolute value (peak detection threshold). In addition the medians of the extracted modulations were calculated and the data point needed to exceed the lowest modulation median by another preset value – this component proved useful in rejecting small local maxima on a high UCM background originating from a highly degraded but high concentration fuel residue.

In this manner the peak detection algorithm looped through all the GCxGC data points in the GCxGC region to be examined for local maxima. All local maxima were tabulated by modulation number, ^{2}D data point number and FID response. In order to quickly examine particularly large GCxGC regions for local maxima the algorithm was speeded up. This was done by first determining if the particular data point being tested

was greater than the proceeding and following ^{2}D data point before the steps outlined above were implemented.

2.4.2 Calculation of GC-FID and GCxGC-FID method uncertainty

The error bars for the GC are calculated from a 1.5% relative uncertainty for calibration uncertainty and precision combined with a 100 ppm uncertainty from blank subtraction of the GC-FID blank from the sample file [106]. The error bars in GCxGC-FID are calculated from a 2.5% relative uncertainty for calibration uncertainty and precision combined with a 7 mg/kg uncertainty from blank subtraction of the GCxGC-FID blank from the sample file. In order to calculate the uncertainty arising from blank subtraction every soil sample extract and TPH standard (n = 120) was corrected with 3 different blank solvent GCxGC-FID analyses. From this a set of 88 TPH values was determined as well as 240 estimates of the variation in TPH value produced by using an alternative solvent blank for correction. The scatter in these 240 estimates corresponded to an uncertainty of 7 mg/kg for blank subtraction.

As a check of this value uncertainty value the average area difference caused by the 3 different blank corrections was calculated (and corresponded to 0.74×10^{6} area units). The median dry sample mass (10.1 g) and the median internal standard area (2.6×10^{6} area units) were also calculated. When these were combined with the calibration data a blank correction standard deviation is estimated at 4 mg/kg in broad agreement with the value form the earlier method.

2.4.3 Estimation of internal standard peak area and uncertainty

The estimation of internal standard peak area the associated uncertainty in this process was carried out with an automated algorithm. In this algorithm peak area was assessed in multiple manners, principally by summing the largest 3, 4 or 5 modulations. In addition to this the peak area in each modulation was estimated by summing the FID responses within ± 2.5, 3.0 and 3.5 multiples of the estimated peak standard deviation from the peak maximum. With this combination of 9 (i.e. 3 x 3) overall internal standard peak area assessments the median result from all 9 methods was taken as the most reliable estimate (as the median is relatively unaffected by a few particularly poor area estimates). The scatter of the other estimates about this median value was used to calculate an estimated uncertainty (as a standard deviation). When these 9 different routines gave an internal standard peak area standard deviation of greater than 2.5% the median value the sample was flagged as a potential outlier. When a potential outlier was identified manual inspection of the GCxGC-FID data was carried out to check if the assigned peak area and uncertainty was in agreement with manual peak integration. In all cases the manual peak area assessment was in agreement with the value returned by the automated algorithm (within ± 2 standard deviations).

2.5 GCxGC-FID calibration, sensitivity and baseline correction.

In order to meet regulatory approval the methodology limit of detection was closely investigated and the critical issue of baseline correction of the GCxGC-FID chromatograms (with higher volume and lower split injections into a low flow ^{1}D column) was examined [96,107,108]. From this a baseline correction approach was developed and validated. For the Macquarie Island series samples no post modulator split

was installed and thus removed an extra fitting, and concurrent dead volume, from the analyte flow path.

Analysis was performed on the differential flow modulator detailed in Table 6. The modulator split vent line was 1.24 m x 0.17 mm i.d. fused silica so that 16 mL/min of the modulator outlet flow entered the FID and 8 mL/min of the modulator outlet flow was vented. 3 µL of extract was injected (1:5 pulsed split) at 285 °C. After 2 minutes, the hydrogen carrier gas pressure was adjusted to maintain constant flow at 0.33 mL/min for the duration of the oven program. Total modulator flow was 24 mL/min over the entire analysis. The oven temperature program was started at 40 °C (held for 2 mins) and increased to 330 °C at 10 °C/min with a total run time of 32 min. FID temperature was 340 °C and operated at 200 Hz. The external valve controlling the modulation switched flows every 3.000 s.

Diesel standards were prepared with the following concentrations of diesel;0 15, 25, 50, 150 and 500 mg/kg based on a 10 g soil sample extracted with the procedures outlined in section 2.2.2. These were spiked with the GCxGC-Internal standard mix (section 2.1.2) so that the internal standard mix was diluted by a factor of 400. An additional set of calibration standards were prepared by diluting the GCxGC-Internal standard mix diluted by the following dilution factors; 400, 800, 1600 and 2000. Prior to the analysis sequence 6 hexane blanks were injected followed by the diluted GCxGC Internal standards and the diesel standards. A hexane blank was analysed after 1 or 2 standards were analysed. All the standards were analysed twice with the duplicate injections space throughout the analysis sequence. The 0 mg/kg standard (i.e. internal standard only) was analysed 8 times throughout the sequence. A given vial containing the

hexane blank was analysed a maximum of 5 times before a new hexane blank was used in the sequence.

2.5.1 Baseline correction.

In order to correct the GCxGC baseline a modulation by modulation approach was used. This was done on the basis that the shape of the particular chromatogram would be maintained from sample to blank but, due to instrument variations, it would be offset and scaled (to some extent). The process can be seen in the following figures. In Figure 3 direct subtraction is implemented while, in Figure 4, scaling and shifting is implemented as described in the caption. The result is a substantial improvement such that no difference can be seen between the red overlay blank chromatogram and the underlying blue sample chromatogram. The residuals in Figure 4 do, however, show that the corrected FID response does not fully return to zero until approximately 120 data points (0.6 s) after the maximum in the blank.

The best approach is shown in Figure 5 with the scaling and shifting targeted towards minimising bias in the regions ≥ 30 data points (150 ms) from the blank maxima. In this a minimisation approach the value to be minimised is the sum of the squared residuals for the region of the modulation free of both eluting analytes and tailing injection solvent. In Figure 5 the entire region outside the hexane maxima has been corrected so that it is within ± 10 FID units of zero. This is very close to the FID noise floor measured at ± 7.7 FID units (measured over 10000 data points in the absence of any

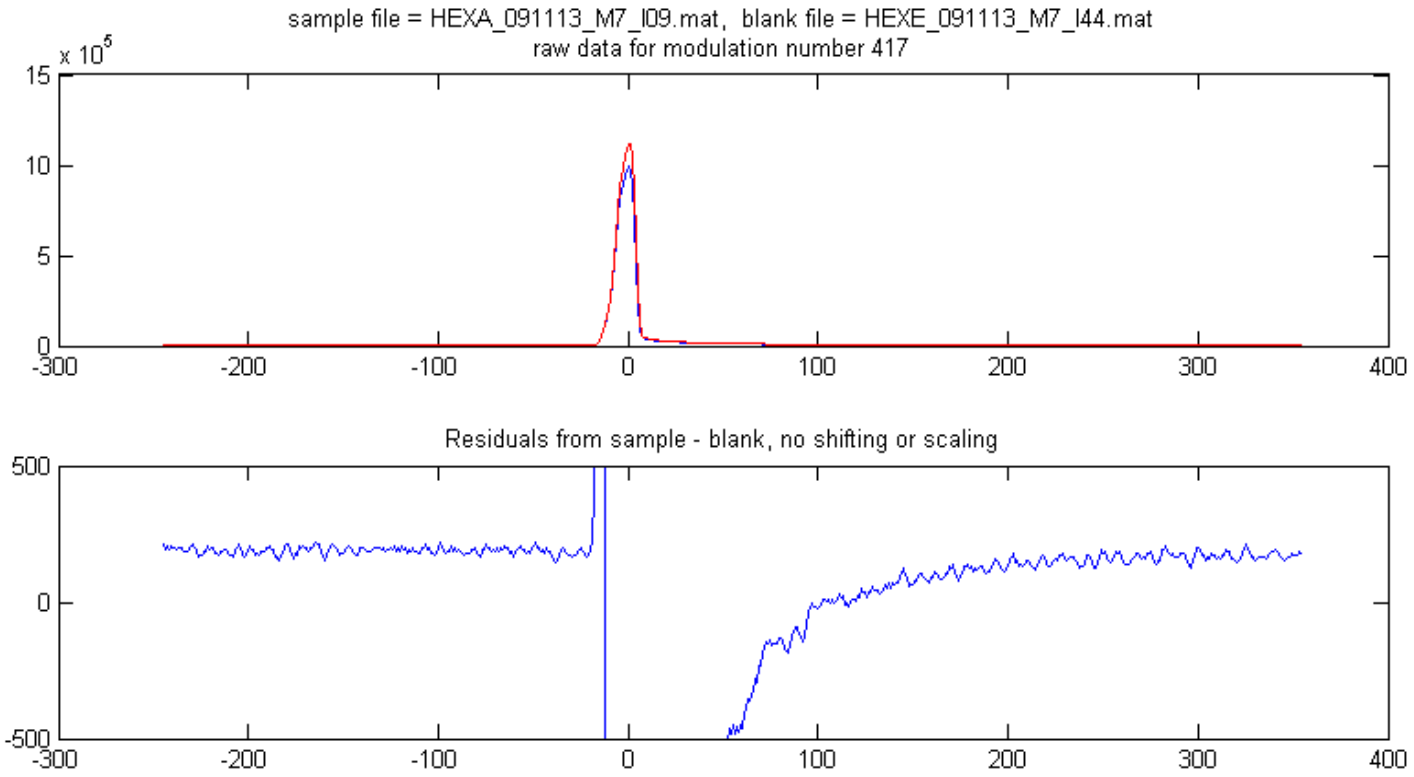

Figure 3. Direct blank subtraction (of modulation 417). The blank used for subtraction is the 44th injection of the sequence while the file it is subtracted from is the hexane injection at position 9 in the analysis sequence. The 35 injections, in this case, between the sample and blank is to test the correction methods after an extended period of instrument drift. During analysis of site samples a blank is within 5 (or less) injections of any given sample. X-axis is scaled in data points from the modulation maximum, Y-axis is scaled in FID detector units.

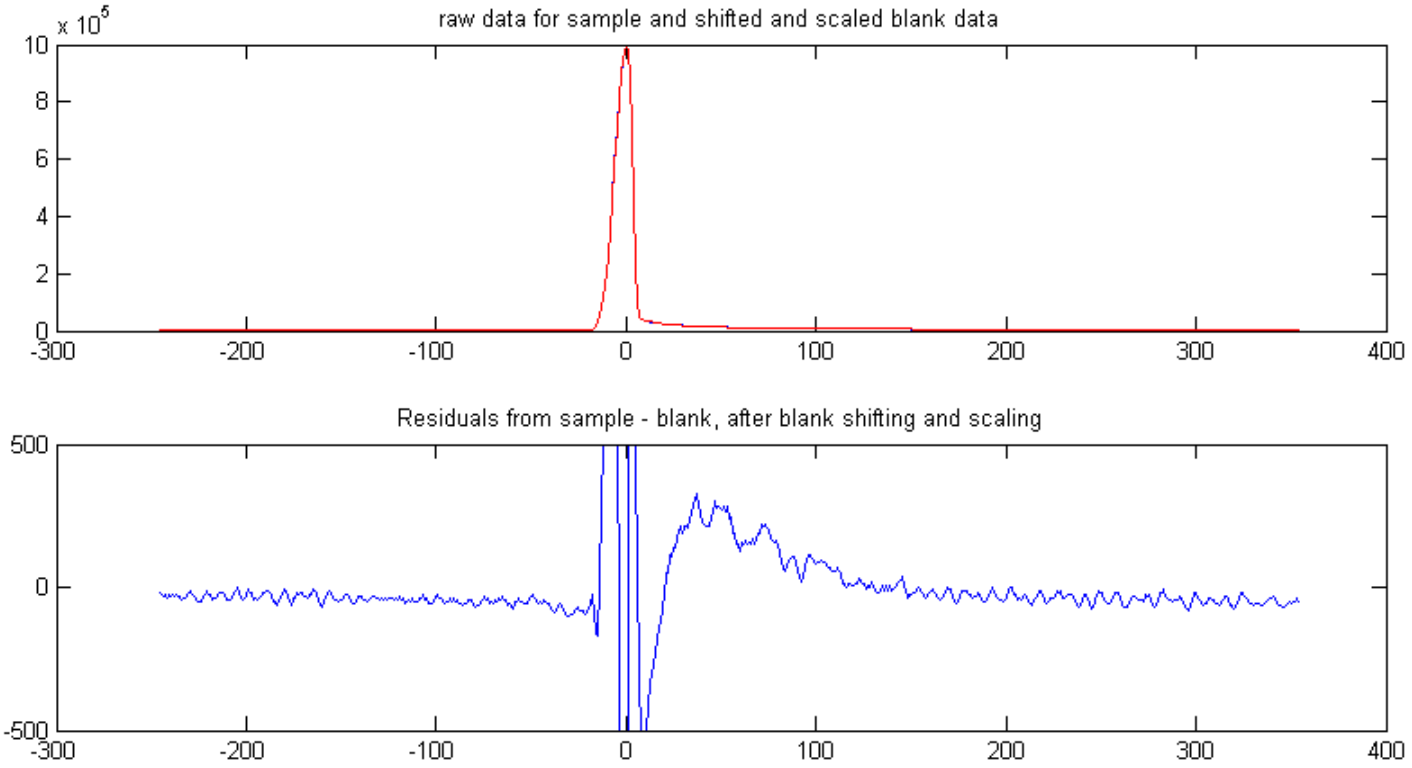

Figure 4. Blank subtraction (of modulation 417) after the particular blank modulation in is aligned and scaled so that the maxima coincide and the median values are also equal. Other plotting features kept as the previous figure.

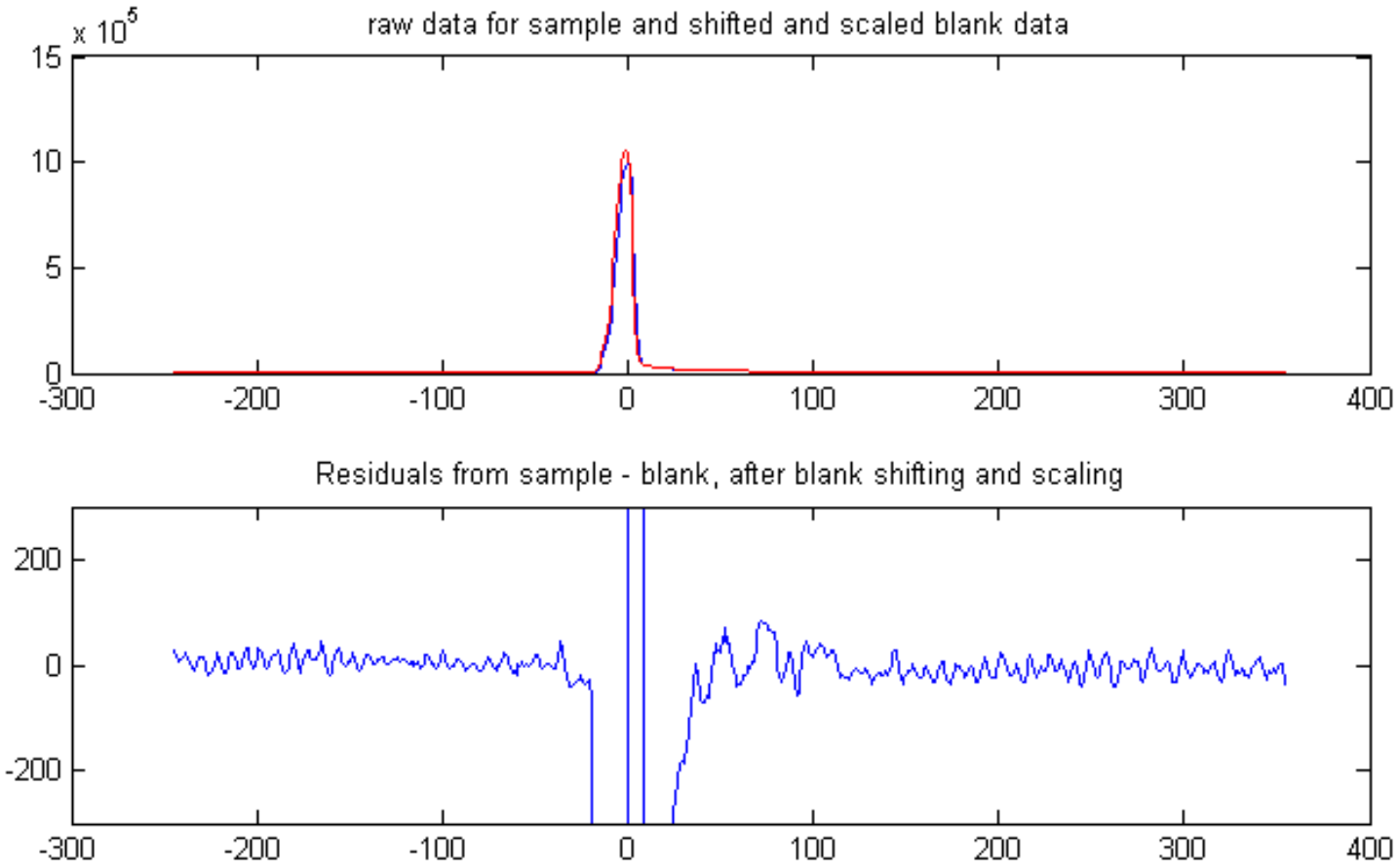

Figure 5. Blank subtraction (of modulation 417) after the particular blank modulation in is aligned and scaled so that the sum of the squared residuals is minimised. The sum of the squared residuals was restricted to the 540 data points ≥30 data points from the modulation maxima. Other plotting features are the same as the 2 previous figures except the y scale of the residuals has been expanded by x2.

eluting material and without valve switching effects).

2.5.2 Diesel limit of detection.

Once the GCxGC baseline correction methodologies (shown in Figure 4 and Figure 5) were established with blank to blank subtractions over the analysis sequence the algorithm was changed for diesel samples standards (and for the soil extracts from the TPH contaminated site). For these samples it is necessary to exclude the analyte elution region as well as the data points about the hexane solvent maximum from the minimisation approach. In the case of the Macquarie Island samples with concurrent silane contamination , the second blank correction method shown in Figure 4 had to be implemented with data points after the last ^{2}D eluting compounds used to assess the median of the modulation.

In the case of the diesel standards examined here the method used in Figure 5 could be implemented with a least squares minimisation over 100 to 300 data points. The exact number of data points used in the minimisation depended on the retention time of the most retained aromatics for that modulation. The exceptional results from this baseline correction method is shown in Figure 6 and Table 7. Using just the 8 repeats of the 0 ppm standard (i.e. GCxGC internal standards only), Student's t-test with 7 degrees of freedom and a 99.9% confidence interval (two tailed) gives a method detection limit of 5.4* σ_{random} = 2.7 ppm for diesel. This exceptionally low limit of detection (~3 mg/kg of diesel) and excellent regression value (0.9996) over all the standards validates the baseline correction approach. This method requires GCxGC-FID regions reliably free of analytes before and after the main diesel elution region as well as well stabilised apparatus. The alternative approach of using the tailing solvent maxima and the GCxGC

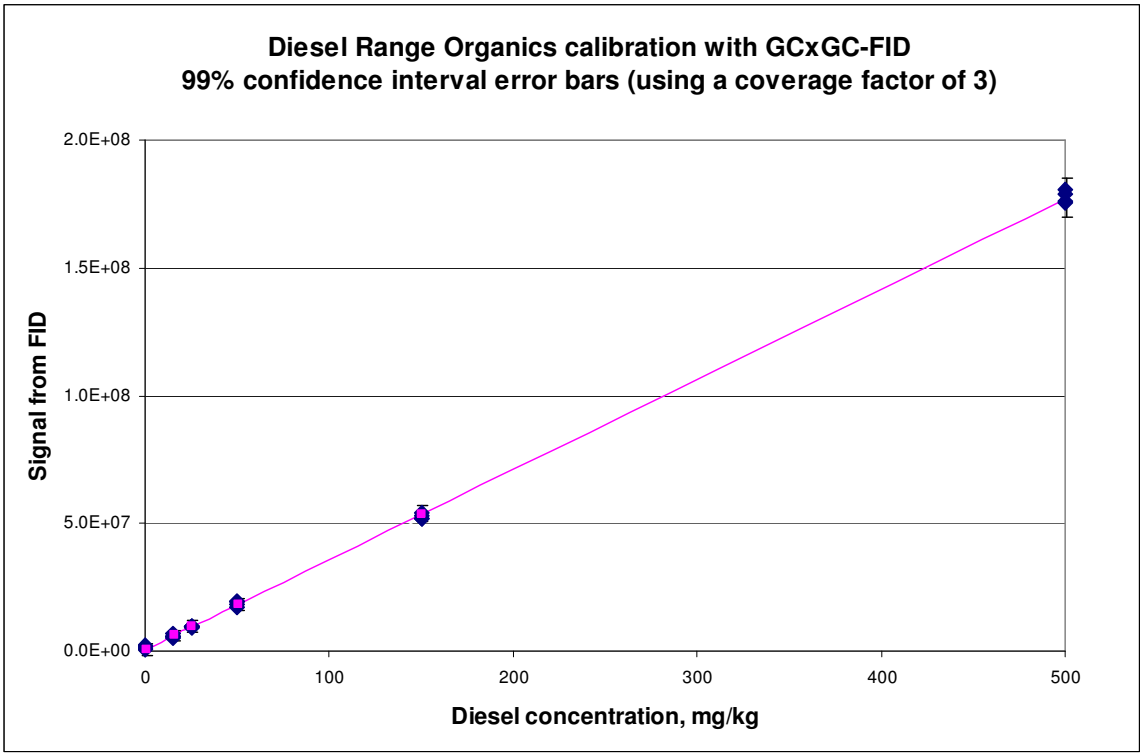

Figure 6. Diesel calibration from 0-500 mg/kg. R^2 value of regression =0.9996

Table 7. Calibration levels with a summary of scatter in calculated area for the separate calibration levels. Data models with an overall method standard deviation of 0.50 mg/kg combined with a 2.0% relative error at higher concentrations. This relative error is in line with standards and blanks from the Macquarie Island extracts while the lower limit of detection is improved.

Calibration level concentration	Number of separate GC injections	Standard deviation, σ, of FID areas from these separate injections	mg/kg equivalent from the **standard deviation** of areas at each concentration level
0	8	56200	± 0.50
15	2	68600	± 0.61
25	2	20500	± 0.18
50	2	83800	± 0.75
150	2	41600	± 0.37
500	2	774000	± 6.9

elution region after the most retained compounds elute from the ^{2}D column is also an excellent strategy and useable when the region prior to the diesel analytes is contaminate with, for example, silanes. By shifting and scaling the blank modulation with a least squares minimisation approach (over all the data points known not to contain eluting material) the regions normally considered wasted empty space can be used to perform a critical step in GCxGC-FID quantitation.

2.5.3 Calibration

Calibration was based on the same calibration standards that were used for conventional GC calibration at Macquarie Island [106]. This set of calibration standards were prepared gravimetrically and were equivalent to 10 g soil samples with TPH values of 3000, 6000 and 12000 mg/kg [96,107]. The GCxGC results from this series (with a gradient of 0.0759) are shown in Figure 7. An alternate series of calibration standards, the "Hobart series" was prepared with the same set of target concentrations. Agreement between the Macquarie Island series and the Hobart series is excellent.

As a separate check of the instrument response, the expected gradient was calculated on the basis of % carbon and hydrogen in the internal standard and in the fuel. This is appropriate for FID detectors since the FID response can be estimated very well from the C and H elemental composition of the compound entering the flame (except with classes of compounds, such as perfluoro-hydrocarbons, that are essentially impervious to the FID flame) [45,47]. Using a nominal fuel composition of $C_{12}H_{23}$ and assuming the bromine in 1-bromoeicosane has no suppression (or enhancement) effect on the FID signal, the expected gradient is 0.0772, shown in Figure 7 as the

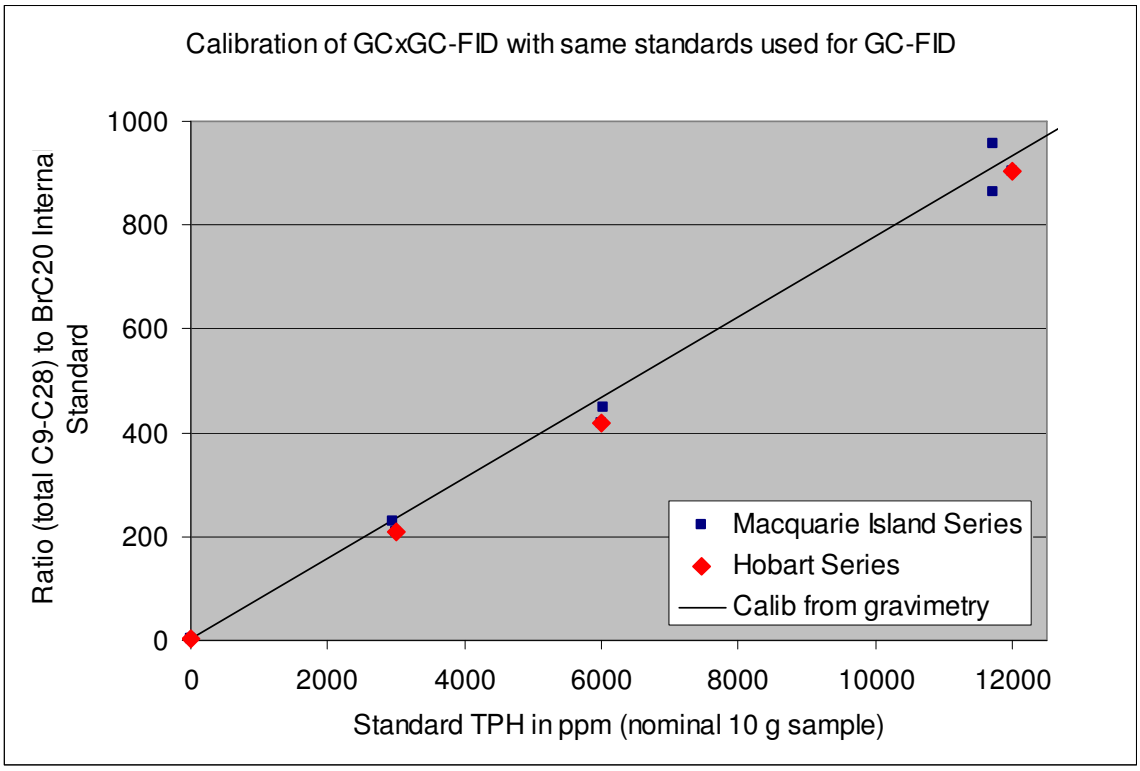

Figure 7. TPH calibration based on different standards. The calibration from gravimetry line is calculated from % carbon in the different components and standard preparation masses.

"Calibration from Gravimetry" line. This expected gradient is slightly susceptible to the assumed composition of diesel fuel. The observed gradient (from the "Macquarie Island Series" of standards) has a relative difference of 1.7 % to this calculated gradient.

The standard uncertainty associated with this calibration gradient (0.0759) is less than 5% since the largest deviation from the expected gradient is 5%. It must be kept in mind that this value also includes an uncertainty component arising from instrument precision between repeat injections and uncertainties from standard preparation.

3 Design considerations for pulsed-flow comprehensive two-dimensional gas chromatography: dynamic flow model approach. J. Chromatogr. Sci. 48 (2010) 245-250

3.1 Introduction

Pulsed flow modulation (PFM) permits GC×GC without recourse to liquid cryogen. A PFM-GC×GC modulation interface can be constructed from readily available capillary connection fittings, a three-way gas switching valve and a suitable timing device to trigger valve actuation [54]. Despite the physical construction of the PFM interface being apparently facile, selection of operating parameters and column dimensions that lead to optimum performance is not necessarily straightforward. PFM-GC×GC has been touted as a low-cost alternative to cryogenic modulation, but one obvious advantage of employing a liquid cryogen to perform GC×GC modulation is that the modulation period can be readily changed to optimise a GC×GC separation. For instance, the LMCS cryogenic modulation system pioneered by Marriott's group has been used without any system modification as fast as 1.0 s for fast GC×GC [109] and up to 7.5 s to accommodate longer second dimension separation times in *enantio*-GC×GC [110]. This flexibility is a common feature in all cryogenic modulation systems. Conversely, a survey

of the literature reveals that the range of modulation conditions utilised with PFM-GC×GC is limited. A summary of these operating conditions is provided in Table 8.

Notwithstanding the demonstrable utility of the PFM-GC×GC modulation device developed by Seeley *et al*. [54,111-114], it is highly likely that extending the types of samples amenable to analysis will require modification of the limited range of conditions hitherto employed. In particular, being able to increase the modulation period is a desirable attribute, which reduces the deleterious effects of wrap-around. Of course other measures such as temperature program and choice of stationary phase are equally important in optimising a GCxGC separation but there is considerable evidence in the literature that it is important to be able to easily change the modulation period. While fuel analysis is often reported using 1.5 s between successive injections into the second dimension separation column [54,90,112,115], a 6 s modulation period is more favourable for analysis of strongly retained analytes such as fatty acid methyl esters [116]. In a more extreme case, Kaal *et al*. used a 10 s modulation period in their GC×GC-MS method for the analysis of hydrolysed sulfonated kraft lignins [117].

Unfortunately changing the modulation period in a PFM-GC×GC system is not as straightforward as the cryogenic modulator example above. Amirav and co-workers have addressed this problem by using a larger volume sample loop, which is partially filled during the "fill time" phase of modulation, demonstrating an extended modulation period of 4 s [90,115]. Currently any modification to a PFM-GC×GC system relies on an iterative re-optimisation of the pneumatic conditions, timing parameters, and the capillary dimensions used to construct the system. This chapter introduces four important developments that improve upon this approach: i) a numerical model that successfully

Table 8. Summary of parameters used for PFM-GC×GC from the general literature. * not shown in reference

sample		^1D column	^2D column(s)	Fill time	Flush time	Sample loop	^1F	^2F	ref
		L, *i.d.*	*L*, *i.d.*			*L*, *i.d.*	sccm	sccm	
1	unleaded gasoline	15 m, 0.25 mm	5 m 0.25 mm 5 m 0.25 mm	1.4 s	0.1 s	0.15m, 0.45 mm	1	20	[54]
2	biodiesel blends	22 m, 0.25 mm	5 m 0.25 mm 5 m 0.25 mm	1.4 s	0.1 s	0.15m, 0.45 mm	1	20	[111]
3	diesel fuel	30 m, 0.25 mm	5 m 0.25 mm 5 m 0.25 mm	1.4 s	0.1 s	0.15m, 0.45 mm	1	18	[112]
4	organic compounds	30 m, 0.25 mm	5 m 0.25 mm 5 m 0.25 mm	1.4 s	0.1 s	0.15m, 0.45 mm	1	18	[112]
5	gasoline	15 m, 0.25 mm	4 m, 0.25 mm	3.7 s	0.3 s	0.5 m, 0.53 mm	0.6	20	[90]
6	gasoline	15 m, 0.25 mm	4 m, 0.25 mm	3.7 s	0.3 s	0.5 m, 0.53 mm	0.7	25	[90]
7	E85 calibration set	40 m, 0.18 mm	5 m 0.25 mm 5 m 0.25 mm	1.4 s	0.1 s	0.15m, 0.45 mm	0.75	15	[113]
8	E85 gasoline	40 m, 0.18 mm	5 m 0.25 mm 5 m 0.25 mm	1.4 s	0.1 s	0.15m, 0.45 mm	0.75	15	[113]
9	diazinon and permethrin in coriander	15 m, 0.25 mm	2.2 m, 0.32 mm	3.7 s	0.3 s	0.5 m, 0.53 mm	*	25	[115]
10	pentane	15 m, 0.25 mm	2.2 m, 0.32 mm	3.7 s	0.3 s	0.5 m, 0.53 mm	0.3	33	[115]
11	pentane	15 m, 0.25 mm	2.2 m, 0.32 mm	3.7 s	0.3 s	0.5 m, 0.53 mm	1	13	[115]
12	organic compounds	40 m, 0.18 mm	5 m 0.25 mm 5 m 0.25 mm	1.4 s	0.1 s	0.15m, 0.45 mm	1	15	[114]

describes how carrier gas flows vary during the modulation cycle throughout the first and second dimension separation columns and the entire set of capillaries used to construct the PFM-GC×GC modulator, ii) use of the model to provide a detailed understanding of the effects on modulation of changing modulation timing and / or carrier gas flow rates iii) the introduction of a symmetrical PFM-GC×GC modulator design to smooth carrier gas flow rate at the outlet of the second dimension separation column(s), iv) demonstration that the inclusion of restrictor tubing in the first dimension adds stability and flexibility to a PFM-GC×GC modulator.

3.2 Theory

The dynamic flow model introduced here tracks the carrier gas flow through a PFM-GC×GC column ensemble, in particular the carrier gas flow is modelled in small time steps through all separation columns, and through the modulator sample loop, during the modulation cycle. A dynamic model is required because the first dimension separation column and the modulator sample loop of the PFM-GC×GC column ensemble have oscillating end pressure during modulation. Figure 8 illustrates a PFM-GC×GC system. In the "load" state, the second dimension carrier gas is delivered *via* the tubing labelled "*c*" and the first dimension column effluent is loaded into the modulator sample loop (*b*). By actuating the three-way valve, the second dimension carrier gas is delivered *via* the tubing labelled "*a*", into '"b" and injects the contents of the modulator sample loop ("b") into the second dimension column and any split transfer line. In a properly functioning modulator, flow from the first dimension column is stopped during this brief "flush" phase of the modulation cycle. In this case a system that employs a cross-union

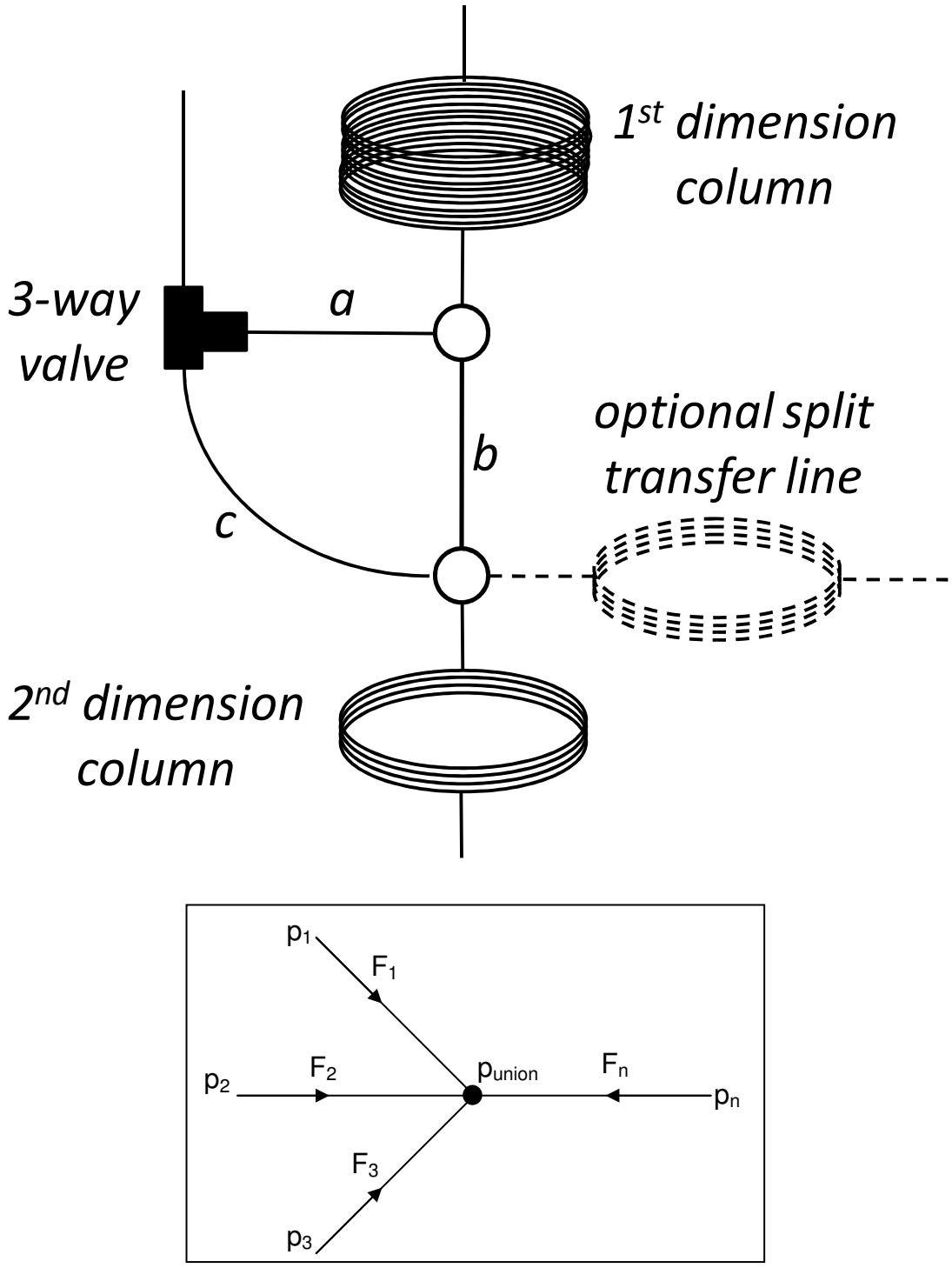

Figure 8. (upper) Typical configuration of a PFM-GC×GC modulator showing the first and second dimension columns, the optional split transfer line, the modulator sample loop (*b*) and the two critical pieces of capillary (*a*, *c*) that connect the three-way valve to the modulator sample loop. (lower) Schematic showing gas flows (F_1 to F_n) into a union with n outlets and pressures throughout the union (p_1 to p_n and p_{union})

connecting the end of the modulator sample loop to the inlet of the second dimension separation column is illustrated. The split transfer line is drawn with a broken line to illustrate that this component is optional. An alternative arrangement employs a tee-union in place of the cross-union and the split transfer line is not installed. The equations necessary to describe the flow through a typical GC×GC column set (i.e. using thermal modulation with two columns joined in series) are described in detail elsewhere [118-120]. In order to model the flow during valve actuation in a PFM-GC×GC system, additional calculations are required to determine the pressure (p_{union}) at the unions in the modulator, so that flow can be correctly apportioned. A union can be considered as a point with *n* inlets. When each arm of a union is considered to be an inlet, we must use +ve or –ve signs to indicate if the *direction* of the gas flow is *towards* the union or *away* from the union respectively. Under steady-state conditions the volume of gas flowing towards the union is equal to the volume of gas flowing away from the union, so:

$$F_1 + F_2 + \ldots + F_n = 0$$

where F is volumetric flow rate and the subscripts indicate particular arms of the union as shown in Figure 8 (lower). For a tee-union n = 3 and n = 4 for a cross-union. It follows that:

$$F_1 + F_2 + \ldots + F_n = K_1(p^2_{union} - p^2_1) + K_2(p^2_{union} - p^2_2) + \ldots + K_n(p^2_{union} - p^2_n) = 0$$

Equation 1. Formula describing steady state gas flow into a union. Terms are described in the text and in Figure 8.

where $K_n = \frac{\pi r_n^4}{16 p_{ref} \eta L_n}$ (and where L_n is the standardised length (according to [118]) of the capillary tubing connected to the union, and r_n is the standardised radius (according to

[118]) of the tubing connected to the union, p_{ref} is a reference pressure, and η is dynamic gas viscosity) and $p_{1\text{-}n}$ are the connecting tubing inlet pressures (*keeping in mind that the union is assumed to be the outlet*). Rearrangement of Equation 1 leads to:

$$p_{union} = \frac{\sum_{j=1}^{n} (K_j p_j^2)}{\sum_{j=1}^{n} K_j}$$

Equation 2. Formula for determining the steady state gas pressure at a union. Terms are described in the text.

Using Equation 2, p_{union} can be determined for a union of n outlets, where $n \geq 2$.

3.3 Dynamic Flow Model

The dynamic flow model computer program uses a finite difference method (explicit method) to calculate gas flow changes induced by repeatedly switching the external 3-way valve in the PFM-GC×GC system. Figure 9 outlines the sequence of calculations. A small set of input data are required, which include the temperature program details and carrier gas type as well as dimensions of the capillary tubing used to construct the PFM-GC×GC device. This capillary tubing is numerically divided into portions of length 0.1 m to 2 m with the smaller 0.1 m length segments clustered around the modulator tubes (a, b and c shown in Figure 8), the outlet of the first dimension column, the inlet of the second dimension column and the inlet of the split transfer line. Hydrogen carrier gas was used for all examples shown in this manuscript. The first- and second-dimension carrier gas flow rates are also required inputs. The program calculates the steady-state pressures $p_1 - p_n$ in the "modulator sample loop fill position" and estimates the number of moles of carrier gas present in each segment of capillary at

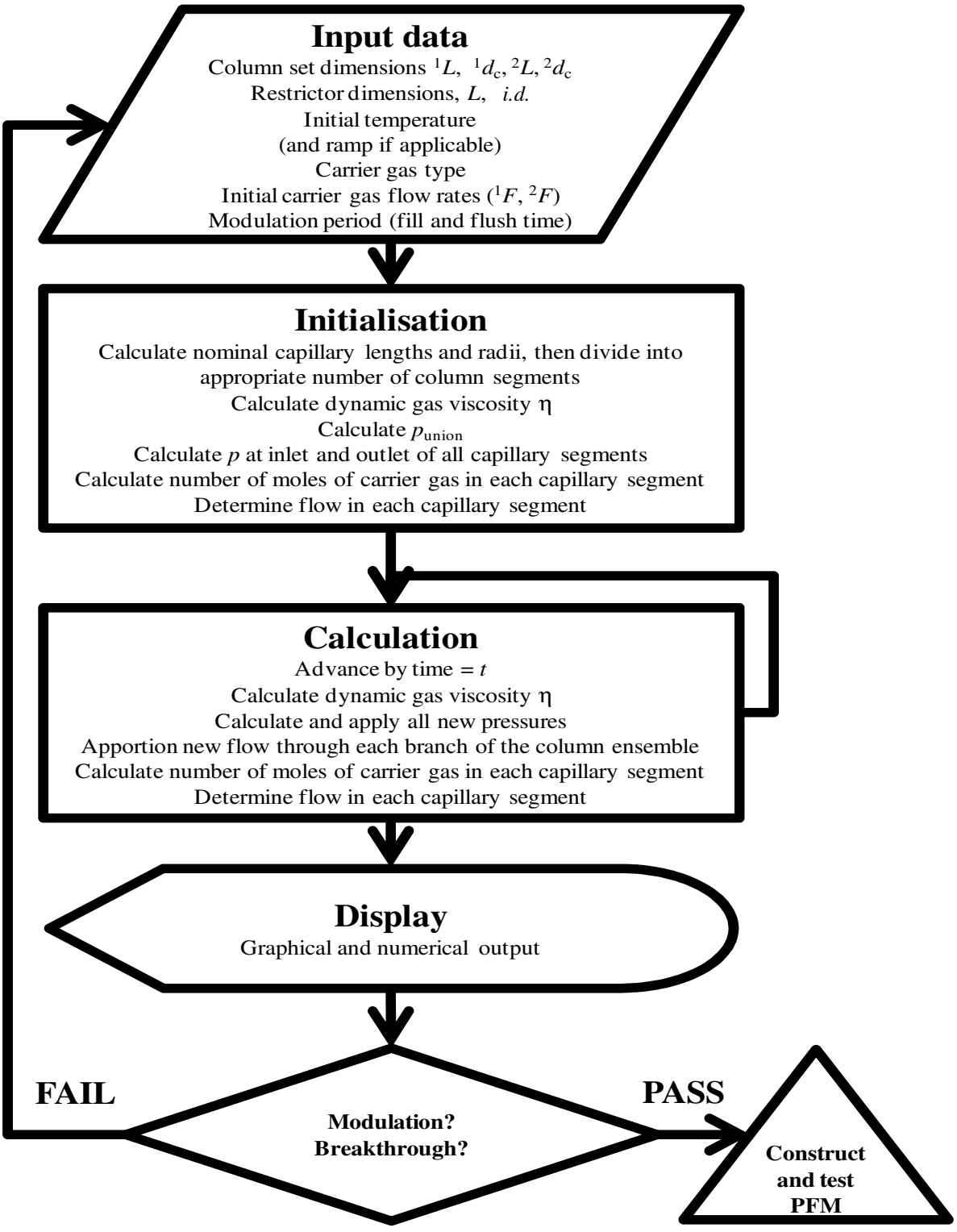

Figure 9. Flowchart of the operations performed by the dynamic flow model computer program.

time $t = 0$. Thus the initial flow at a reference pressure in each segment of the column ensemble is calculated. The calculated flow rate in each segment is assumed to remain constant for a small (< 0.001 s) time step t which permits the number of moles of gas leaving each segment during the time step t to be calculated.

The program recognises that the number of moles of carrier gas exiting one column segment during the time step equals the number of moles entering the next column segment in the column ensemble during the same time step. A new set of p_o values for every connected column segment(s) is calculated during each calculation cycle and a sequence of repetitive calculations is performed. Valve actuation is modelled by changing the allowable boundary pneumatic conditions. It is usually sufficient to model only a few modulation cycles, which are represented by *ca.* 10^4 individual time steps, and it is also appropriate to check that the conditions are suitable at the start and end of the temperature program as well as one point at the middle oven temperature. If the criteria for modulation are met at these three points, by interpolation between these points, we assume that all other conditions are appropriate.

3.4 Results and Discussion

The preliminary work leading up to the present study essentially sought to reproduce published modulator configurations and investigate the potential to use different modulation periods. However, large detector signal fluctuations were observed when the external three-way valve was actuated. These findings are consistent with comments made by Poliak *et al*. [115] who revealed that the second dimension carrier gas flow rate using their PFM-GC×GC setup varies between 20 mL/min and 25 mL/min due to the difference in flow impedance in the transfer lines connecting the three-way valve to

the modulator sample loop. This systematic and periodic flow rate perturbation will lead to some FID detector signal instability. A plot of the calculated second dimension column outlet flow (F_{co}) as a function of time over four successive 3 s modulations (2.7 s fill; 0.3 s flush) using two modulation devices is shown in Figure 10. This flow is just the *F*co value over time from an entire PFM device set of calculations using the dynamic flow model of the entire column set shown in Figure 8.

Figure 10A tracks the second dimension column outlet flow in a PFM-GC×GC device with a 0.5 m × 0.45 mm i.d. modulator sample loop "b". This is coupled with a 0.35 m x 0.25mm i.d. capillary tube "a" and a 0.65 m × 0.25 mm i.d. length of tubing designated "c" (see Figure 8). While the valve is in the "fill" position, a constant flow rate of 12.5 mL/min flows through the second dimension separation column. When the three-way valve is actuated (and held in this position for 0.3 s), the flow impedance between the valve and the second dimension column outlet is lower and the second dimension column outlet flow rapidly increases by *ca.* 7%. When the valve returns to the original position, the second dimension column outlet flow returns exponentially to 12.5 mL/min, and returns to the 'normal' second dimension column outlet flow rate after *ca*. 1 s. These calculated flows represent the maximum flow surge that would be produced by such a configuration and that in practice flow impedance within the valve might minimise the magnitude of the surge. It is also rather intuitive that a symmetric flow path modulator design could have potential in flattening the baseline perturbation. Briefly, in the symmetric flow path design investigated here, the modulator sample loop, and the two connection lines are constructed from the same internal diameter fused silica capillary tubing. The lengths (*L*) of tubing (shown in Figure 8) must satisfy the criterion

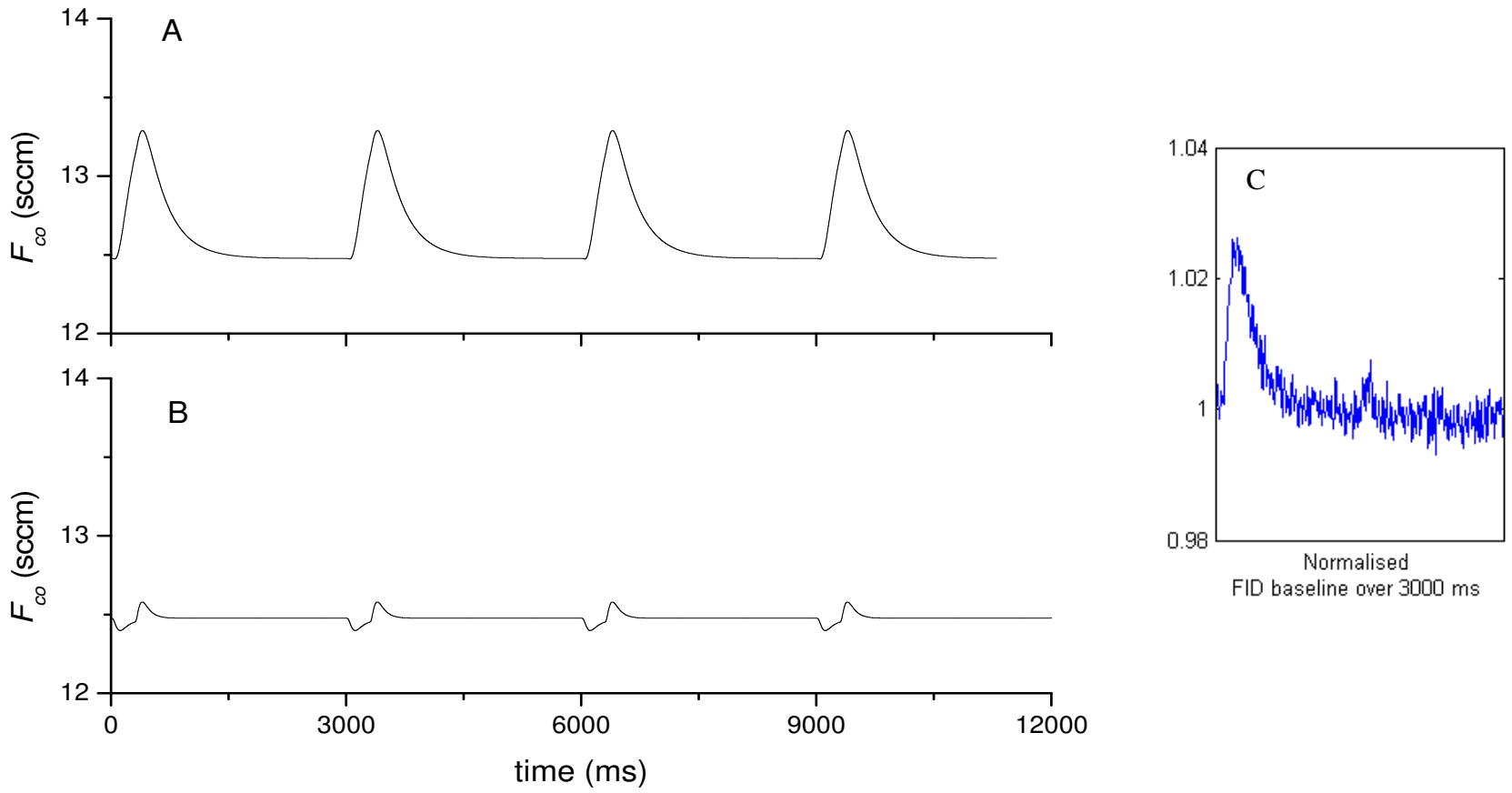

Figure 10. Comparison of the simulated second dimension column outlet flow in a typical PFM-GC×GC design (A) a simulated symmetric flow path design (B) and the normalised FID baseline for a operating symmetric flow path design with 3.0 s modulation (C). Conditions for (C) are described in experimental section and the caption of Table 9.

$L_a + L_b = L_c$. This way the second dimension column head pressure perturbation is minimised. Figure 10B highlights the advantage of using a symmetric flow path design, by tracking the second dimension column outlet flow in a symmetric flow path PFM-GC×GC device, which uses 0.25 mm i.d. tubing throughout. The lengths of the *a*, *b*, and *c* tubing were 0.35 m, 0.30 m and 0.65 m respectively. While the valve is in the fill position, a constant flow rate of 12.5 mL/min flows through the second dimension separation column. Figure 10C shows the experimentally obtained FID baseline for a constructed symmetric flow path system. In the constructed system outflow from dead volumes within the valve lead to additional gas being delivered to the FID compared to the simulated symmetric flow system shown in Figure 10B. For this reason the timing and shape of the observed FID perturbation is very similar to the calculated shape shown in Figure 10A (a typical PFM-GCxGC system with additional gas delivered during modulation) while the magnitude of the FID signal change is closer to the changes calculated for ideal flow in a symmetric flow path system with no dead volumes (Figure 10B).

Compared to the former scenario, there is substantial flow impedance in the modulator sample loop itself, so when the valve switches to the flush position for 0.3 s, the second dimension column outlet flow dips slightly while the carrier gas in this arm of the modulator is compressed and the column pressure is reached. There is a slight perturbation in the second dimension column outlet flow when the valve returns to the fill position, but notably, the magnitude of flow perturbations (both in the negative and positive directions) is less than 1% throughout the entire modulation process. The duration of this flow perturbation is also substantially shorter when a symmetric flow

path design is employed, resulting in a more stable baseline in the two-dimensional separation space. The performance of the symmetric flow path design is highly satisfactory and all results presented in this manuscript were obtained using a symmetric flow path device.

Finely tuned pneumatic conditions are needed for a PFM-GC×GC device to function correctly. To achieve proper modulation the flow direction of the carrier gas needs to periodically and systematically change at the end of the first dimension column during a GC×GC separation. The modulator sample loop has a fixed volume, so increasing modulation period can lead to breakthrough. Increasing the modulator sample loop volume is one way to address this breakthrough problem [90,115], but it will take longer to empty the modulator sample loop and this requires the three-way valve be held in the flush position for a longer time. Increasing the flush time requires a higher pressure at the outlet of the first dimension column to achieve the necessary stop flow state. Both longer pulse times, and higher pulse pressures lead to greater flow perturbation in the first dimension column. An alternative way to alleviate this breakthrough is to reduce the first dimension column flow rate but this option needs to be used with caution because the pressure pulse caused by actuating the valve can again easily cause unnecessarily high flow perturbation in the first dimension column. Iterative optimisation of these parameters is not desirable for two reasons, namely i) the time required to construct and test the PFM-GC×GC device is potentially excessive, and ii) the final parameters may not be truly optimal.

The dynamic flow model program correctly apportions the flow of carrier gas through each arm of the tee- or cross-union and then quickly and unambiguously shows if

the conditions are suitable for PFM-GC×GC. A typical output of the dynamic flow model program is shown in Figure 11. Figure 11 is a contour plot of flow (as sccm) along the length of the primary column (x-axis) over a period of time (y-axis). In this figure, two modulations are shown with backflow towards injector set as negative (and white in colour) and normal flow towards the modulator as shown in the coloured contours. Importantly EVERY piece of capillary tubing (i.e. primary column, secondary column, optional split transfer line AND the modulator tubes a, b and c from Figure 8) has a similar output of calculated flows across length and time during the modulation process. Investigation of the flow profile for each capillary will show how this flow responds to valve actuation.

A narrow internal diameter retention gap (before the first dimension separation column) is included in this column set. We have determined that this retention gap is often important because it increases the required injector pressure. In scenarios in which low first dimension carrier gas flow rates are used (and therefore which have a small pressure drop in the first dimension column), this additional inlet pressure provides a greater difference between the first and second dimension inlet pressures (measured at the electronic pressure controller) and improves modulator stability. It is also difficult to accurately control the carrier gas flow rate in a column with a small pressure drop when there is a fluctuating column outlet pressure. The *x*-axis in Figure 11 represents distance along the first dimension column assembly, and the direction and magnitude of the carrier gas flow during the modulation cycles (represented by the *y*-time axis) is represented by the colour contours. A 3 s modulation period (2.9 s fill time, 0.1 s flush time) is chosen for this illustration with a first dimension column flow rate of 0.3 mL/min and a second

dimension flow rate of 12.5 mL/min (plus 12.5 mL/min in the split transfer line). An ideal modulator would stop the flow from the first dimension column assembly for 0.1 s and the flow rate would rapidly return to the original flow rate of 0.3 mL/min. Here, it is apparent the outlet pressure is excessive and the direction of flow in the first dimension column assembly is reversed up to 4 m along the column. The original flow rate of 0.3 mL/min is not regained before the valve actuates to perform the next modulation. This extreme flow perturbation cannot be alleviated by making changes to the carrier gas flow rate(s) alone.

Having performed many calculations with the dynamic flow model we have determined that placing a narrow-internal diameter restrictor at the end of the first dimension column is highly beneficial. Figure 12 shows the dynamic flow model output from a PFM-GC×GC device which employs the same modulator design, modulation timing parameters and carrier gas flow rates as those already discussed in Figure 11, with the exception that the last 0.5 m of the first dimension column assembly is changed from 0.25 mm I.D. to a 0.5 m × 0.10 mm i.d. flow restrictor. Although the flow slows in the last 3 m of the first dimension column assembly, the flow is only reversed (stopped) in the restrictor tubing. The original flow rate of 0.3 mL/min is rapidly regained following the modulation pulse. An additional benefit of the restriction is a substantial amount of the pressure drop in the first dimension column assembly is in this restrictor, so it is possible to change the length of the first dimension separation column without having any impact on the modulator performance.

The addition of the restrictor at the end of the first dimension column was a critical breakthrough in this investigation, because extension of this concept eliminates the

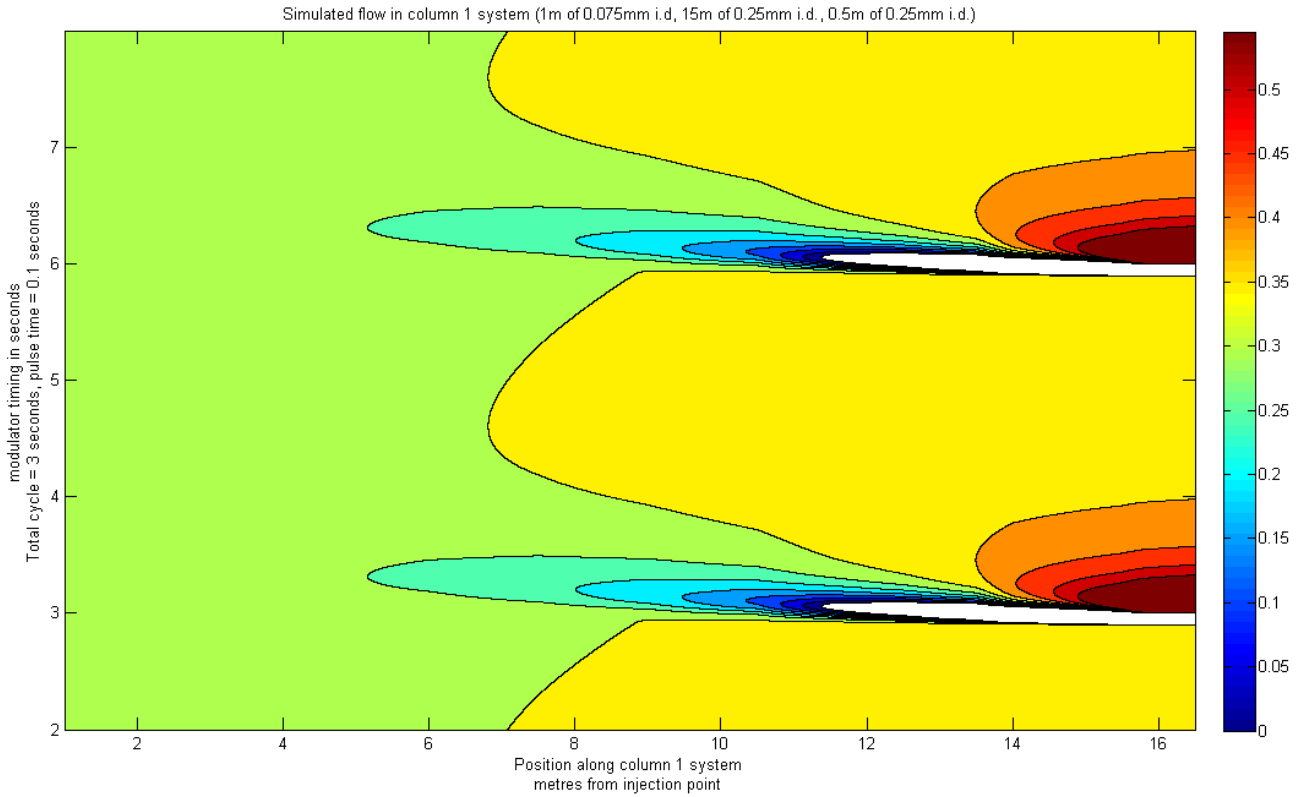

Figure 11. Typical output from the dynamic flow model program illustrating the flow perturbation in the first dimension column assembly during two full 3.0 s modulation cycles. The program is also able to report the flow profile at any distinct position along the first dimension column assembly.

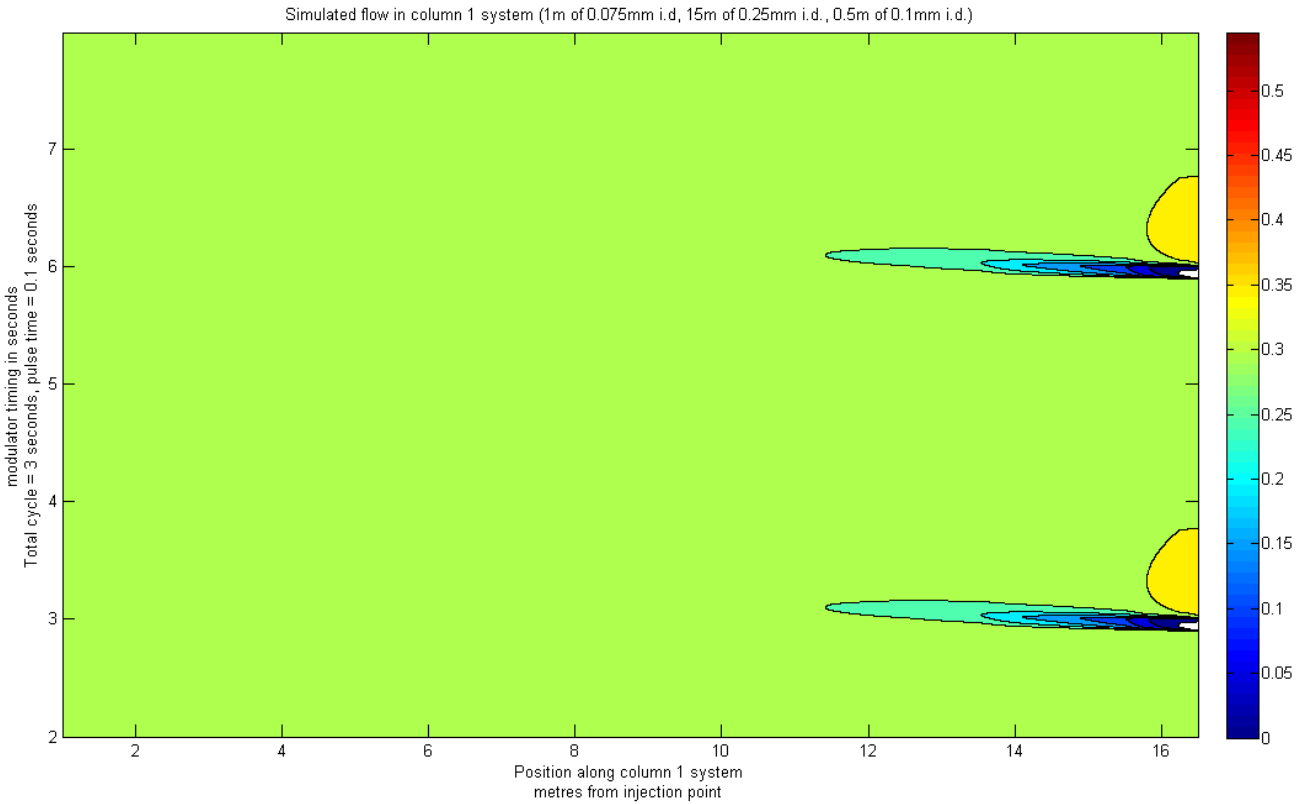

Figure 12. Typical output from the dynamic flow model program illustrating the flow perturbation in the first dimension column assembly during two full 3.0 s modulation cycles after inclusion of a post-column restrictor in the first dimension column assembly.

inherent modulation frequency inflexibility of PFM-GC×GC. In fact by simply making an appropriate change to the first dimension carrier gas flow rate and incorporating an additional restrictor it is possible to increase the modulation period substantially. Table 9 suggests a series of operating parameters determined using the dynamic flow model program that are required for correct modulation between 3 s and 9 s. The first dimension carrier gas flow rate and the additional restrictor dimensions are shown in bold typeface because these are the only parameters that require adjustment. All other parameters are constant. This represents a significant improvement in timing flexibility compared to equivalent systems without a post-column restrictor in the first dimension. Conditions for longer modulation periods have been determined *in silico*, but the Scielex timer used in the present study is configured for a maximum of 9 s so longer modulation periods are not reported in Table 9. Obviously, by using very low volumetric flow rates in the first dimension column there will be concomitant loss of separation efficiency in the first dimension column. Our recommendation is therefore to employ a narrower first dimension column.

The appropriateness of the parameters shown in Table 9 were tested and confirmed experimentally. A typical PFM-GC×GC separation of SAB using 3 s modulation is shown in Figure 13 and the two-dimensional separation space for a typical result using 9 s modulation to analyse the same SAB sample is presented in Figure 14. The scale used for both chromatograms ranges from the lowest baseline response to 10% of the most intense peak in each separation. The similarities of the chromatograms highlights that the integrity of the modulation system is maintained despite tripling the modulation period. The appearance of the first dimension peak tailing in Figure 14 is put down to the low

Table 9. List of appropriate column and connecting tubing dimensions for PFM-GC×GC which permit different modulation periods employed using the same device. The only modifications required are the additional restrictor column at the end of the first dimension column assembly and a change in first dimension carrier gas flow rate. * if a split transfer line is used the flow in the second dimension column and the split transfer line is 7.5 mL/min in each column. The connecting tubing (*a* and *c*) are 0.35 m and 0.65 m × 0.25 mm i.d. respectively. All modulation periods are performed with a 0.15 s flush time

Modulation period	3 s	4.5 s	6s	9 s	Modulation period	3 s	4.5 s	6s	9 s
retention gap					**restrictor**				
L (m)	0.1	0.1	0.1	0.1	*L* (m)	2	2	2	2
i.d. (mm)	0.075	0.075	0.075	0.075	I.D. (mm)	0.15	0.15	0.15	0.15
first dimension column					**additional restrictor**				
L (m)	15	15	15	15	***L* (m)**	**n/a**	**0.1**	**0.2**	**0.1**
i.d. (mm)	0.22	0.22	0.22	0.22	**I.D. (mm)**		**0.1**	**0.1**	**0.075**
***F* (sccm)**	**0.3**	**0.2**	**0.15**	**0.1**	**second dimension column**				
modulator sample loop (*b*)					*L* (m)	5	5	5	5
L (m)	0.3	0.3	0.3	0.3	I.D. (mm)	0.25	0.25	0.25	0.25
i.d. (mm)	0.25	0.25	0.25	0.25	*F* (sccm)	15*	15*	15*	15*

.

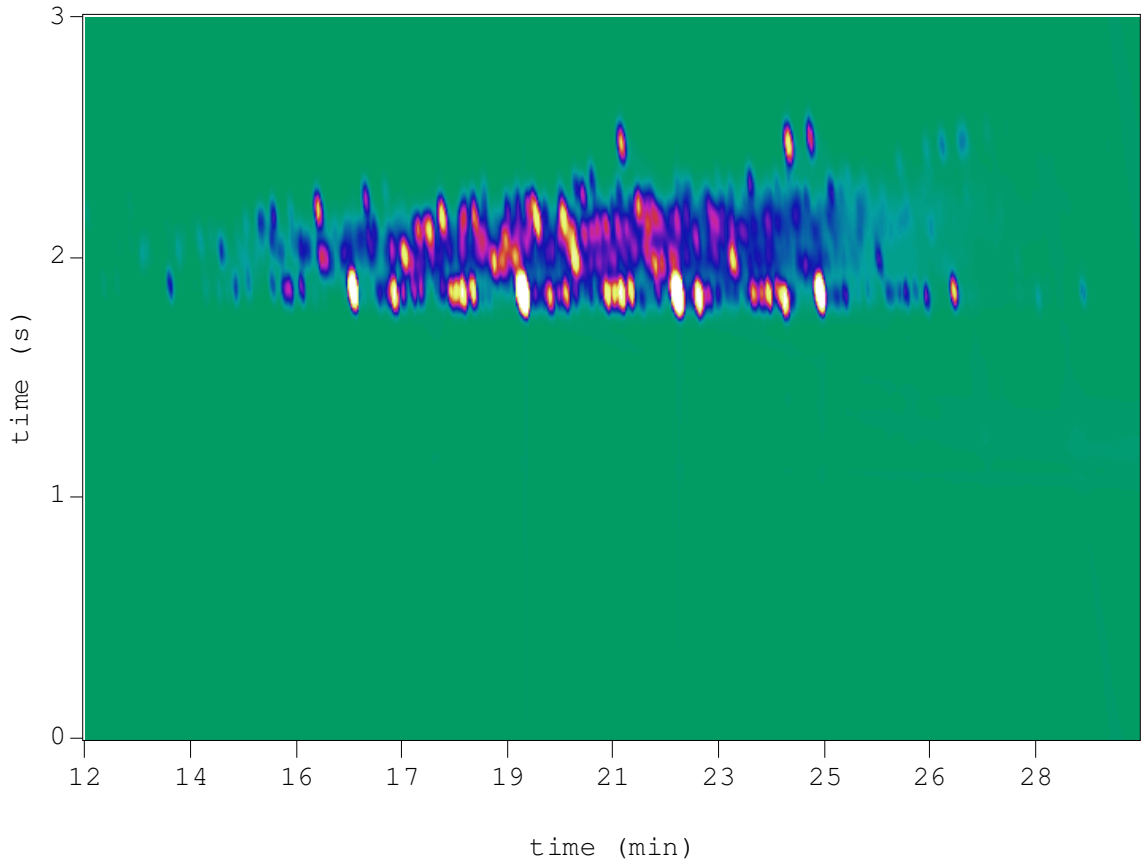

Figure 13. Two dimensional separation space illustrating the GC×GC separation of Special Antarctic Blend (SAB) diesel with 3.0 s modulation. Conditions are described in experimental section and the caption of Table 9. Each 3s modulation of naphthalene gives pwhh 110 ms in the second dimension.

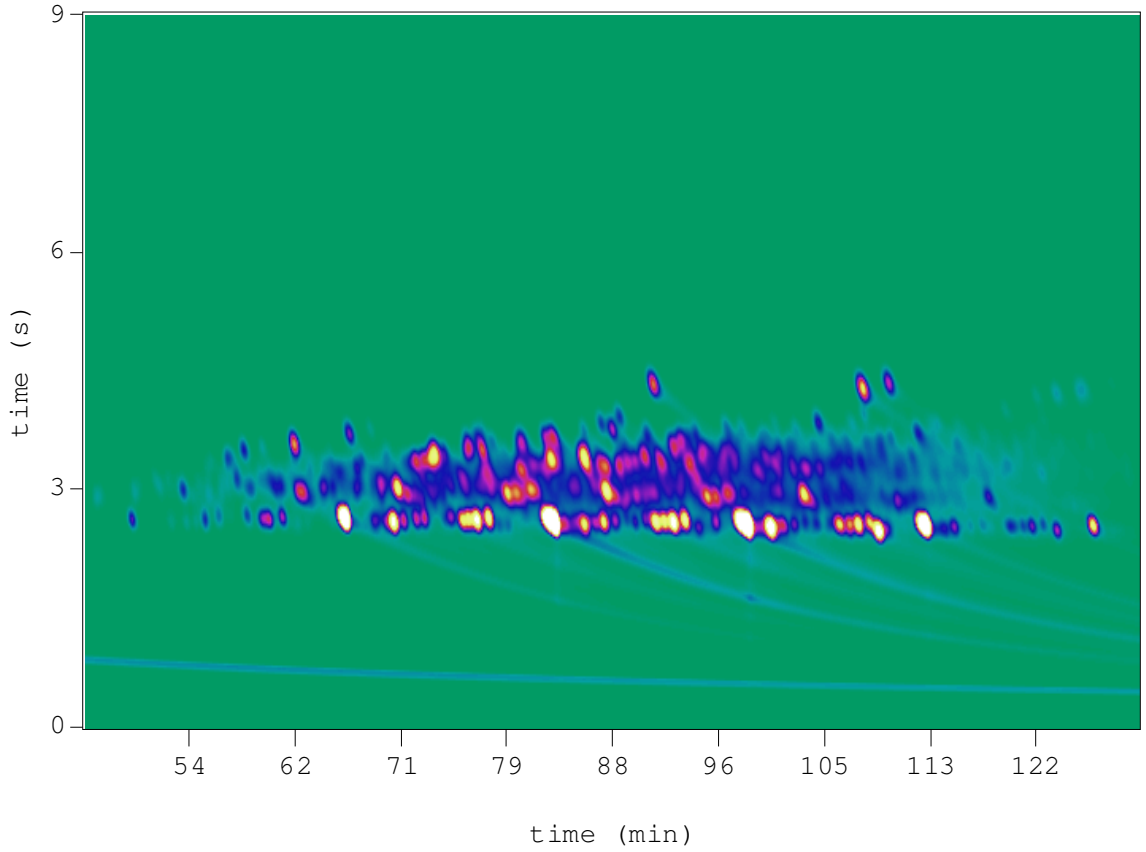

Figure 14. Two dimensional separation space illustrating the GC×GC separation of Special Antarctic Blend (SAB) diesel with 9.0 s modulation. Conditions are described in experimental section and the caption of Table 9. Each 9s modulation of naphthalene gives pwhh of 220 ms in the second dimension. Peaks are broader in the second dimension of this separation primarily due to temperature effects.

flow exacerbating poorly swept volumes in the tee pieces used to construct the modulator. It is likely that by using dedicated equipment in place of the universal tee-unions employed in the present investigation the tailing caused by poorly swept union fittings may be improved.

3.5 Conclusions

The dynamic flow model described here is a very useful tool for designing a PFM-GC×GC system. By performing a detailed investigation of the flow through a PFM-GC×GC system, several key observations have been made. First, the use of a symmetric flow path PFM-GC×GC design reduces valve actuation induced flow perturbations at the detector, leads to a more stable baseline. Second, inclusion of a narrow internal diameter retention gap prior to the first dimension column and a narrow internal diameter restrictor at the end of the first dimension column are highly desirable additions to the PFM-GCxGC column ensemble because they lead to a generally more stable and robust system. Third, the narrow internal diameter restrictor column at the end of the first dimension column provides a substantial increase in modulator flexibility, in terms of making the system amenable to a wider range of modulation times. Extreme changes in modulation time may need an adjustment to the length and / or internal diameter of the restrictor.

4 Factors affecting peak shape in GCxGC with non-focusing modulation. J.Chromatogr. A 1218 (2011) 3153-3158

4.1 Introduction

PFM-GCxGC operates by periodically introducing the first-dimension column effluent to the second dimension column(s) via a series of open-tubular conduits. A PFM-GCxGC modulation interface can constructed using capillary connection fittings, a gas switching valve and a sufficiently accurate timing device to trigger valve actuation. When the first-dimension column effluent is delivered to the second column by a pressure pulse, the pressure pulse concurrently stops the flow of effluent from the outlet end of the first-dimension column. Unlike thermal modulation, analytes are not focused in the modulator in a PFM GCxGC system. To this end, there are two factors that contribute to peak shape in the second dimension column; first, band dispersion continues within the modulator sample loop during the modulation cycle by diffusion, second the concentration profile of the peak from the first dimension is partially preserved in the resulting second-dimension peak meaning that the elution profile of the first-dimension peak has a significant influence on second-dimension peak shape. Poliak *et al*. previously alluded to the preserved peak-shape in the modulation process, stating that the observed GCxGC peak

width is due to a combination of injection width and second dimension elution time width [90]. The present chapter further explores this observation and discusses a systematic investigation of peak shape in PFM-GCxGC.

A model of peak shape was developed to illustrate the various contributions that the modulation process imparts upon GCxGC peak shape. Understanding these effects is useful in determining appropriate dimensions of the open-tubular conduits used to set up a PFM-GCxGC system and aids in carrier gas flow rate choices. Experimental peak data can be de-convoluted using the model into contributions from the first- and second-dimension separations as well as modulation effects.

4.2 Results and Discussion

The primary contributions to peak width and shape in PFM-GCxGC separations can be classified as those that can be attributed to chromatographic effects and those that can be attributed to modulation effects. Chromatographic effects are not deeply described here because this information can be found elsewhere [121,122], however modulation effects are discussed in detail. Unlike thermal modulation GCxGC where solutes are focused into narrow bands between the first- and second-dimension columns, Figure 15 illustrates how the concentration profile from the first-dimension peak is preserved in PFM-GCxGC. Here the reconstructed first dimension peak profile for a solute having a first dimension retention time of 13.44 min and peak width (4 σ) of 11.4 s. Injection into the second dimension column occurs every 3 s as indicated by the vertical bars giving a modulation ratio (M_r) of 3.8. Seven individual peak slices are labelled A-G in Figure 15. One of the more abundant peak slices (slice C) is discussed further. This peak slice is a suitable candidate to illustrate modulation effects. The peak slice has a large change in

response during the loading portion of the modulation period and the response is always substantially greater than zero. PFM-GCxGC modulators are non-focusing and although modulation leads to peak compression in time, the shape of this peak slice is maintained as it is delivered to the second dimension. The second dimension column injection bandwidth can be estimated using Equation 3 [53,90] where *PM* is the modulation period and *Flow Ratio* is the ratio of flush : fill volumetric flow rates in the modulator.

$$\text{Second dimension column injection bandwidth} = \frac{P_M}{Flow\ Ratio}$$

Equation 3. Second dimension column injection bandwidth. Terms are described in the text.

Figure 16A illustrates the peak compression (in time) for a single peak slice (slice C from Figure 15) produced from a 3 s modulation period and flow ratio of 100:1 and shows the effect that increasing peak width as a result of second-dimension chromatographic effects (σ_c) has upon peak shape following separation in the second column. In this case the initial width of the compressed peak slice will be 30 ms. In the absence of chromatographic band broadening, this compressed version of the portion of the first-dimension effluent would be exactly maintained and would be reflected by the detector response. However in any real scenario this peak shape is altered by band broadening. The result of the band broadening imparted on each of the segments within the compressed peak slice is also shown in Figure 16. For a 30 ms wide injection plug of uniform concentration a simplified standard deviation estimate for the sample plug, σ_L, is 8.7 ms. This 8.7 ms estimate (= 30 / 2√3) is obtained from the standard deviation of a uniform (or boxcar) distribution lasting 30 ms and assumes a loading profile of constant

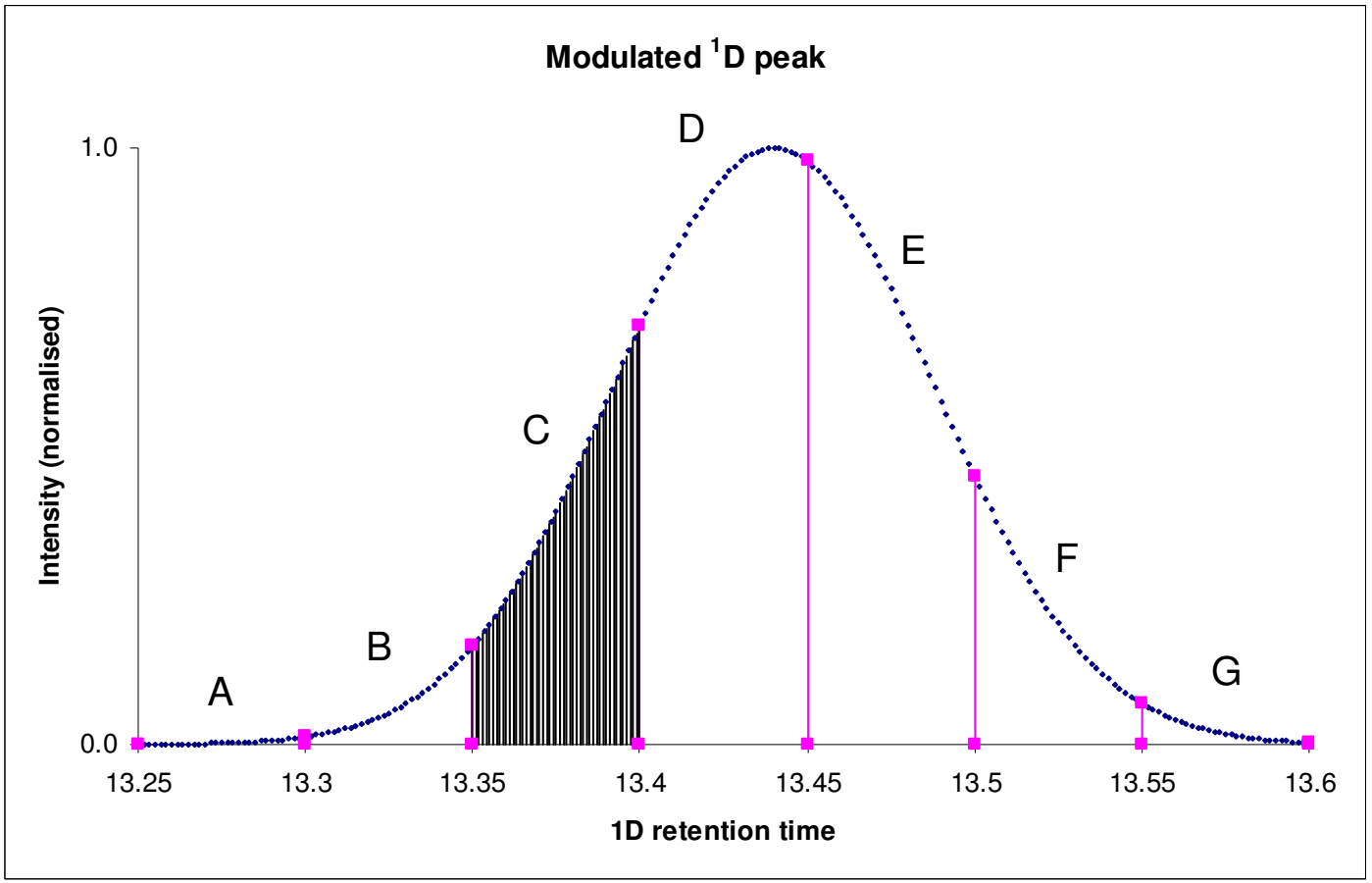

Figure 15. Simulated first dimension peak profile for a solute having a first dimension retention time of 13.44 min and peak width (4 σ) of 11.4 s. Injection into the second dimension column occurs every 3 s as indicated by the vertical bars giving a modulation ratio (M_r) of 3.8. A-G represent individual peak slices.

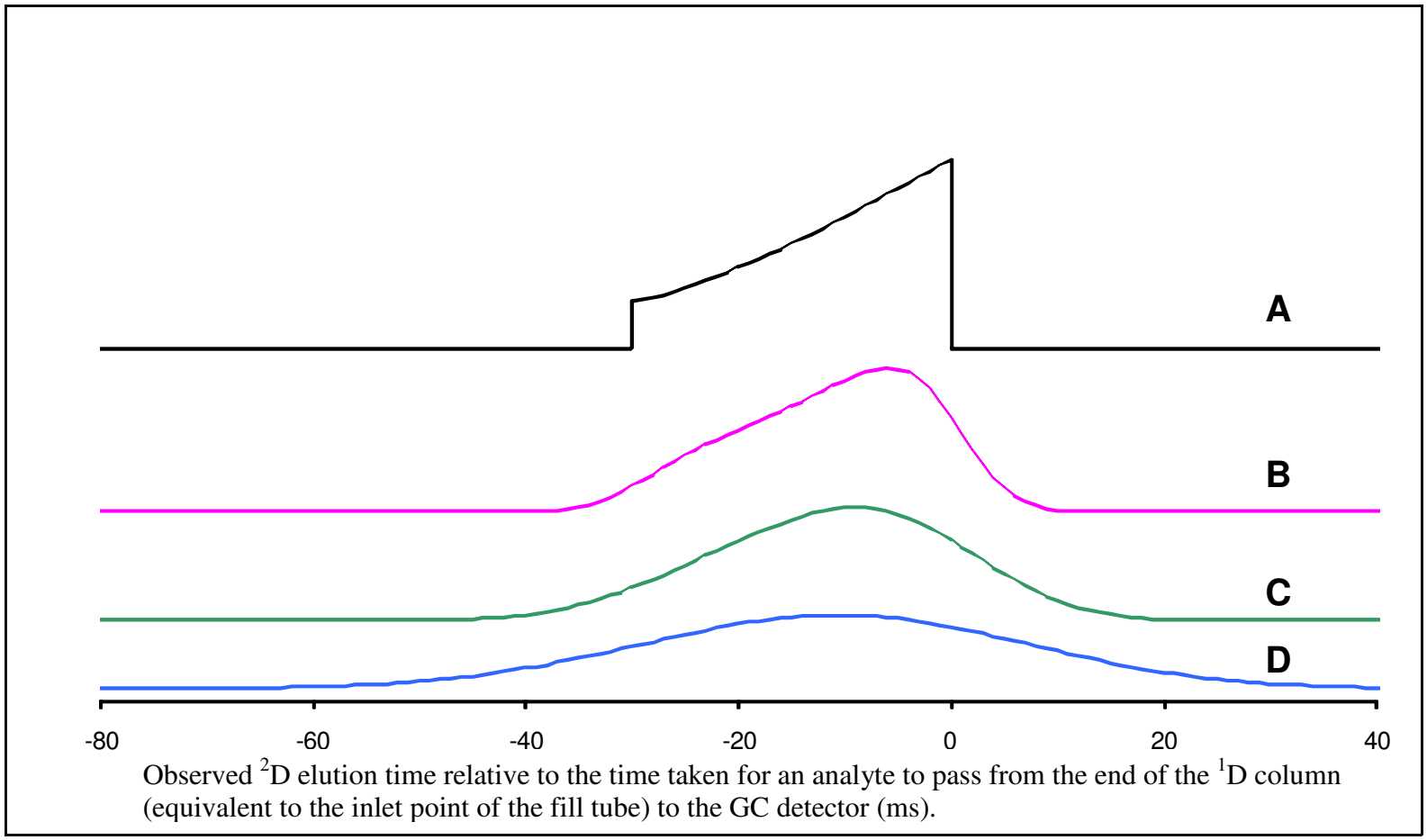

Figure 16. Single compressed (in time) peak slice modelled from a 3 s modulation period and flow ratio of 100:1. The simulated effect that increasing σ (B-C-D) has upon peak shape following separation in the second column.

concentration. Combining σ_L with the additional broadening during the separation on the second dimension column (σ_C) gives an estimate of peak width for any peak slice following the second dimension separation (σ_T). When σ_C is 4 ms (Figure 16B) the resultant peak has significant asymmetry ($A_s = 0.46$) and retains much of its profile from the first dimension peak shape. The resulting final peak width, σ_T, is $\sqrt{(4^2 + 8.7^2)} = 9.6$ ms. The width and shape of the peak are consistent with the loading effect being the major contributor towards these parameters. As σ_C is increased to 8 ms (Figure 16C) the profile has less resemblance to the injection plug. When σ_C is further increased to 16 ms (Figure 16D) the resulting profile is close to a Gaussian peak ($A_s = 0.95$) with a standard deviation of $\sqrt{(16^2 + 8.7^2)} = 18.2$ ms and second-dimension column broadening is the major component to σ_T. A critical observation associated with the partial retention of the first dimension peak shape is its effect on second dimension retention time. Note that the peak apex in each of the cases in Figure 16 is different. An additional effect on two-dimensional peak shapes is caused by the fact that loading profiles of contiguous first dimension peak slices are different from one another (Figure 15A-G). This has a significant influence on the cross-peak shape when the chromatogram is plotted as a two-dimensional colour plot (Figure 17). In this case the simulated GCxGC peak has a flow ratio of 30. Modulation ratio (M_r) also has a very important influence on peak-skewing. Very low M_r will lead to substantial skewing and high M_r reduces it, however there are practical considerations which rule out the use of very high M_r. In this discussion all calculations have been made using a favourable $M_r > 3$. A clear downward trend in the retention times of the peak maxima is expected in the two-dimensional colour plot due to the modulation effects described above. A systematic comparison of varying the flow

ratio and second dimension σ_C (Figure 18) shows that low flow ratio exacerbates this effect and increasing the flow ratio reduces the magnitude of peak-slice to peak-slice retention time differences. The efficiency of the second dimension column can disguise this peak shape effect. As σ_C increases, the peak skewing becomes less obvious and the contribution of σ_L towards the total peak bandwidth is reduced. As σ_C increases the loading profile has reduced effect on the resulting peak. Examination of the literature reveals that the majority of separations achieved by using PFM-GCxGC devices have been performed with a 20-30:1 flow ratio. Coincident with moderate second-column efficiency this moderate flow ratio is in the regime of partial retention of first-dimension peak shape and the contribution to peak shape from modulation effects should not be ignored. Either manual interpretation or automated software based interpretation of PFM-GCxGC chromatograms needs to be mindful of this peak shape phenomenon, particularly when relatively low flow ratio is combined with low σ_C (noting that σ_L is often be the major component of peak width since $\sigma_c = \frac{t_M(k+1)}{\sqrt{N}}$ and both k and t_M are small in GCxGC second-dimension separations). Given that the peak shift is predictable suitable software can be expected to adequately compensate for the modulation effect. The peak-picking algorithm needs to be informed to minimise the likelihood of either incorrectly summing the area of closely eluted peaks in the two-dimensional separation space, or incorrectly assigning portions of a single component to two separate peaks. Temperature programming effects can also cause predictable peak shift [123] that should also be considered for peaks eluting during an oven temperature ramp. It is advisable to employ a flow ratio > 30:1 in method development to minimise the modulation (peak-shape) effect.

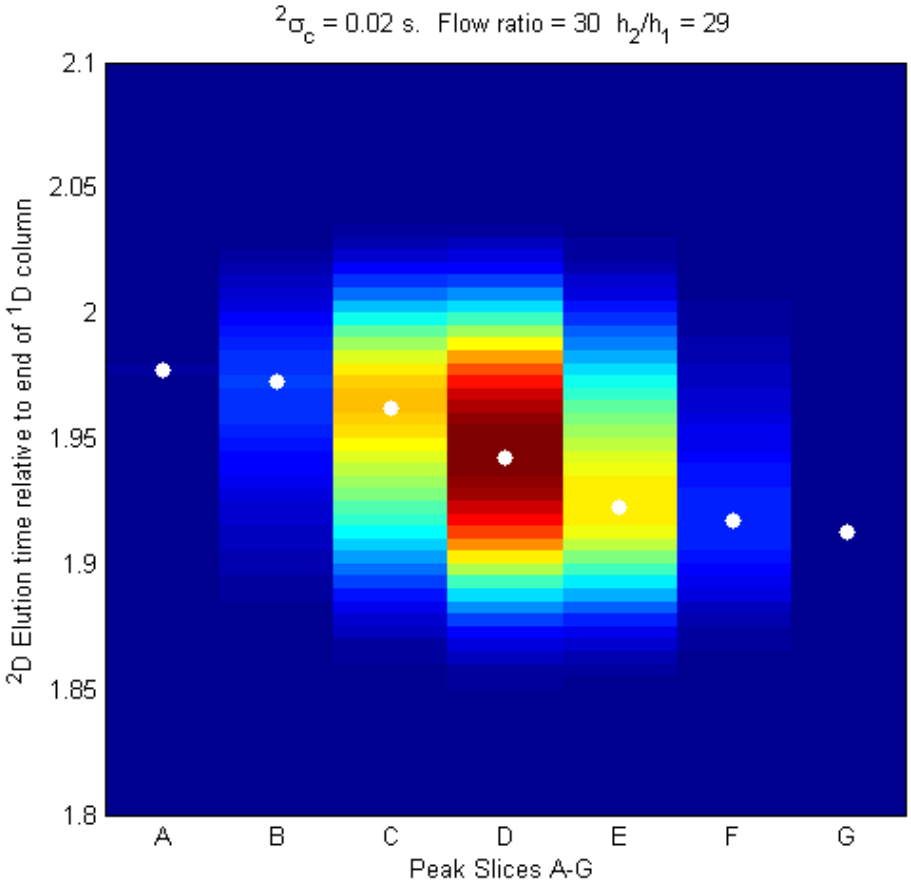

Figure 17. Two-dimensional projection, from numerical modelling, of all simulated peak slices across a modulated peak. First dimension profile and modulation period the same as Figure 15. Flow ratio in modulator = 30. The maximum of each peak slice is marked with a white dot.

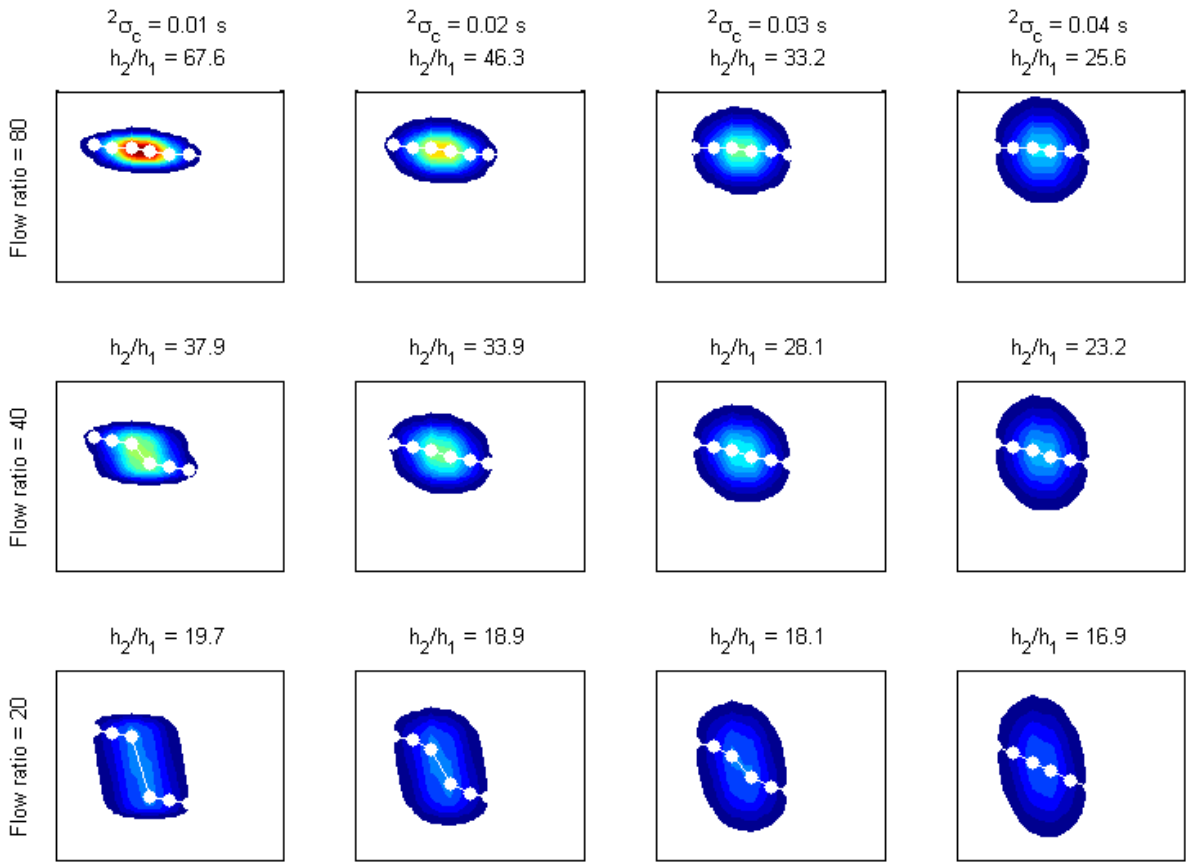

Figure 18. Simulated PFM-GCxGC peaks showing a systematic comparison of varying the flow ratio highlighting the peak skewing effect and peak amplitude enhancement brought about by modulation. First Dimension peak width (4 σ) is 11.4 s, modulation time is 3.0 seconds, first dimension retention time in phase with modulation timing.

It would be advantageous to be able to predict the amplitude enhancement available in PFM-GCxGC by marrying Equation 3 with the model shown by Lee *et al*. [124] to predict peak amplitude enhancement as a function of relative peak widths in the first and second dimensions respectively. Lee uses the Error Function to calculate the amount of material entering the modulator from the ^{1}D column and assumes all this material subsequently elutes at the GCxGC detector as a sharp Gaussian peak. When considering non-focusing GCxGC peak amplitude enhancement there are, however, a few important considerations since the model used by Lee requires that analyte release from the modulator onto the ^{2}D separation column does not contribute to peak width. Figure 16D shows the second-dimension peak height / width relationship is influenced only marginally by the modulation effect. Under these circumstances (where σ_C is large compared to σ_L) the observations made by Lee *et al*. are applicable without change and since performance (*N*) of the second dimension column can be reliably predicted it should not be arduous to predict peak amplitude enhancement. However, although it is possible to achieve close to theoretical minimum peak width if an uncoated transfer line is used after the modulator (Poliak *et al.* [90] have shown 20 ms (FWHH) peaks using a 70 cm × 0.25 mm i.d transfer line to the detector in a system that had a calculated width of 16 ms), it was shown in Chapter 3 that the concurrent reversal of flow at the first-dimension column outlet following valve actuation may effectively increase the first-dimension flow entering the modulator. Consequently the actual flow ratio is always slightly lower that the theoretical flow ratio. When $\sigma_C < 2\sigma_L$ retention of the original peak profile is likely to be observed and the simple approach of using the relative peak widths in the first- and second-dimension to predict peak amplitude enhancement will not

be sufficient. However peak amplitude enhancement can be predicted in all scenarios using the model described here. Figure 18 highlights the contributions of flow ratio and modulation period (two factors that influence σ_L) towards peak amplitude enhancement (h_2/h_1) in PFM-GCxGC (where h_1 and h_2 are non-modulated and modulated peak heights respectively). Validation by comparison of experimental data is discussed further below.

Since PFM-GCxGC relies on stopping the flow from the first dimension column temporarily and periodically, retention times are different in modulated vs. non-modulated experiments so the proposed peak shape models were validated using the following hypothesis:

Since the approach described above can predict peak shapes across all modulations for any given set of system parameters, it is also possible to determine first and second dimension peak width and time parameters from a GCxGC chromatogram by deconvolving the various contributing factors described above.

The peak shown in the left panel of Figure 19 was obtained by the analysis of *n*-eicosane that was eluted in an isothermal plateau (252 ^{o}C) of a GCxGC temperature programmed analysis. Six peak descriptors describe a three-dimensional peak in a PFM-GCxGC chromatogram. i) first dimension peak width, ii) second-dimension peak width, iii) first dimension retention time, iv) second dimension retention times, v) σ_L (which is determined from the flow ratio, modulation period and first dimension peak shape), vi) peak area. Peak shape can be described by a Gaussian function or contain additional terms for other chromatographic shapes such as skew Gaussian, exponentially modified Gaussian etc. [125]. For a set of real multidimensional chromatographic data it is possible to accurately project the first dimension peak profile. Here successive iterations of a

simulated three-dimensional peak are compared to the real data until the difference between the real peak and simulated peak is minimised (a multivariate, non-linear minimisation problem). The simulated GCxGC chromatogram was generated using the peak modelling approach described herein from an initial estimate for the six peak descriptors. The projected multidimensional chromatogram was compared directly with the raw GCxGC chromatogram and the peak descriptors were changed until the projected GCxGC chromatogram and the experimental data are in agreement. The specific parameter minimised was the sum of the square of the difference between real and simulated value (ie. a least squares approach). The projected GCxGC chromatogram for *n*-eicosane after this peak-fitting approach is shown in the right panel of Figure 19. The two peaks match with outstanding congruity. The residuals from the fitting process vary between – 1.5% and + 2.6% (normalised to the maximum detector response).

This ability to de-convolute the contributions of modulation and separation efficiency offers both a validation of the new approach for predicting the two-dimensional peak shape as well as a new model for determining first dimension retention time and width. Previously there have been a number of approaches for determining the first dimension retention time and width. A simplistic approach uses the most intense second-dimension peak pulse as an estimate of the first dimension retention time. Shellie *et al.* briefly described an approach for determining first dimension retention time, based on fitting the cumulative peak area to a normal cumulative distribution curve [120]. Adcock *et al.* recently extended this approach and provided a detailed description [126]. Here the new approach for determining first-dimension retention time and peak width were compared with the peak-area method proposed by Adcock *et al*. The *n*-eicosane

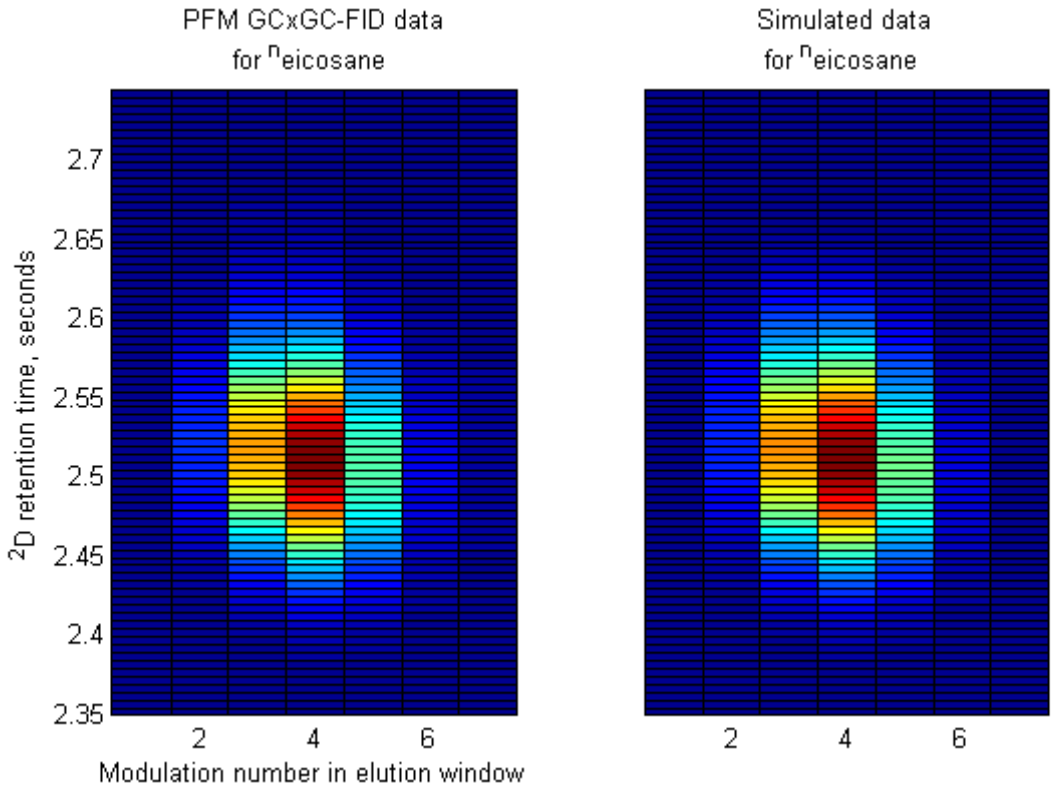

Figure 19. (left) Experimentally obtained PFM-GCxGC data for *n*-$C_{20}H_{42}$ eluting during an isothermal (252 °C) plateau in a temperature programmed method. (right) Simulated data.

peak shown in Figure 19 is again used for illustrative purposes. Adcock's method was used to determine the first-dimension peak parameters based on summation of all eight modulations during the isothermal plateau. The simplified approach of Adcock *et al.* using the three most intense modulations was not used in order to permit a fair comparison between methods. Comparison of the two approaches is summarised in Table 10. The best fit using the new model was achieved using a skew Guassian so Adcock and co-workers' approach was slightly modified to a skew-Gaussian approximation.

Table 10. Comparison of best fit peak parameters for *n*-eicosane using different fitting methods on experimentally obtained data.

Approach	**First dimension retention time (min)**	**σ (First dimension; s)**
n-eicosane (isothermal)		
Adcock *et al*.	31.116	2.720
Modified Adcock *et al*. (skew Gaussian)	31.116	2.614 (left) 2.808 (right)
Isothermal model (skew Gaussian)	31.112	2.533 (left) 2.873 (right)

The correspondence between the approaches is highly satisfactory and offers additional support to the effectiveness of the approach used here to understand PFM-GCxGC modulation effects.

All observations above are drawn from isothermal / isobaric models. However GCxGC uses a programmed temperature gradient to maximise differences in separation mechanisms in the two separation dimensions [127]. Notwithstanding, it is generally accepted that second dimension separations are treated as pseudo-isothermal, since the change in temperature during a single modulation period (P_M) is small (often < 0.5 ^oC).

Considering a case in which a desirable modulation ratio of four is achieved (where $M_R=4\sigma / P_M$), the oven temperature is not likely to increase more than a couple of degrees during the elution of the peak from the first dimension column. However, if temperature effects are ignored the residuals from the fitting process vary between – 8 % and + 17 % (normalised to the maximum detector response) for *n*-hexadecane eluting during an 8 ºC/min oven temperature ramp. This is considerably worse than the isothermal example above but is still quite satisfactory - in spite of the temperature effect. The reasonable fit for *n*-hexadecane is ascribed to the estimated σ_L peak descriptor (and resulting peak distortion from this parameter) offering compensation for the temperature effect. Although the numerical value for σ_L will now have no physical meaning the ability to estimate the first dimension retention time and peak width is only slightly compromised.

In the temperature-programmed situation a number of additional steps may be incorporated improve the methodology (and thus determination of the first dimension peak descriptors) for temperature-programmed operation. For instance the effect of temperature on retention factor is well described by the van't Hoff equation or one of its many variants (Equation 4).

$$\ln(K_C) = m.\frac{1}{T} + c$$

Equation 4. The van't Hoff equation

The temperature dependent retention data were obtained from an isovolatility curve [128] for the analyte at a wide range of temperatures. The multivariate, non-linear minimisation now changes marginally from the isothermal case in that a single second-dimension time difference (applied equally across all the modulations) according to the van't Hoff relationship is included. In this manner the temperature dependent second-dimension

retention time change is rigorously incorporated. In doing so σ_L once also again has a physical meaning. The peak shown in the left panel in Figure 20 obtained by analysis of *n*-hexadecane that was eluted in a temperature programmed GCxGC analysis and is compared in the right hand side with the predicted (projected) response.

The residuals from the fitting process vary between – 1.0 % and + 3.0 % (normalised to the maximum detector response). By doing so the fit is substantially improved over the isothermal method.

4.3 Conclusions

With increasing interest in GCxGC instrumentation that is less expensive, bulky, and / or fragile than conventional thermal modulation systems, the application of PFM-GCxGC has a growing number of supporters. With increasing use of this technology comes an expectation of more systematic investigations of system performance and more studies that improve understanding of the fundamental parameters leading to the chromatogram appearance. Here a systematic investigation of modulation induced peak shape effects has conclusively shown that significant peak skewing can be expected when a low flow ratio is utilised. Typically, high flow rates are used in the second-dimension column in this type of GCxGC experiment. These are substantially above optimum and lead to reduced efficiency (N), however σ_L is often be the major component of peak width since $\sigma_C = \frac{t_M (k+1)}{\sqrt{N}}$ and both k and t_M are small in GCxGC second-dimension separations. Therefore minimising the injection pulse width in the second dimension is recommended. Although the peak skewing is somewhat disguised by using a second-

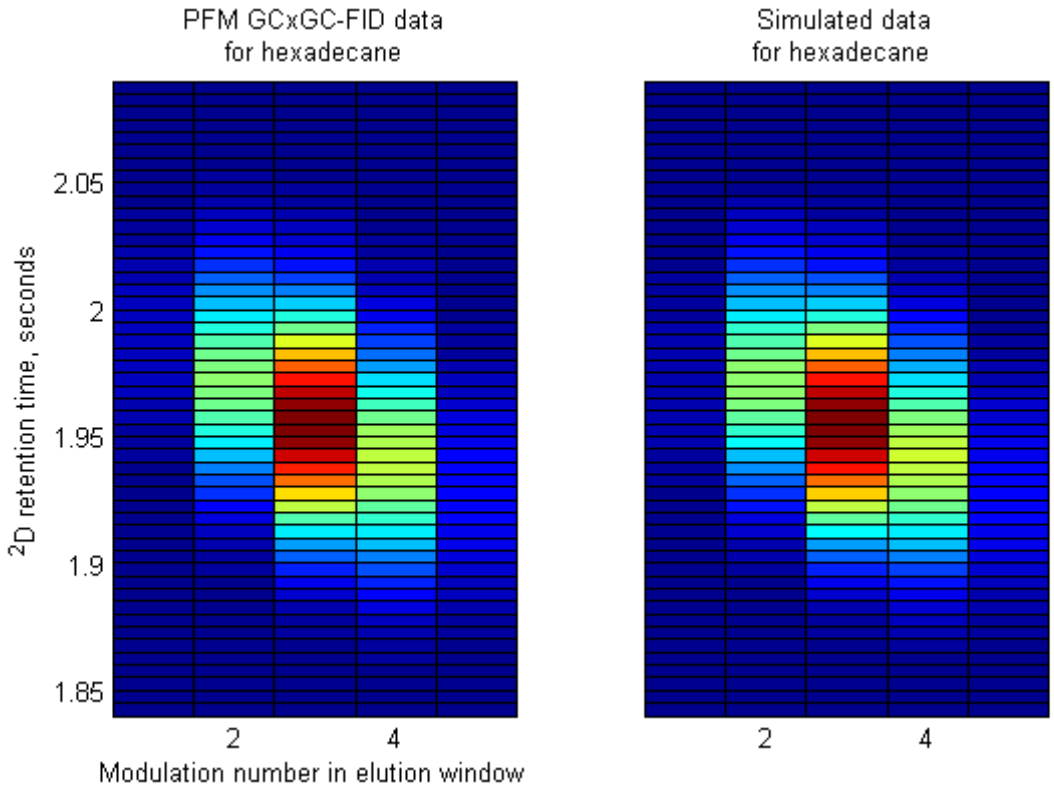

Figure 20. (left) Experimentally obtained PFM-GCxGC data and for *n*-hexadecane acquired during an 8 °C temperature programmed oven ramp. (right) Simulated data.

dimension column with low efficiency, investigations into improved second-dimension column efficiency are already being made [129]. In the simplest experimental set-up, flow ratio is determined by the flow rates in the first- and second-columns respectively. High flow ratio can be achieved by using low first-dimension column flow rate, or high second dimension column flow rate. In the simple set-up high flow ratio may have several drawbacks, including high pressures in both primary and secondary columns, either very low flow rates in primary column or very high flow rates in secondary column. Using a dual secondary column arrangement can largely alleviate these drawbacks. The flow parameters described here provide a new guideline for appropriate choice of experimental conditions. The modelling approach is validated by excellent agreement with experimental data and has been shown for both isothermal and temperature-programmed analysis.

5 GCxGC-FID assessment of a PHC contaminated site and comparison to GC-FID and GC-MS, parts submitted in Anal. Chem., March 2012

5.1 Introduction

GCxGC is uniquely suited to environmental PHC spill site assessment [130]. Pneumatic modulation GCxGC-FID methods offer a low cost, portable and robust site assessment tool for tasks such PHC analysis and are particularly well suited for site assessment and risk monitoring following a PHC spill at a remote site. The GCxGC separation space can be used to calculate parameters such as volatility and water solubility of PHC components in addition to separating the (generally) dominant aliphatic components from alkyl benzenes, alkyl naphthalenes and other alkyl PAHs [131,132]. GCxGC-FID data from 88 Macquarie Island Fuel Farm soil sample extracts were compared with GC-FID results [106].

Following this 13 samples were selected for further analysis with GC-MS methods. In order to accommodate the requirement of minimal operator input and manipulation of the sample extract at the remote site, sample preparation required neither concentration nor any aliphatic – aromatic fractionation prior to analysis. A mixed set of internal standards compatible with each technique was added and was suitable for GCxGC-FID,

GC-FID and GC-MS analysis. While the GCxGC-FID and GC-FID TPH values from all 88 site samples are compared in this chapter only selected samples are discussed in depth to illustrate how GCxGC-FID data can be used to obtain biomarker information. This biomarker information from the selected samples is used to derive the extent of biodegradation or water soluble aromatic transport and is compared to biomarker information obtained from GC-MS data. Analysis of the TPH composition in the entire set of GCxGC-FID data, and the implications this has to overall site assessment, is presented in Chapter 6.

5.2 TPH measurement

5.2.1 Considerations for developing the GCxGC approach for TPH determination

Considerations for development of a GCxGC approach for TPH determination are described here. Various data acquisition requirements and requests were presented by AAD scientists, AAD collaborating scientists (including research staff from Macquarie University and the University of Saskatchewan) and by examining documents available from various regulatory authorities [96,107,108]. It was mandatory that the approach provided quantitative data in order to satisfy regulators. The ability to analyse *n*-alkanes from *n*-C_9 to *n*-C_{36} and all 16 priority EPA PAHs while giving consistent ordered structures (of the different analyte classes) [66], was viewed as an essential analysis capability that covered all regulatory and research requirements. The TPHCWG Documents [93,94,133] mandate the evaluation of the concentrations of indicator carcinogenic compounds (e.g., the EPA PAH benzo[a]pyrene). The Australian NEPM

documents [134-136] also require evaluation of indicator carcinogens. In each case the assessment of indicator compounds is the first step during a risk assessment for petroleum-contaminated media.

The starting point of *n*-C_9 is, in this investigation, derived from the fact that AAD operations use bulk SAB diesel, a product that essentially starts at *n*-C_9. AAD operations utilising more volatile fuels are limited to jet fuels used in aviation (intra-station flights in Antarctica and helicopter operations at all stations) and some petrol (gasoline) for small petrol engines. Due to transport regulations (for the shipping of bulk flammable and volatile fuels) jet fuel and gasoline are shipped in 200 L drums, to limit the magnitude of potential spills.

Outside the *n*-C_{36} region it was seen as important to ensure elution of *n*-C_{40} as (i) some guidelines require measurement of TPH components up to *n*-C_{40} [137] and (ii) some soil samples from AAD stations have engine lubrication oil hydrocarbons extending into this range [106].

5.2.2 GCxGC separation of diesel

The separation obtained by GCxGC analysis of diesel shown in Figure 21 demonstrates that the current approach meets these requirements. The chromatogram also indicates that alkyl naphthalenes are plentiful. The sample also contains alkyl anthracenes and phenanthrenes (up to C3 alkylation). Finally trace levels of pyrene and methyl pyrenes (or possibly methyl fluoranthenes) can be detected.

The ability to measure the 16 priority EPA PAHs (Figure 22) and alkylated analogues covers most of the compounds required for long term monitoring of spilled fuel [49]. The components not directly observable using the GCxGC approach proposed

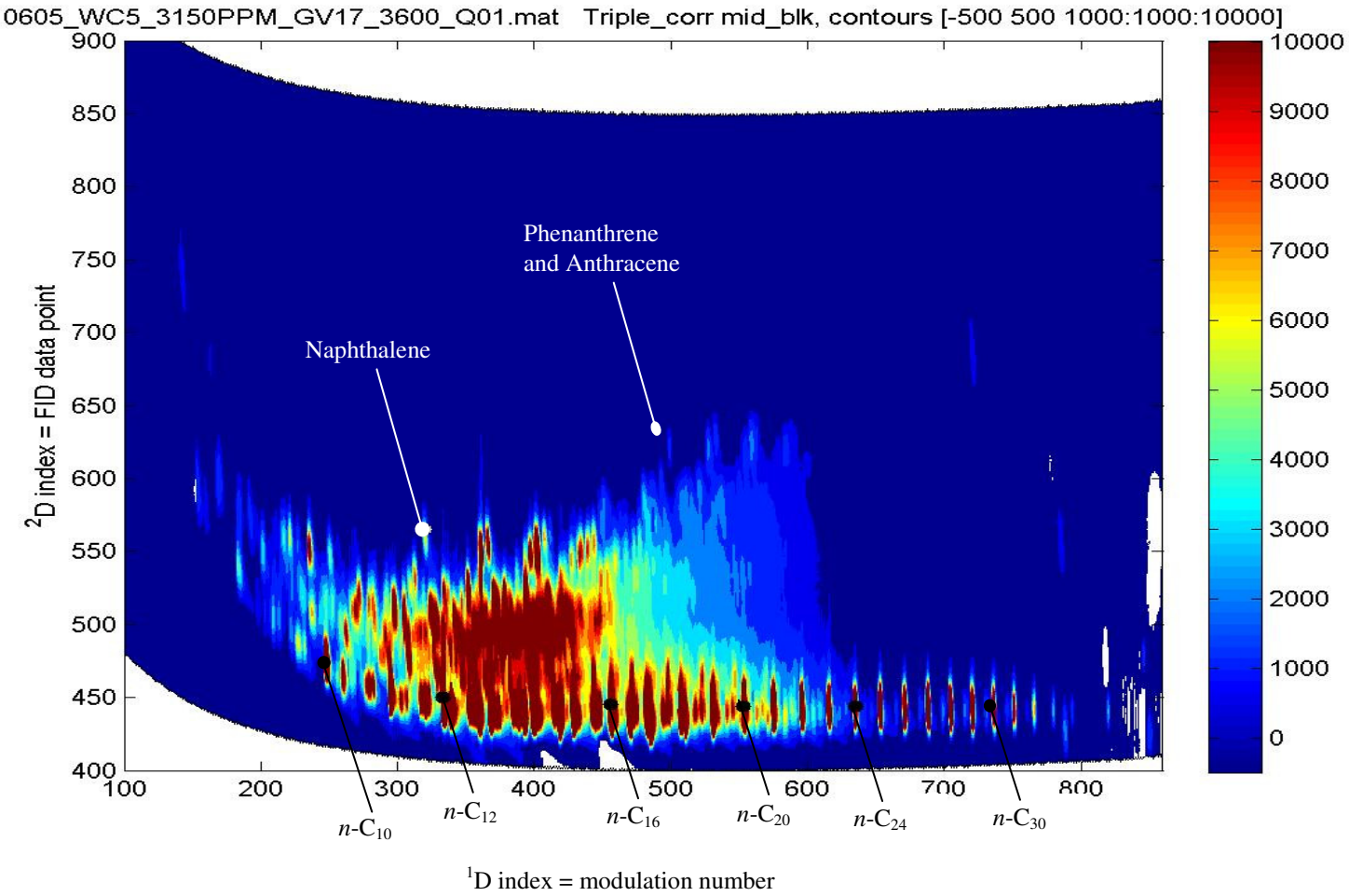

Figure 21. Usage of GCxGC separation space as shown by the separation of the WC5 standard (prepared from mixed SAB, Diesel and *n*-alkane rich candle wax, total TPH in standard is 3150 mg/L).

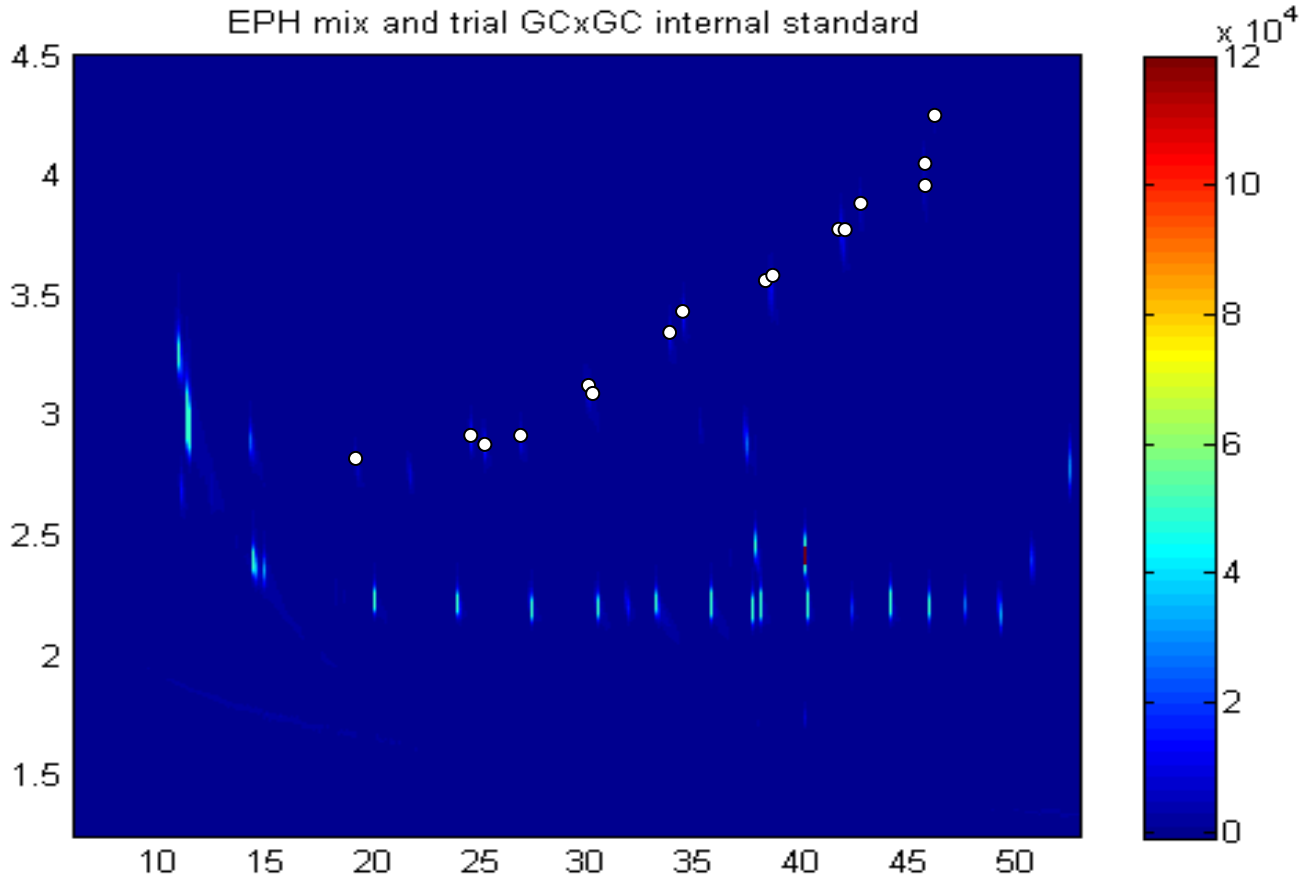

Figure 22. Usage of GCxGC separation space showing the positions of the 16 priority EPA PAH components (white dots) and alkanes up to *n*-C_{36} without wrap around and with class structure preserved by a consistent temperature and pressure ramp. Alkanes *n*-C_{38} and *n*-C_{40} elute on the final, isothermal part of the GC method. See Table 15 (page130) for ^{1}D and ^{2}D retention times of aromatic components

here include C4 phenanthrenes/anthracenes, C1 to C4 alkylated chrysenes, dibenzothiophene and C1 to C3 alkylated dibenzothiophenes. Of these components it is likely that, due to the consistent class structure of the separation and the separation of the parent PAHs demonstrated in Figure 22, all but the dibenzothiophenes will be separated as distinct, measurable classes. The dibenzothiophenes are not resolved from other fuel components in the GCxGC analysis of the fuel. Analysis of dibenzothiophenes is more suited to determination by using GC-MS (or GCxGC-MS), utilising unique m/z ions of these compounds.

The measurement of specific biomarkers [92,138] was given a relatively low priority in GCxGC method development. On the other hand, the information about PHC environmental fate that is normally gained from the measurement of such biomarkers was given a high priority. The method was developed with the aim of being able to detect and estimate the extent of PHC evaporation, dissolution and biodegradation. No particular separation of closely eluted isomers or biomarkers had to be obtained but it was seen as advantageous to preserve a separation between *n*-C_{17} and pristine and well as *n*-C_{18} and phytane. These particular *n*-alkane - isoprenoid pairs, which are easily separated on non-polar dimethyl-siloxane columns, are frequently used for determining the extent of biodegradation [139].

In addition to the abovementioned requirements, short analysis time and high sensitivity were desirable. A single GCxGC analysis can separate aliphatics and aromatics. Compared to GC, which would require fractionation and two GC analyses [107], an initial target of a GCxGC analysis runtime of less than (or equal to) twice the existing GC method time seemed appropriate. It is worthwhile noting that shorter

analysis times aid sensitivity, by increasing the signal-to-noise ratio for eluted components, although often at the expense of resolution.

Modulation period (P_M) is an important method consideration. Increasing the modulation period permits the use of slower (more efficient) second dimension separations, which leads to an increase in the number of separable classes in the ^{2}D column. Longer P_M also aids sensitivity by compressing a given analyte band into fewer modulations. Excessively long P_M can reduce the quality of the ^{1}D separation [140]. The frequency of sampling of the ^{1}D column is defined by the Modulation Ratio, M_R, with formula shown in Equation 5 [141]. When the precise quantitative analysis of specific trace analytes is required [141], or when separating the maximum number of individual compounds in a given time [141,142], a $M_R \geq 3$ is recommended. A $M_R \approx 1.5$ is suitable for the analysis of abundant compounds or semiquantitative analysis.

$$M_R = \frac{4 \times {}^1D\ peak\ \sigma}{P_M}.$$

Equation 5. Definition of the Modulation Ratio (M_R) in GCxGC analysis.

In the fuel analysis in this work the M_R is ~1.0. This is broadly similar to the recommendation for semiquantitative analysis and is suitable because preserving within-class separation is unnecessary for gaining PHC environmental information and allows for a faster GCxGC method. The class structure of the separation is paramount because it provides an analogous approach to that used to monitor the *Exxon Valdez* spill, where a single estimate for all C2 Naphthalenes or all C2 phenanthrenes /anthracenes provides a surrogate for the separation of all the individual isomers [49]. Several papers analysing the long term fate of alkyl aromatics from the *Exxon Valdez* spill simply summed all the

different reported aromatic fuel classes to provide a single number for persistent total PAH (TPAH) components of interest [49,143]. Clearly, in the case where TPAH is of interest, preserving any within-class separation is completely unnecessary (a consideration that is exploited further in Chapter 6, especially Section 6.2 'Binning of GCxGC data', and the subsequent analysis of binned data).

An additional advantage of a long modulation time is that the unoccupied separation space can be used to aid baseline correction. This is especially useful when correcting drift between the GCxGC analysis of an instrument blank and an environmental extract. Given that this work employs experimental early generation differential-flow GCxGC modulators, blank correction is a significant issue in achieving the best possible sensitivity, and quantitative accuracy and precision. Any pneumatic modulator, even if perfectly constructed, will experience some flow perturbations with valve switching. As the gas in the capillaries of the modulator either compresses, with an applied higher pressure, or decompresses (towards an equilibrium state with a lower pressure) flow changes are unavoidable. As system sensitivity is pushed towards measuring an analyte signal near the noise floor (especially when measuring a co-eluting analyte class appearing as the GCxGC equivalent of an UCM) baseline correction and removal of instrument artefacts will ultimately be the limiting factor for sensitivity.

5.2.3 GCxGC-FID vs. GC-FID for TPH measurement

To compare the GCxGC data with those from a long-established GC-FID method [42,96], 88 soil extracts were analysed by GC-FID and GCxGC-FID. All GC analyses were conducted at Macquarie Island. While some preliminary GCxGC-FID analysis was

done at Macquarie Island, all the site extracts were analysed at Hobart (on a different instrument) following 15 months of storage at -20 °C. Despite the difficulties of shipping over the Southern Ocean and the lengthy storage, agreement between the initial GC-FID result and the GCxGC-FID result is excellent, when the GC-FID result was greater than twice the GC-FID reporting limit of 200 mg/kg, as shown in Figure 23 and Figure 24. The two outliers identified in Figure 23 are from samples containing high levels of PHCs are eluted near 1-bromoeicosane. This situation is illustrated by Figure 25 which shows the analysis of sample 53184. This sample, which has a PHC concentration of ~13000 mg/kg, has a PHC profile similar to that seen in the diesel sample purchased at a Hobart service station. The expansions of the 1-bromoeicosane internal standard region illustrate the problem of defining a baseline for the integration of the internal standard itself. These outliers were identified with an automated algorithm (as outlined in the experimental section 2.4.3). The estimated uncertainty introduced by the additional compounds eluted near the internal standard was subsequently incorporated into the overall uncertainty for that result as shown in the error bars of Figure 23 for the series labelled “high signals near IS”. For these two samples an error assessment of the GC-FID data was not undertaken so these particular GC-FID error bars (that would be aligned with the x-axis) have been omitted in Figure 23.

The final check of the quality of the instrument data acquisition and the post-acquisition data analysis was the repeat GCxGC-FID analysis of eight randomly selected site extracts. The TPH results from this process are shown in Table 11. Agreement between replicate analyses is good. The sample with greatest difference between the results (sample 53187 with TPH results of 434 ± 13 mg/kg and 404 ± 13 mg/kg) has a

difference that does not fall outside a 95% confidence interval for the comparison of 2 such results (z-score less than 2). It is evident that the GCxGC measurement of TPH is both reliable and sensitive as reported elsewhere and has not been adversely affected by the lower than usual modulation ratio ($M_R \approx 1.0$) [111,144].

5.2.4 Biodegradation index

The display of the biodegradation index, based on composition changes in crude oils from a geological context, is shown in Table 12 (page 111) [145-147]. The complication of fuel spill evaporation is potentially very important in a shallow soil setting where the fuel has originated from above-ground tanks. The possibility of volatile component evaporation makes disentangling volatile *n*-alkane losses between evaporation and biodegradation difficult and therefore it is hard to unambiguously identify stage 1 biodegradation.

Given that the soil bound PHC biodegradation can be much faster with a high availability of nutrients and oxygen [148-150], selectivity during degradation will be affected by what limits biodegradation. In a setting where the local soil community is limited chiefly by access to the fuel components, selectivity will be low – fuel components will be used (biodegraded) as they are encountered. Conversely, where access to fuel components is high (i.e. high TPH levels) but nutrient and oxygen flux is limited (i.e. at a greater soil depth where nutrient and oxygen components are limited by biological activity in the upper soil layers) selectivity during biodegradation will be higher [151-155]. For these reasons, in a soil setting, it is not possible to simply state that a certain biodegradation index indicates a particular percentage of fuel loss to

Table 11. Repeat GCxGC-FID analysis and TPH assessment in 8 randomly selected site sample extracts. Estimated uncertainty is from combining the uncertainty arising from method blanks (7 mg/kg) and calibration (2.5% of the TPH estimate). The raw value of -1.4 ± 7 mg/kg for the repeat analysis of sample 52514 would be changed to 0 mg/kg should that value be needed in a site assessment report for an external body.

barcode	TPH estimate from injection 1 mg/kg	TPH estimate from injection 2 mg/kg	estimated uncertainty, mg/kg	abs difference / combined uncertainty' (z-score)
53058	133	142	8	0.9
53085	508	507	14	0.1
53131	632	621	17	0.5
53166	11	11	7	0.0
53187	434	404	13	1.7
52514	0.1	-1.4	7	0.2
53232	9	15	7	0.6
53259	19	22	7	0.3

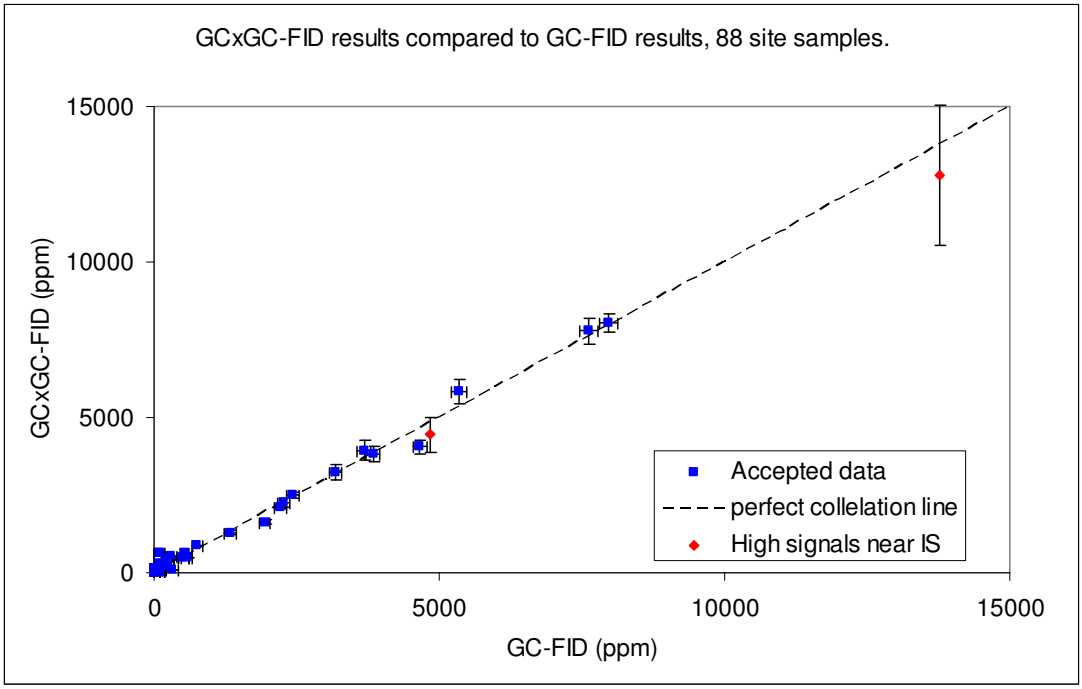

Figure 23. Comparison of all 88 GC-FID results and the corresponding GCxGC-FID result

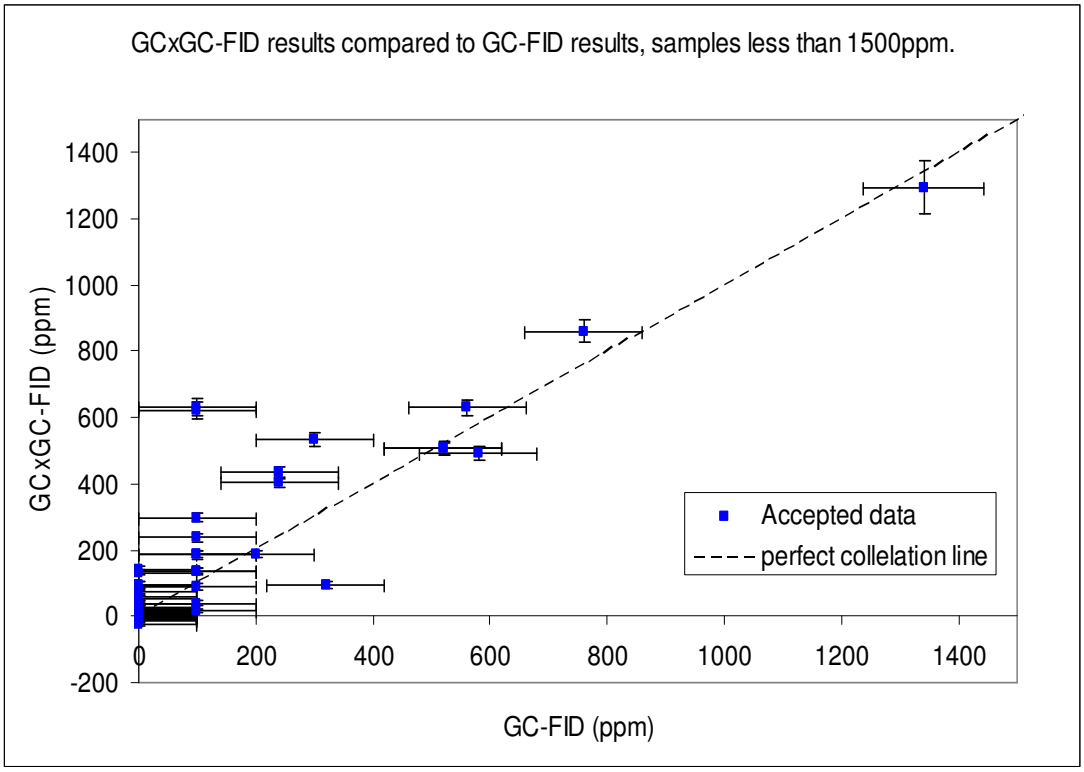

Figure 24. Comparison of all the GC-FID results less than 1500 ppm with the corresponding GCxGC-FID result (error bars left off for clarity). GC-FID result "ND" set to 0 ppm. GC-FID result "< 200" set to 100ppm.

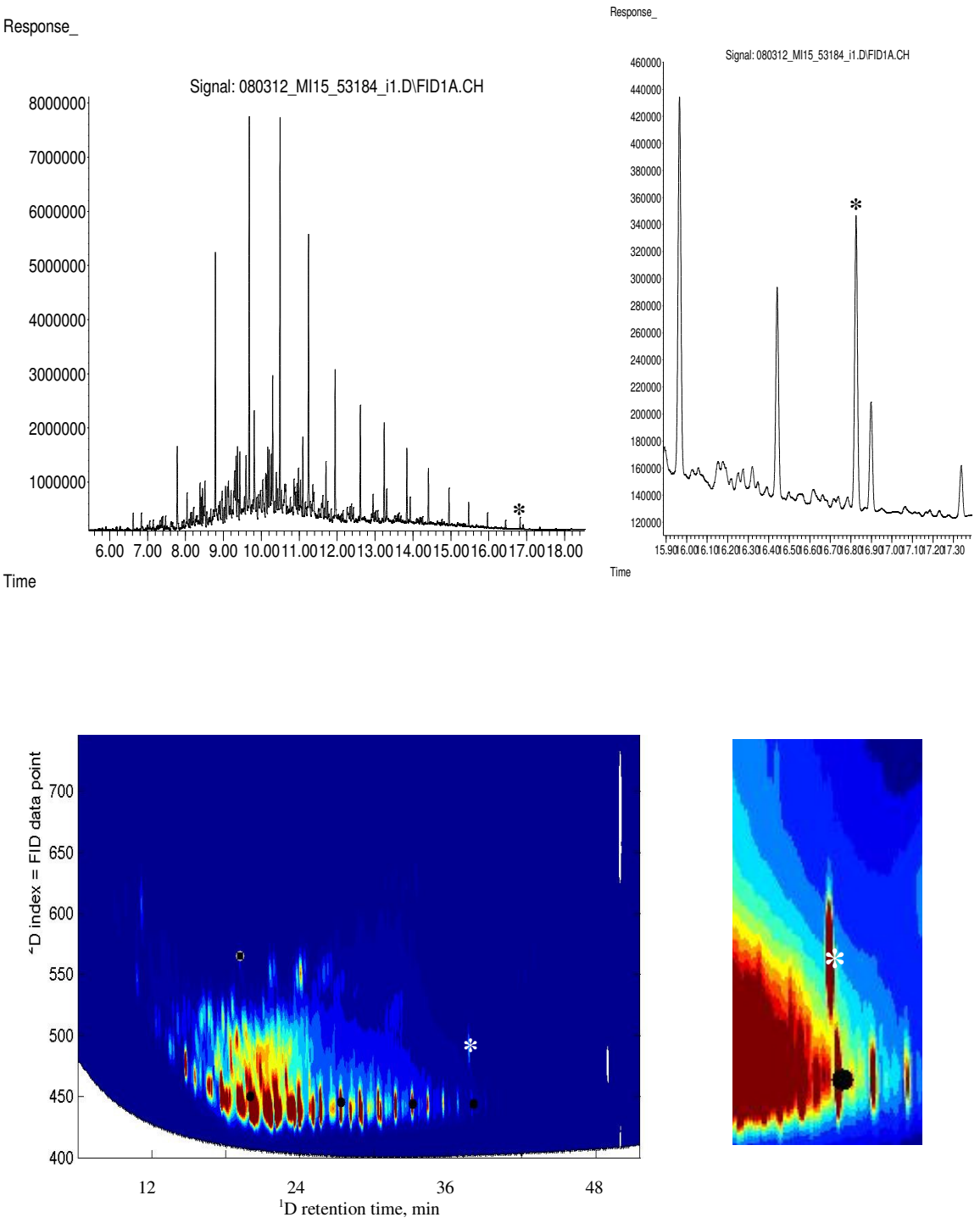

Figure 25. GC-FID and GCxGC-FID analysis of sample 53184. 1D GC-FID expansion is for region *n*-C_{22} to *n*-C_{25} showing the internal standard, 1-bromoeicosane. 2D expansion is *n*-C_{21} to *n*-C_{26} with a lower set of contours. In each case the co eluting compounds can be seen at, and around, the elution time of the internal standard. *n*-C_{12}, *n*-C_{16}, *n*-C_{20} and *n*-C_{24} are indicated with black dots on the GCxGC chromatograms. 1-bromoeicosane is indicated with an asteric (*).

Table 12. Typical effects of biodegradation on crude oil taken from Volkman *et al*. [146]. See list of abbreviations on pages iv to vi.

Level of biodegradation	**Saturated hydrocarbons**	**Aromatic hydrocarbons**
1 (Minor)	Low molecular weight *n*-alkanes depleted	MNs depleted
2	General depletion of *n*-alkanes	DMNs altered
3	>90% *n*-alkanes absent, alkylcyclohexanes affected	DMNs, TMNs, MBPs, EBPs and MDPM altered, DMBP slightly altered
4 (Moderate)	*n*-Alkanes and alkylcyclohexanes absent, acyclic isoprenoids depleted	DMNs, TMNs, MPs altered, MBPs, EBPs, MDPM and DMBP severely depleted, TMBP altered
5	Acyclic isoprenoids absent	DMNs severely depleted, TMNs. TeMNs and DMPs altered
5-6	Bicyclic alkanes affected	DMNs absent, TMNs severely depleted, TeMNs and DMPs altered, MPs depleted
6 (Extensive)	Bicyclic alkanes severely depleted, steranes affected, 25-norhopanes present	TMNs and MPs absent, TeMNs depleted, DMPs altered, EPs unaltered
7 (Very extensive)	>50% ααα steranes removed, 25-norhopanes present	DMNs, TMNs, TeMNs, MPs, DMPs, EPs, MBPs,
8 (Severe)	Hopanes affected, steranes absent	
9	Hopanes absent, diasteranes affected	
10 (Extreme)		Aromatic steroids affected

biodegradation pathways. In order to gain an insight into site mechanisms for fuel fate, and the rate of those mechanisms, it is necessary to consider the context of each sample within the setting of the whole fuel plume [155]. While this Chapter considers several representative samples in detail, Chapter 6, analyses the entire sample set after the data is binned into environmentally based GCxGC regions. Examples of evaporation and biodegradation identified with the techniques used in Chapter 6 can be seen in Figure 40 and Figure 41 and are discussed in the associated text.

5.3 Analysis of Aliphatics

5.3.1 Assessment of n-alkanes, isoprenoids and biodegradation

The elution regions for the aliphatics *n*-C_{16}, *n*-C_{17} and *n*-C_{18} are shown in Figure 26 (for samples 53091 and 53268). The region also contains three important acyclic isoprenoids; norpristane, pristane and phytane [139]. The aliphatic elution regions are summed to give a reconstructed ^{1}D aliphatic chromatogram (Figure 26, bottom). As is evident in both the GCxGC plots and in the reconstructed ^{1}D aliphatic profile some separation exists for the biomarkers *n*-C_{17} - pristane as well as *n*-C_{18} – phytane. The isoprenoid norpristane is well separated from every *n*-alkane. Numerous other unidentified low abundance aliphatics are seen in the elution region of these compounds.

The presence of these compounds makes it impossible to determine a definitive baseline for the *n*-alkanes and isoprenoids eluting in this region. Despite the difficulties in assessing the baseline around the compounds it can be easily seen in Figure 26 that the isoprenoids in sample 53091 are equal to or higher in concentration than the *n*-alkane(s) eluted near them. In contrast sample 53268 has concentrations of *n*-alkanes substantially

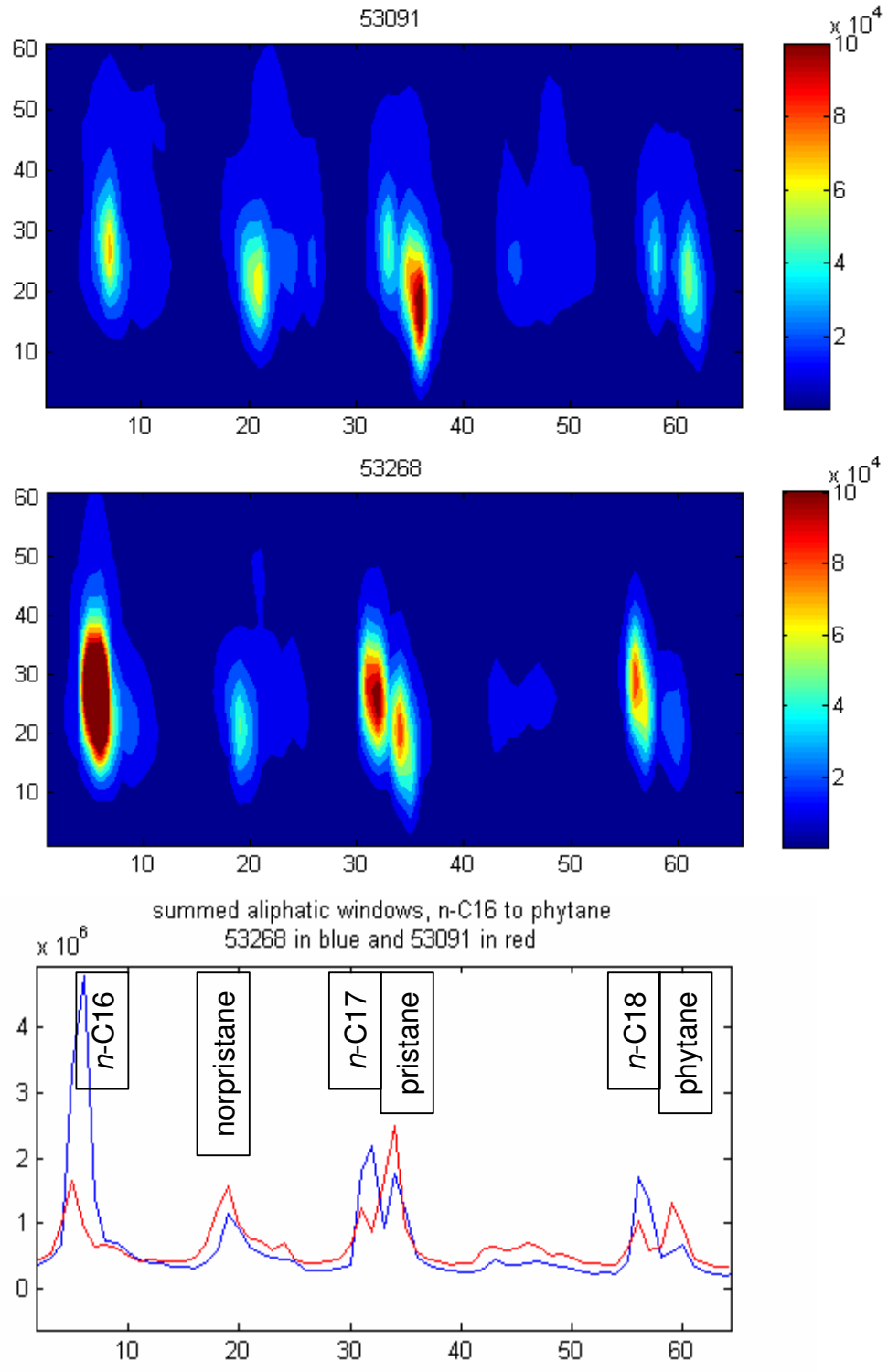

Figure 26. Top and middle, GCxGC-FID trace for aliphatics in the region *n*-C_{16} to phytane inclusive. Sample barcodes above figure. X-axis is the modulation number within the elution region, Y-axis is the FID data point number within the aliphatic elution window. Bottom, reconstructed ^{1}D elution profile of the aliphatics shown in the top and middle figures. X-axis is the modulation number within the elution region, Y-axis is the summed FID response from aliphatics in the modulation.

higher than the local isoprenoids. In both samples the *n*-alkanes are clearly present as the peak corresponding to the *n*-alkane is significantly higher than the peaks observed from the unidentified aliphatics in the elution window. It is evident that sample 53091 has experienced a moderate level of biodegradation such that it has entered, approximately, stage 2 on the aliphatic biodegradation index shown in Table 12. Sample 53268 has experienced less biodegradation.

A comparison to the initial fuel composition would need to be undertaken if marker ratios such as *n*-C_{17}/pristane were to be used as evidence of biodegradation [139]. Unfortunately, as the spill is of unknown age and from a different batch to the current SAB shipped to Macquarie Island, a sample of the particular diesel is unavailable. Research into AAD shipping records [156] for the previous 20 years indicates that, at no stage in the last 20 years, has any bulk fuel product other than SAB been shipped to Macquarie Island.

The sample showing enhanced biodegradation (53091) was obtained from bore MI08FF #07 from a depth of 500 to 600 mm from the surface and with a TPH value of 1340 mg /kg. The sample showing less extensive biodegradation (53268) was obtained from bore MI08FF #29 from a depth of 1000 mm (the maximum depth of the excavated hole) and with a TPH value of 3680 mg /kg. Given the greater depth, with concurrent limited availability of oxygen and nutrient for biodegradation, as well as the higher fuel loading it is not surprising that sample 53268 shows less fuel composition change, from biodegradation, than sample 53091. This conclusion is entirely consistent with the GC-FID analysis of these same extracts. Figure 27 shows the GC-FID analysis results for these samples.

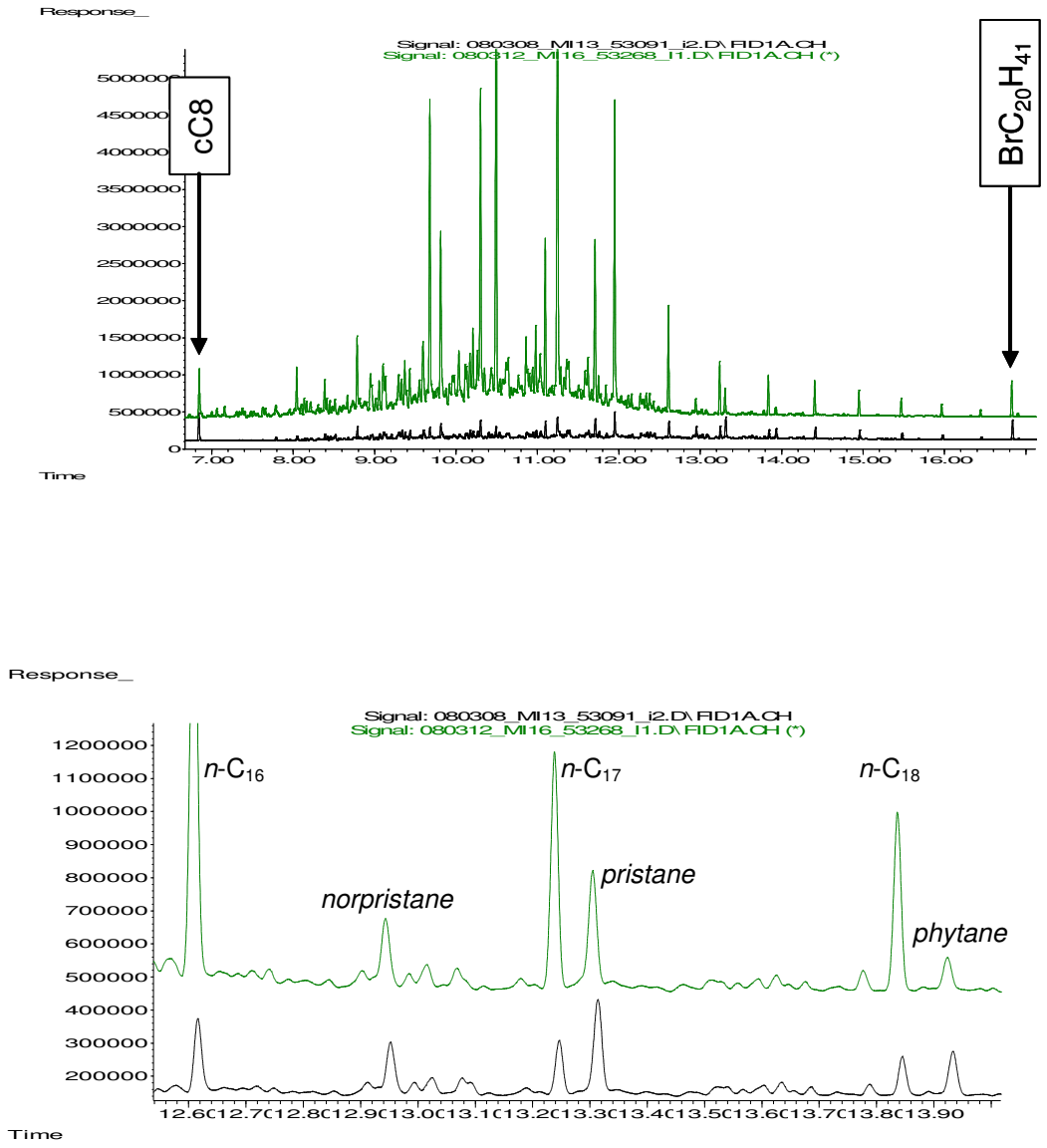

Figure 27. GC-FID chromatograms for samples 53091 and 53268. Top Chromatogram from *n*-C_9 to *n*-C_{24} inclusive, internal standards cyclooctane (cC8) and 1-bromoeicosane marked. Bottom expansion of *n*-C_{16} to *n*-C_{18} region. Sample 53091 shows significant losses of the *n*-alkanes *n*-C_{16} to *n*-C_{18} inclusive compared to 53268.

5.3.2 GCxGC-FID assessment of alkyl-cyclohexanes and biodegradation

Alkyl-cyclohexanes form an important homologous series of aliphatics that have long been used to monitor biodegradation [5,11,145,146,157] with commercially available standards for this purpose [158]. This is apparent in the notes regarding biodegradation scales 3 and 4 in Table 12. In the direct GC-FID analysis of fresh (non-degraded) SAB and other diesel fuels, this series has insufficient abundance to stand out from the large numbers of co-eluting analytes. This can be appreciated from Figure 27 as, in the expansion, only the labelled *n*-alkanes and acyclic isoprenoids stand out from the mass of other PHC peaks. In contrast, the class structure of the GCxGC separation and the slightly higher polarity of the cyclohexyl ring allow these compounds to be seen as a series with different ^{2}D retention (compared to the *n*-alkanes and the acyclic isoprenoids). In published literature, this can be seen in the GCxGC-FID separation of crude oil from the *Exxon Valdez* spill [64].

The series of *n*-alkyl-cyclohexanes can be identified on the basis of retention factors in both dimensions. In Figure 28 local maxima are identified when a point is thelargest point within ± 5 data points on the y-axis and within ± 1 modulation (giving a ^{1}D window of ± 3.6 s and a ^{2}D window of ± 25 ms). This method of locating maxima finds the series of cyclohexanes, which is marked as the upper series of white dots in both Figure 28 and Figure 29. For plotting purposes only maxima well above the local signals are shown in the plots.

The usefulness of these cyclohexanes in identifying evidence for biodegradation can be seen in Figure 29. In this figure the display window is centred on the maximum of heptyl-cyclohexane found with an automated peak search algorithm. Upon examination

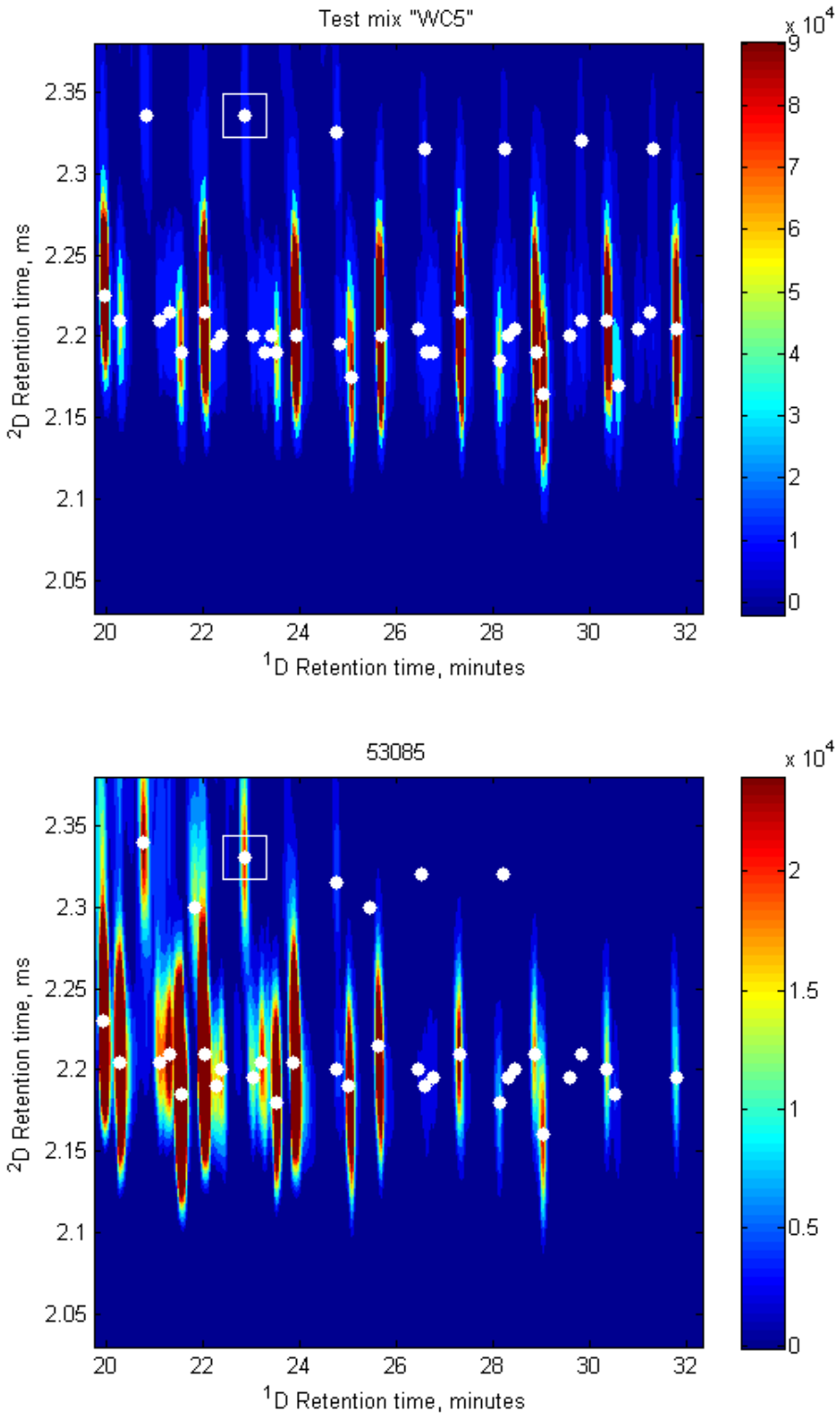

Figure 28. Top. Resolved cyclohexane series in test mix WC5. Upper white dots show the location of the alkyl-cyclohexanes. Lower white dots represent local maxima for all the acyclic aliphatics. The white square corresponds to heptyl-cyclohexane. Bottom, Field sample 53085 with the same local maxima auto-search routine but with revised peak detection thresholds.

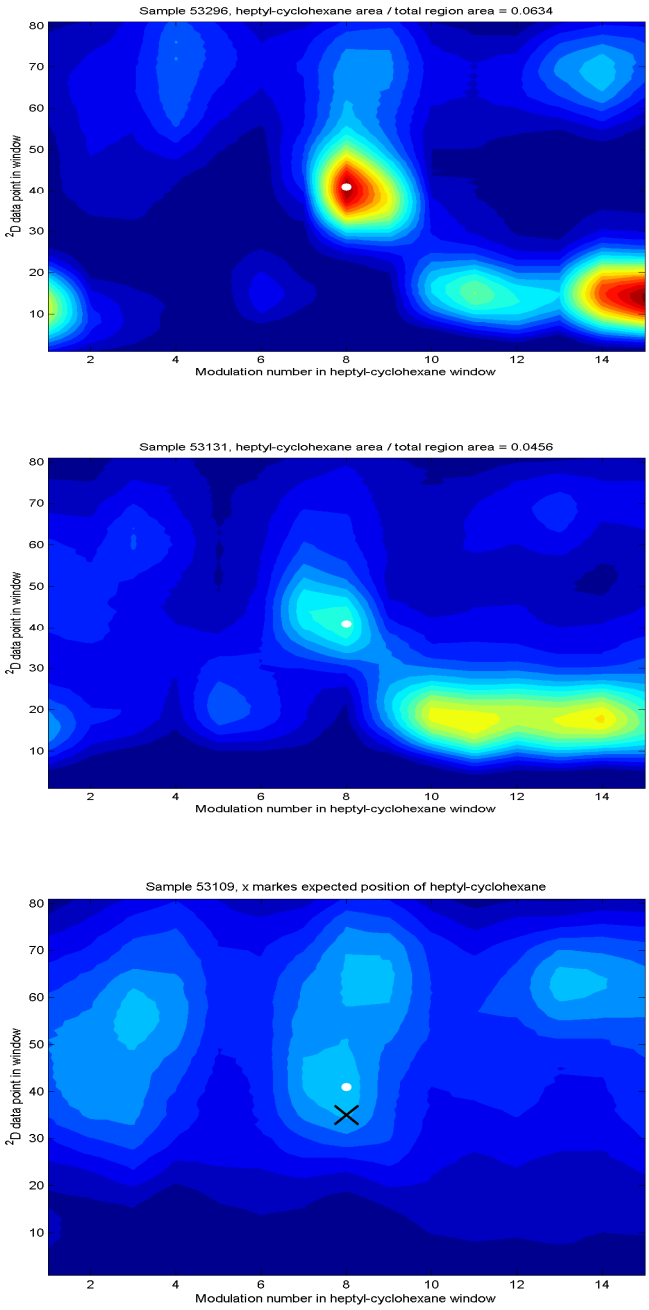

Figure 29. GCxGC-FID plots of the resolved compounds in the heptyl-cyclohexane region. In all cases the white dot is the local maxima corresponding to the automatically assigned position of heptyl-cyclohexane. Each subplot is contoured equally after the subplot was normalised such that total response in the elution window equals 1. Degradation increases from top to bottom. The cross in the lowest figure is located at the expected position of the heptyl-cyclohexane which is different to the located peak maxima in this case.

of the heptyl-cyclohexane region for the different samples, it is evident that they have undergone changes in composition to different extents. Since the GCxGC elution window is small the other compounds in this window possess similar volatility and polarity [131,132] when compared to heptyl-cyclohexane. The only mechanism able to induce such a targeted compound reduction is biodegradation. The samples are arranged such that biodegradation increases from the top to bottom. This extent of biodegradation is partially captured in the ratio of heptyl-cyclohexane area to the total area in the region shown. This ratio drops from 0.063 to 0.046 from sample 53296 to sample 53131. In the case of sample 53109 (the lowest plot in Figure 29) degradation has proceeded to the extent that formally minor compounds in the elution window now have similar concentration to the peak that would be automatically assigned to heptyl-cyclohexane. In such cases, especially given the presence of a peak partly overlapping the peak of interest, the automatic calculation of a reliable area for heptyl-cyclohexane is very difficult or impossible. Consequently the ratio of heptyl-cyclohexane area to the total area in the region shown is assessed as approximately zero.

It is also important to note that the PHC concentrations in the samples in Figure 29 were all identified as " < 200 " mg/kg with the GC-FID method employed at Macquarie Island [2]. In contrast the GCxGC approach is able to both reliably detect fuels at concentrations at and below 200 mg/kg and give compound / region specific fingerprinting information that is simply not possible with direct GC analysis of PHCs in

[2] Method TNRCC 1005 has an estimate method quantitation limit of 50 mg/kg TPH in the range *n*-C_6 to *n*-C_{35}. This TNRCC GC-FID method uses a 1.0 to 1.5 µL splitless injection, large diameter GC columns accepting 3 to 6 mL/minute carrier gas and TPH calibration standards up to 5000 mg/kg. As the 'Macquarie Island' GC-FID method uses a 15x to 20x reduction in initial injection and 0.25 mm i.d. GC columns (allowing greater compound separation) the higher method quantitation limit with the 'Macquarie Island' GC-FID method is expected and inline with expectations. In this case the method emphasis on greater separation of individual compounds was required by AAD staff.

a soil extract. The TPH results for these samples are shown in Table 13. As the GCxGC instrument baseline is observed for a significant portion of each modulation the within run, FID drift can be corrected much more reliably, compared to GC-FID analysis. This is reflected in the standard uncertainty for blank correction of ± 7 mg/kg compared to the Macquarie Island standard uncertainty for GC-FID blank correction of approximately ± 100 mg/kg.

Table 13. GC-FID and GCxGC-FID results for samples showing different extents of biodegradation and indicative biodegradation ratio heptyl-cyclohexane / local region (GCxGC-FID area / area).

Sample number	GC-FID TPH mg/kg (dry soil)	GCxGC-FID TPH mg/kg (dry soil)	Ratio heptyl-cyclohexane / local region	Level of biodegradation
53296	<200	300	0.063	0-1
53131	<200	620	0.046	3
53109	<200	240	~0	3~4

Examination of the biodegradation index, shown in Table 12, would indicate that sample 53296 is only at an early stage of biodegradation (at most) since the *n*-alkane signature is unaffected. Sample 53131 is at, approximately, biodegradation level 3 since the heptyl-cyclohexane is depleted (as well as the other alkyl-cyclohexanes).

Examination of the rest of the GCxGC chromatogram for sample 53131 shows that the *n*-alkanes are difficult to detect or absent (i.e. >90% depleted), which is the other expected composition change. Sample 53109 shows no evidence of any *n*-alkanes and the presence of alkyl-cyclohexanes (including heptyl-cyclohexane shown in Figure 29) is doubtful. The problem of measuring a particular, low abundance, biomarker against a

background of many co-eluting compounds a universal problem across fuel analysis. As degradation depletes the marker compound it leaves an UCM with numerous components that have the same, or very similar, retention behavior. The presence of significant acyclic isoprenoids but the absence, or near absence, of alkyl-cyclohexanes puts this sample (53109) at biodegradation level 3 or 4.

GC-MS methods, for the analysis of alkyl-cyclohexanes, typically use the 83^+ m/z ion (from $C_6H_{11}^+$) for identification and quantitation [159,160]. This extracted ion, from the analysis of several samples with a full scan GC-MS method, is shown in Figure 30 with comparison to the total ion chromatogram. As can be seen the 83^+ m/z ion is somewhat selective for the series of alkyl-cyclohexanes but there are clearly many other components that give this fragment ion. It can be seen that direct GC-MS analysis on the soil extract is useful for detecting elevated concentrations of alkyl-cyclohexanes but is not without its own set of problems, particularly baseline assessment, at lower alkyl-cyclohexane abundance. This is similar to the problems identified with the GCxGC approach shown in Figure 29. As such, both methods have the capability to detect this class of compounds but the reliability of that detection will depend on the exact instrument method, the sample composition and the efforts taken when examining the available data

5.4 Analysis of Aromatics

For a GCxGC analysis of PHCs in environmental samples to be effective it is necessary to be able to differentiate between aromatic and aliphatic fractions and measure each fraction [96,107]. It is of particular importance to be able to implement this at a remote site since clean-up guidelines for aliphatics and aromatics (of the same carbon range) differ by up to a factor of 20 [93]. The aromatic / aliphatic separation is also important as it reveals, when enhanced aromatics are seen, that aqueous transport is

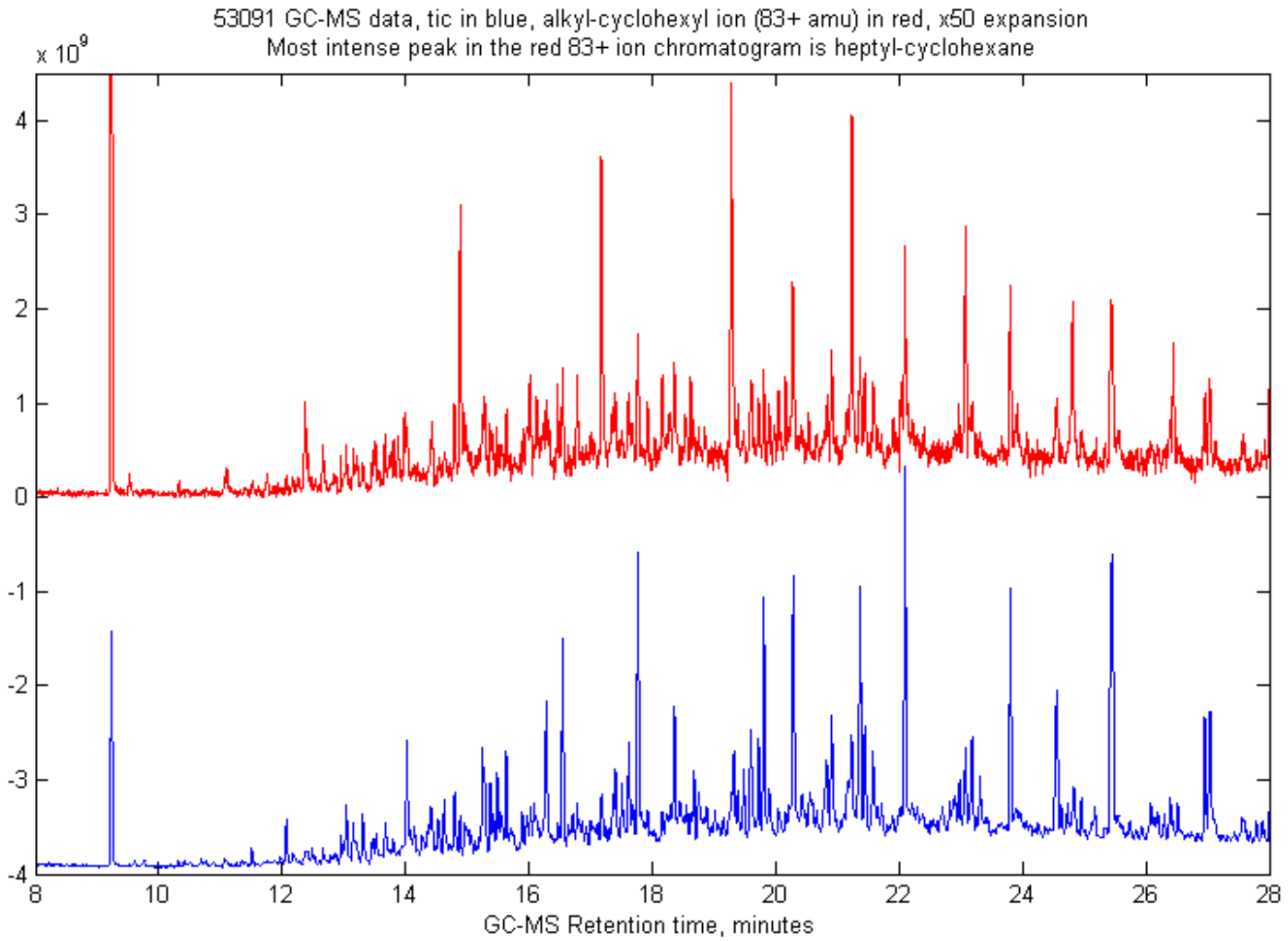

Figure 30. GC-MS data for sample 53091. Blue trace is for the total ion chromatogram, red trace is for the alkyl-cyclohexyl quantitation ion, 83^{+}.

moving the more soluble aromatic components from the NAPL into the surrounding environment [139].

5.4.1 Enhancement of water soluble aromatics via ground water flows

A careful review of the GCxGC data from the analysis of the 88 site samples indicated that only two samples showed clear evidence of an enhanced aromatic content, samples 53115 and 53187. The separate data mining techniques presented in Chapter 6, especially Figure 41 and the associated text, independently identify these two samples as being markedly different to other samples and enriched with soluble aromatic components. These samples are both found in similar settings on the outlet side of water flow through the SAB contamination plume. To a significantly lesser extent, sample 53223 shows some aromatic enhancement but the extremely low concentration of fuel in this sample (~4 mg/kg) makes the presence of any PHC components difficult to confirm (and makes it impossible to make any definitive comment on fuel composition). Sample 53115 has a reported TPH value of 320 mg/kg from the GC analysis while the GCxGC puts it at 95 mg/kg. Given the amount of drift seen in the GC baseline, as shown in Figure 31, and the difficulty of assessing GC baseline when components from *n*-C_9 to *n*-C_{40} may be eluting as a broad, low concentration UCM, it is likely that the GC result is a significant overestimate of TPH. The return of the GCxGC baseline (to FID noise) can be seen at the minimum and maximum ^{2}D retention times shown in the top plot in Figure 32.

For bore MI08FF #05 (the bore containing sample 53115) combining the available analysis data (for all the bore sub-samples) and the corresponding field excavation notes is informative. The combined data from bore MI08FF #05 samples [161], and the notes

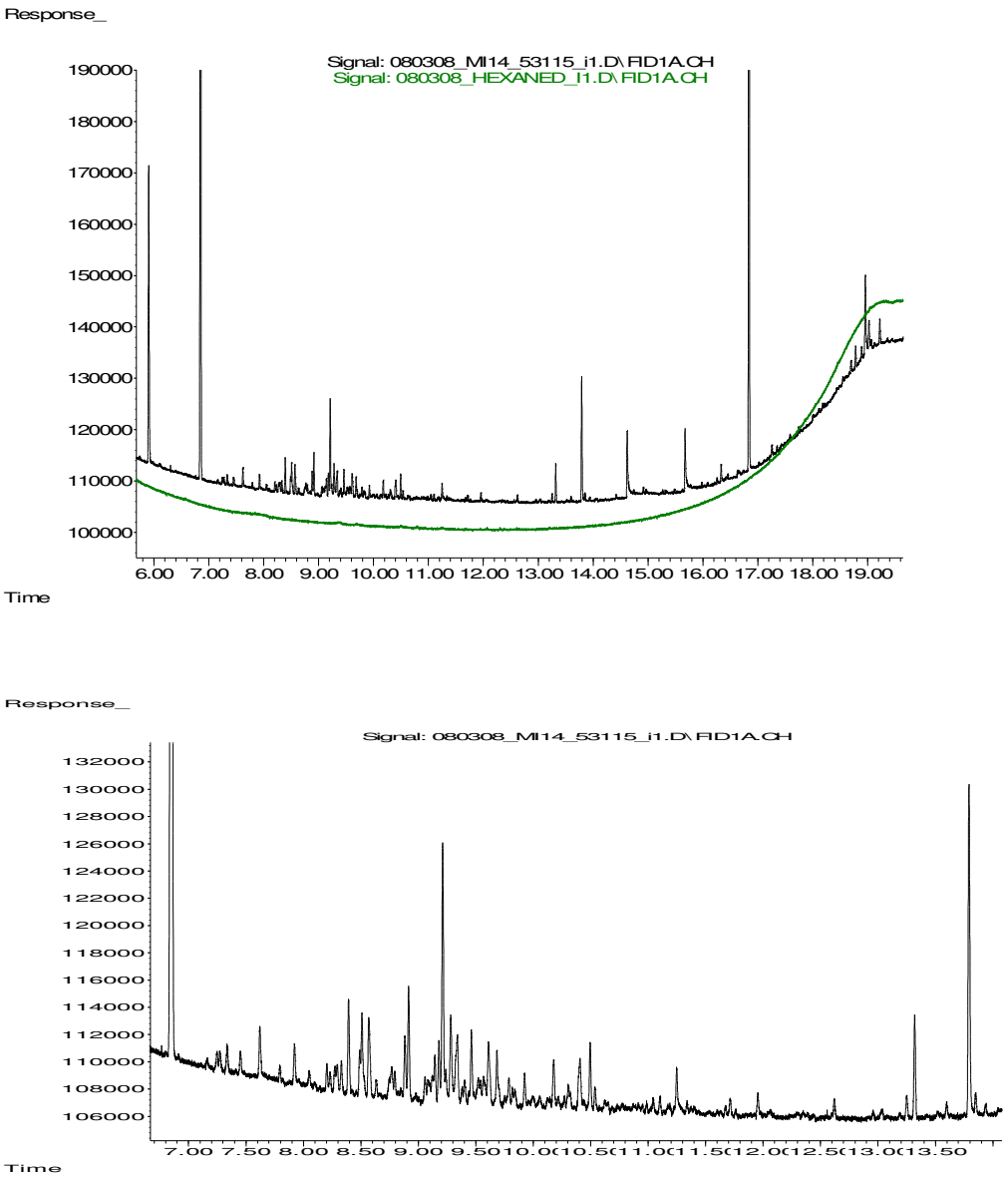

Figure 31. Top GC-FID analysis of sample 53115 (black) and a blank (green), from within the same analysis sequence, showing the deviation of the GC-FID baseline during an analysis. Bottom, Expansion of the GC-FID chromatogram from the internal standard cyclo-octane (on left) and d_{10}-anthracene (on right). The presence of some biomarkers (*n*-alkanes and acyclic isoprenoids) can just be discerned in the last third of the expansion. No other peaks are able to be identified.

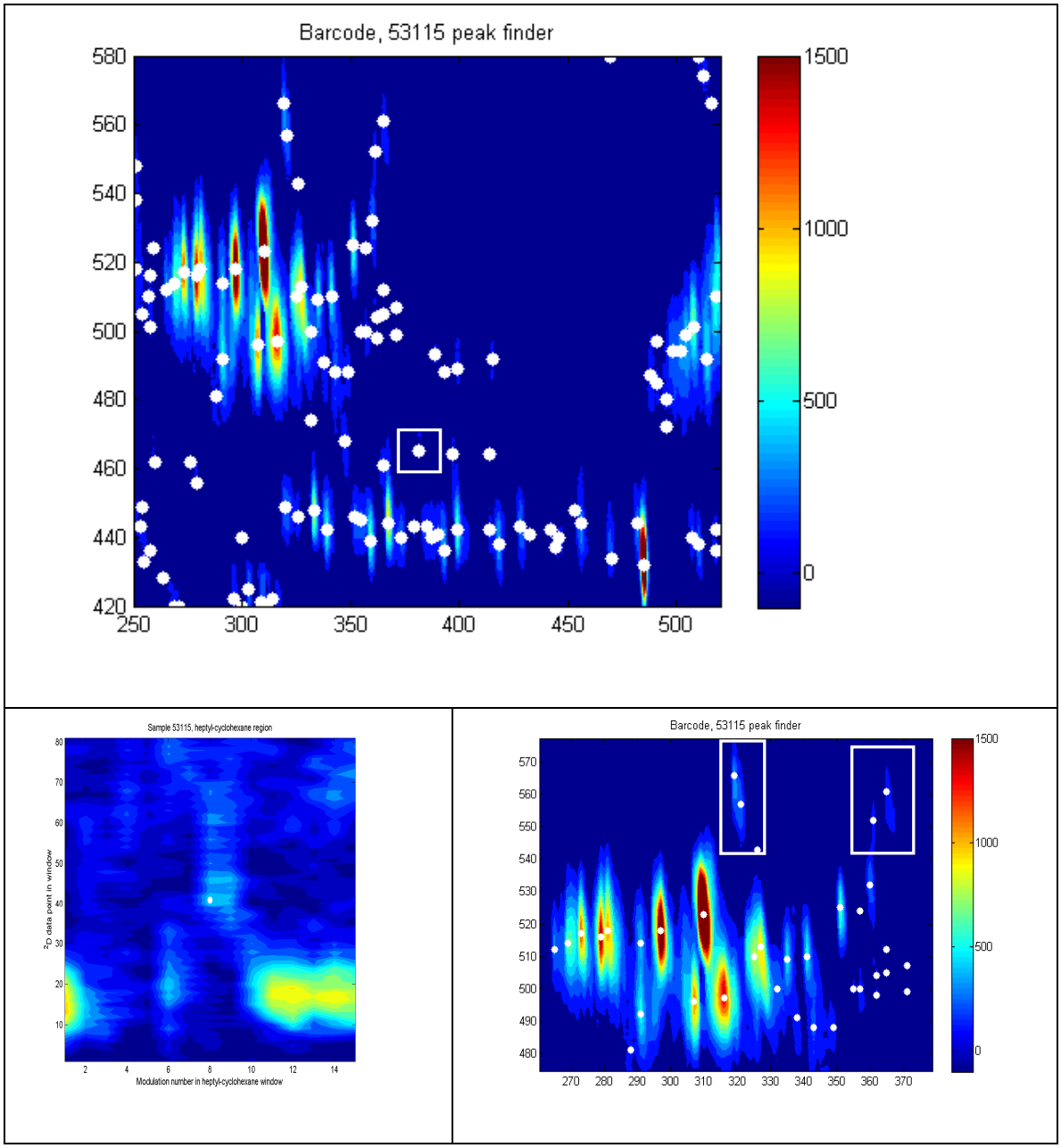

Figure 32. Top, GCxGC-FID analysis of sample 53115 contoured from -100 to 1500. White dots are the identified local maxima with a height of 100 or greater. The white square is the local maxima in the elution region of heptyl-cyclohexane. Bottom left, expansion of the heptyl-cyclohexane region for sample 53115. Pattern is consistent with minimal aliphatic biodegradation and the presence of *n*-alkanes in the sample confirms this. Bottom right, expansion of the aromatic region, white squares identify the regions for naphthalene and the region containing the two different methyl-naphthalene isomers.

that were written during bore excavation are shown in Table 14. In terms of the excavation notes the absence of PHCs in the top layer was correctly noted as was the presence of PHCs in all the lower layers. The excavation notes are not, however, useful in determining the concentration of PHCs. The sample with the highest TPH value (sample 53112 with ~7700 mg/kg PHCs) is merely noted as "some PHC" during excavation.

A feature that is particularly interesting in the excavation notes is the layer at 800 to 900 mm which is described as "cobbles and rocks" implying the presence of a soil layer with high water permeability. The observation of "free phase PHC" at a depth of 1700 to 1800 mm indicated a high water content and the presence of NAPL. While this does not correlate with a high soil TPH value it is below the layer with "cobbles and rocks". The cobble and rock layer itself has a very low PHC content, presumably because the pore structure and low surface area of the cobbles is unable to retain significant amounts of NAPL. The layers above and below this layer have high PHC content. The PID values from the bore correlate relatively well to TPH value with the most notable exception coming from the cobbled layer. This device responds to volatilised organics so the relatively high PID response for this sample is consistent with poorly absorbed NAPL that easily evaporated when bore MI08FF #05 was dug.

The θg values (% water content calculated relative to soil mass after drying the soil at 105 °C) sharply increase at a depth of 1400 to 1500 mm [161]. This is below the cobbles and rocks, but above the level of observed free phase NAPL, so the water table may well be located at this point. The sample from a depth of 1400 to 1500 mm has an anomalously high total carbon content of 6.4% when compared to the entire Fuel Farm average and standard deviation (0.77 % ± 0.92 %). This is very unusual as it is almost

Table 14. Excavation notes and available data for bore MI08FF #05. θ_g, is the m/m % water based on the mass of dry soil in a given subsample. Sample 53115, shown in bold, has enhanced aromatics in the extracted PHCs.

Sample barcode	Sample depth mm, upper	Sample depth mm, lower	θ_g, (water content of the TPH sample)	TC (% w/w)	Excavation Notes/ Observations.	GCxGC-FID TPH	GC-FID TPH	Chromatogram Interpretation from GC-FID	Bore PID response
53100	50	150	13.0%	0.5%	sandy peat	0	ND		1.9
53103	200	300	22.3%	0.8%	PHC gravel	38	ND		1.9
53106	500	600	19.1%	0.7%	PHC layer	4443	4860	diesel	37.9
53109	800	900	31.1%	1.2%	Cobbles and rocks	239	<200	SAB	40.7
53112	1100	1200	19.8%	0.4%	some PHC	7775	7620	SAB	88.8
53115	**1400**	**1500**	**117.9%**	**6.4%**	**PHC, tar balls**	**95**	**380**	**NOM & SAB?**	**8.1**
53131	1500		98.5%			632	240	SAB & NOM	
53130	1500		74.0%			185	240	SAB & NOM	
53118	1700	1800	21.8%	1.9%	free phase PHC	26	ND		7.6
53121	1900	2000	17.5%	0.2%	PHC	17	<200	SAB	2.9
53124	2050	2150	14.7%	0.2%	Gravel with PHC	39	<200	SAB	2.6
53127	2190	2300	18.4%	0.1%	Gravel with PHC	1634	1960	SAB	65.8
53132	2393		17.6%			631	560	SAB	

double the value of the next highest sample from the Fuel Farm. The near surface sample with a high TPH value (53106, with ~4500 mg/kg PHCs) is noted, in the GC-FID chromatogram interpretation, as diesel. Since no records exist for the shipping of anything but SAB to Macquarie Island, it appears likely that the PHCs profile observed in 53106 is the result of extensive gas phase loss of volatiles from SAB itself. The profile of lost components is, however, not consistent with direct evaporation of liquid SAB at site temperatures [162,163]. Rather, it seems likely that the near surface sample has had gas phase loss / evaporation controlled by component diffusion within the NAPL to the NAPL surface in the soil pore structure.

Bore (MI08FF #05) is located at the ocean edge of the Fuel Farm site. As such the ground water passing through the bore has passed through the PHC plume that is located back towards the Fuel Farm tanks and associated pipes. Combining all this site analysis indicates that the sample 53115 is uniquely situated to be exposed to aromatic saturated ground water flows while being sufficiently deep to avoid evaporative loss of these volatile aromatics. Additionally, the high carbon content of the soil can absorb these aqueous aromatics and therefore accumulate and concentrate the water-soluble fraction from the up-gradient SAB spill. Given the low concentration (~95 mg/kg by GCxGC-FID) of aromatics in sample 53115 and given that no other sample showed enhanced aromatics it is reasonable to conclude that ground water aromatic transport of PHCs at the site is slow with low concentrations of aromatics in the ground water. The unique combination of site setting, water table level and very high carbon content all combine to make it possible to detect this transport mechanism in the case of sample 53115.

5.4.2 Identification of 2-4 ring PAHs with GCxGC-FID and GC-MS

With the injection of retention time marker standards (such as the WC5 and EPH mixes) a range of 2-4 ring PAHs and alkyl PAHs can be identified. The compounds of interest are identified in Table 15, with the retention times taken from the first two injections of the sequence used to assess the Macquarie Island Fuel Farm samples. The GCxGC data for the retention time assessment is shown in Figure 33. Examination of site sample 53184, (with ~13000 mg/kg PHC) indicates that the largest PAH identified in site samples is pyrene (peak #11, with the adjacent peak #12 tentatively assigned to a methyl pyrene isomer). The C1, C2 and C3 alkylated naphthalene groups have ^{2}D retention times of ~2.8 s and appear as identifiable groups. The C1, C2 and C3 alkylated phenanthrene and anthracene groups have a ^{2}D retention time of ~3.1 s and appear as separated bands in Figure 33. The raw GCxGC-FID data for sample 53184 is shown in Figure 34.

A more direct comparison of sample 53184 and the retention time marker mix is shown in Figure 35. Retention time alignment is based solely on making the maxima of the internal standard 1-bromoeicosane coincide [66], a process that is able to be quickly implemented automatically with the algorithm written to find local maxima in a specified ^{1}D and ^{2}D elution window. Due to phase shifts of the compounds entering the modulator from the ^{1}D column, and the PFM skewing effect, such an alignment approach will not be perfect. Despite this, the obvious correlation between the marker mix and the sample is excellent, especially when it is considered that the sample was analysed after 68 other injections. A significant virtue of such an alignment approach is that no computationally intensive interpolation is required when mapping the sample data onto the data points of the retention time marker mixture. Avoiding an interpolation step also avoids any bias

Table 15. PAH and alkyl PAH GCxGC-FID retention table and numbering scheme for following figures.

Number	Name	^{1}D retention time, minutes	^{2}D retention time, seconds
1	Naphthalene	19.20	2.780
2	2-Methylnaphthalene	21.66	2.750
3	1-Methylnaphthalene	21.96	2.770
4	Acenaphthylene [ND]	24.48	2.905
5	Acenaphthene [ND]	25.08	2.880
6	Fluorene [ND]	26.82	2.900
7	d_{10}-Anthracene * [#]	29.88	3.120
8	Phenanthrene [#]	29.88	3.120
9	Anthracene	30.00	3.090
10	Fluoranthene [ND]	33.78	3.320
11	Pyrene	34.44	3.415
12	Methylpyrene isomer [(tentative assignment)]	36.24	3.465
13	Benz(a)anthracene [ND]	38.40	3.510
14	Chrysene [ND]	38.52	3.515
15	1,1':4',1"-Terphenyl *	35.16	2.970
16	2,2'-Dimethyl-1,1'-binaphthalene *	37.32	2.890
17	Benzo(b)fluoranthenes [# ND]	41.82	3.745
18	Benzo(k)fluoranthenes [# ND]	41.82	3.745
19	Benzo(a)pyrene [ND]	42.6	3.900
20	Indeno(1,2,3-cd)pyrene [ND]	45.6	3.93
21	Dibenzo(a,h)anthracene [ND]	45.6	4.045
22	Benzo(g,h,i)perylene [ND]	46.14	4.225

* = Internal standard or trial internal standard, [ND] = Not Detected in Macquarie Island soil extracts.

[#] = co-eluting compounds leading to a single GCxGC maximum.

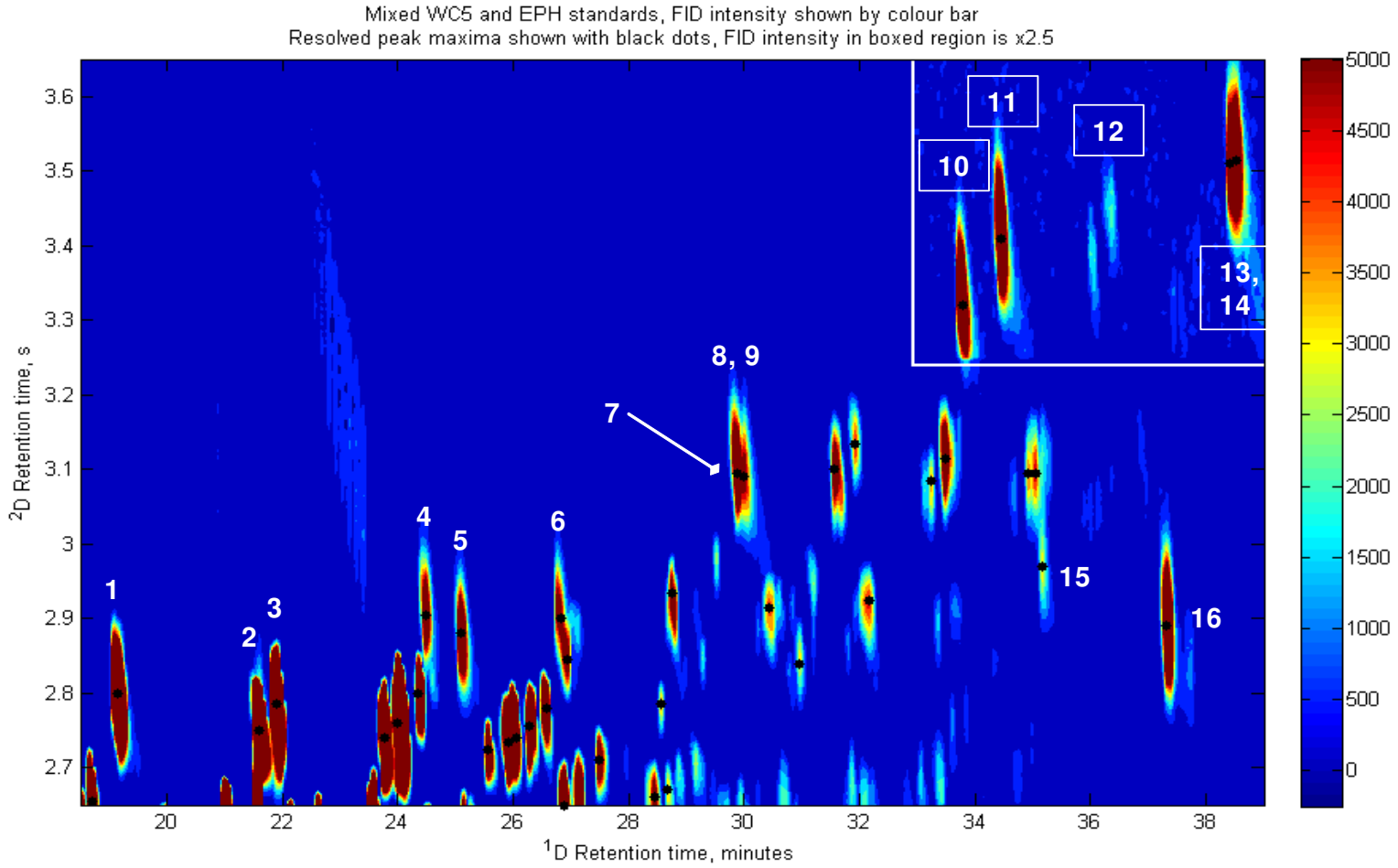

Figure 33. Identified 2-4 ring PAHs in retention time marker mixes, WC5 and EPH. See Table 15 for the compound names for the numbered peaks.

that can arise during interpolation and lets the user see the acquired instrument data in a form as close to the raw data as possible.

While more sophisticated warping approaches are possible, so that GCxGC retention time correlation is improved, these methods require the identification of equivalent features in the samples to be correlated [66]. While many such equivalent features appear between a relatively fresh fuel and a retention time marker mix, changes due to biodegradation (Table 12) and abiotic weathering will make such feature selection harder when a range of site samples are investigated.

The boxed region in Figure 34 and Figure 35, with the FID data intensified by a factor of 50, is the elution region for four-ring PAHs in sample 53184. In sample 53184 fluoranthene (peak 10, Table 15) is absent while pyrene (peak 11) is present in very low concentrations (15 µg/kg). The additional peak in the elution region of 4 ring PAHs (peak 12) has GCxGC retention times consistent with it being a methylpyrene isomer (with an estimated concentration of 10 µg/kg). The absence of fluoranthenes is expected since fluoranthenes are less thermodynamically stable than the pyrenes. Reported analysis of diesel range fuels indicates that pyrenes are more abundant than fluoranthenes. Pyrenes have been measured at similar mass fractions in neat diesel fuels to the pyrene / fuel mass fraction measured for this sample (1.2 mg/kg).

5.4.3 Identification of 3-4 ring PAHs with GC-MS.

Sample 53184 was analysed by GC-MS and the quantitation ions [159,160] for the C1-C3 alkylated isomers of phenanthrene + anthracene are shown in Figure 36 (middle and lower plots respectively). While pyrene and methyl pyrene can be identified (at 31.7

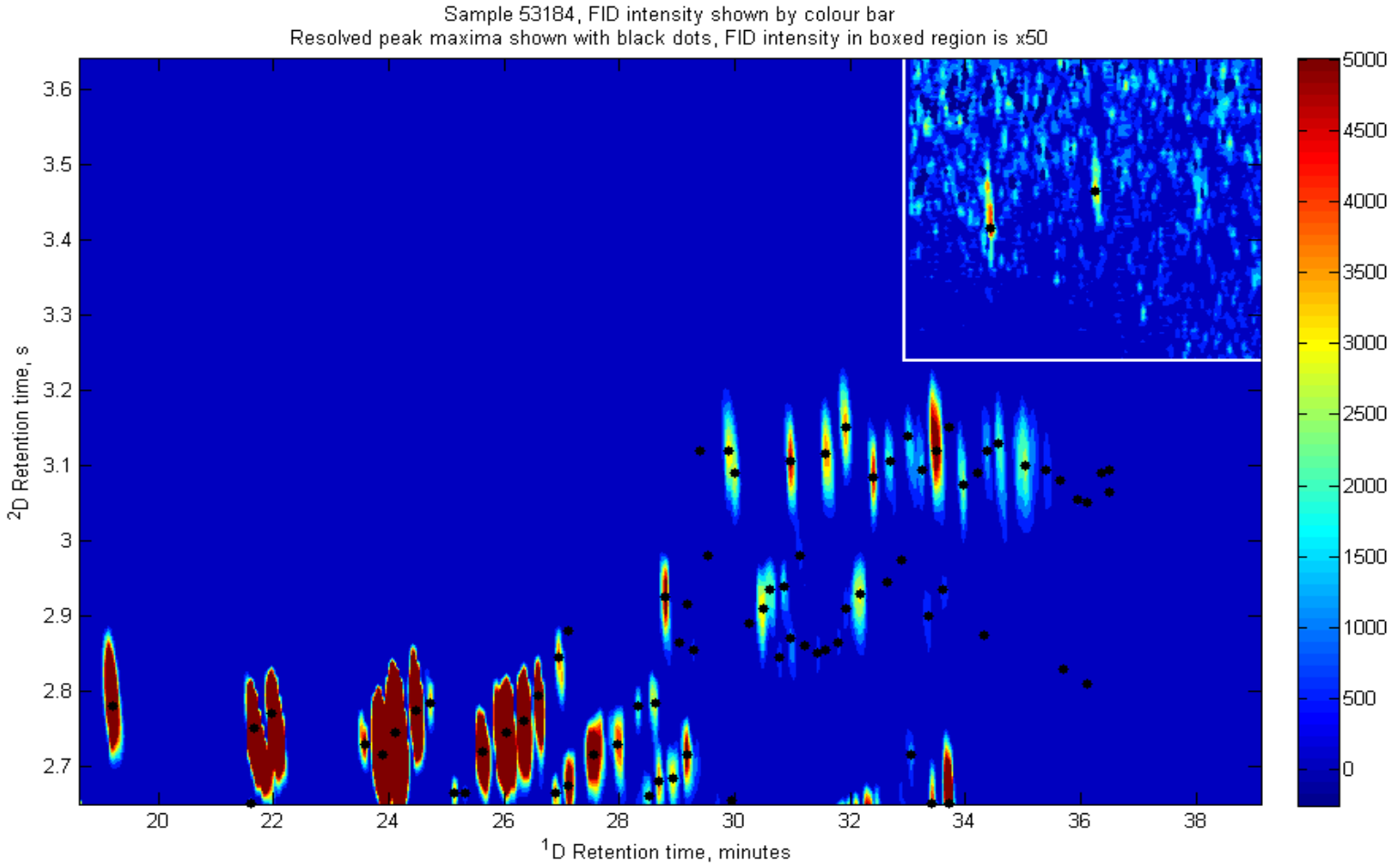

Figure 34. Sample 53184, GCxGC-FID elution region for 2-4 ring PAHs with identification of local maxima.

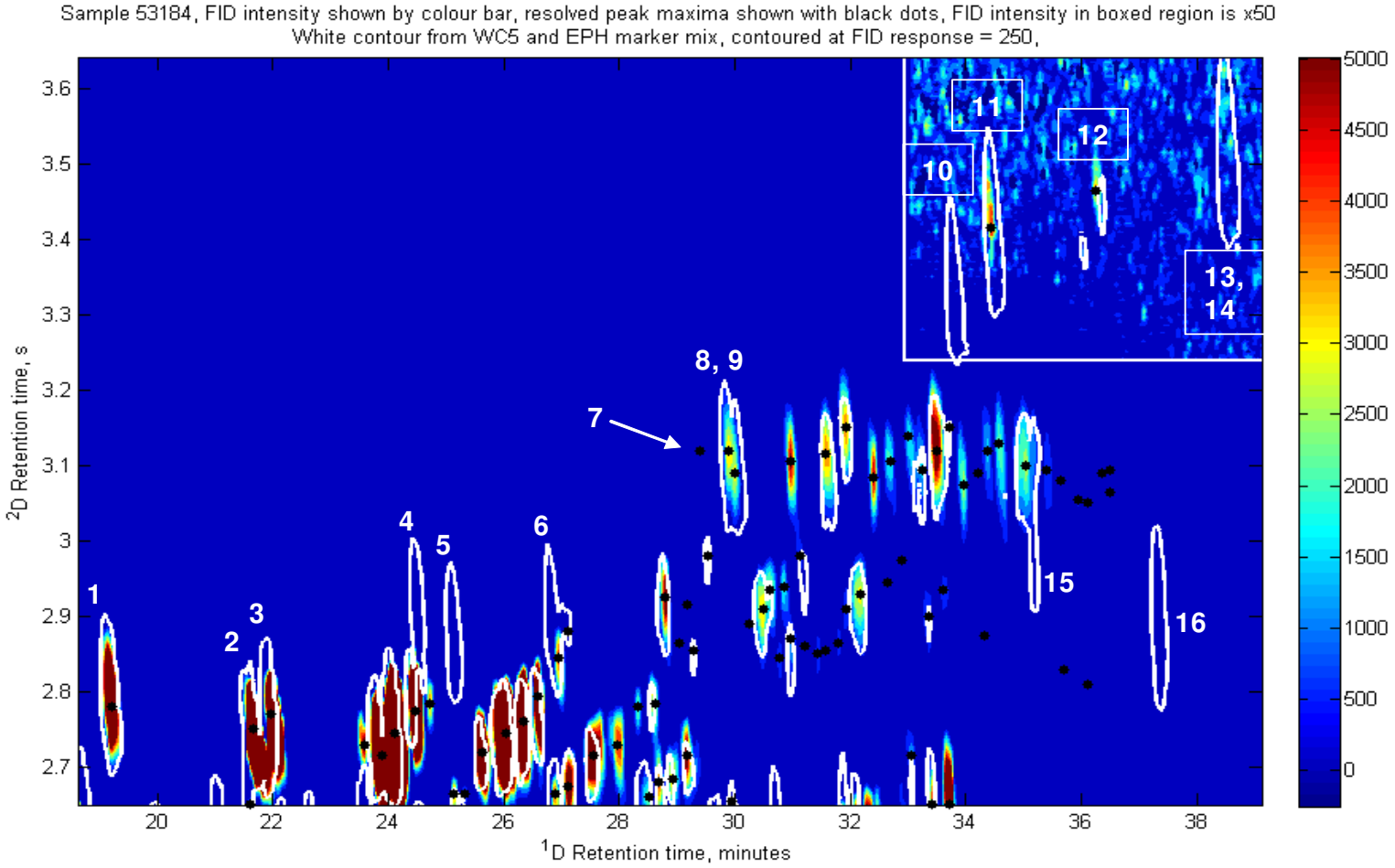

Figure 35. Sample 53184 shown as the filled colour contour plot. Overlay is a single contour from retention time marker mixes. Alignment carried out with the internal standard bromoeicosane (sample 53184 had 0.12 minutes added to ^{1}D retention time and 0.010 s subtracted from ^{2}D retention time).

min and 33.5 minutes respectively) the presence of other signals in the GC-MS data for m/z 202 indicates that the GC-MS data is not perfectly selective. These other signals occur at the same retention times as the major C2 and C3 phenanthrenes + anthracenes (a situation similar to the attempted quantitation of low C2 naphthalene concentrations against a high fuel background).

5.5 Conclusions

The ability of PFM GCxGC to reliably analyse a batch of >100 samples and standards for PHC contaminated site assessment has been demonstrated. The hardware has proved satisfactory for extended use with little operator input or repair. Quality of TPH assessment from the acquired GCxGC-FID data matches or exceeds that acquired with GC-FID [94,96,107,108], a technique widely used for PHC assessment. The GCxGC separation space not containing eluting PHC components or siloxanes is used to effect an automated modulation by modulation baseline correction (see experimental section 2.5) and thus give a very low limit of detection.

The information obtained from GCxGC approach greatly exceeds that obtained with GC-FID and allows site processes (especially soluble aromatic transport) to be directly observed [139] as illustrated by the detailed analysis of selected samples. This is coupled with the ability of the technique to predict PHC component volatility and water solubility based on retention position [131,132,164,165]. The technique is therefore especially effective for an assessment of a PHC spill in an environmentally sensitive region. Furthermore, with a PFM modulator, this site assessment can be carried out anywhere a conventional GC instrument can be installed and operated.

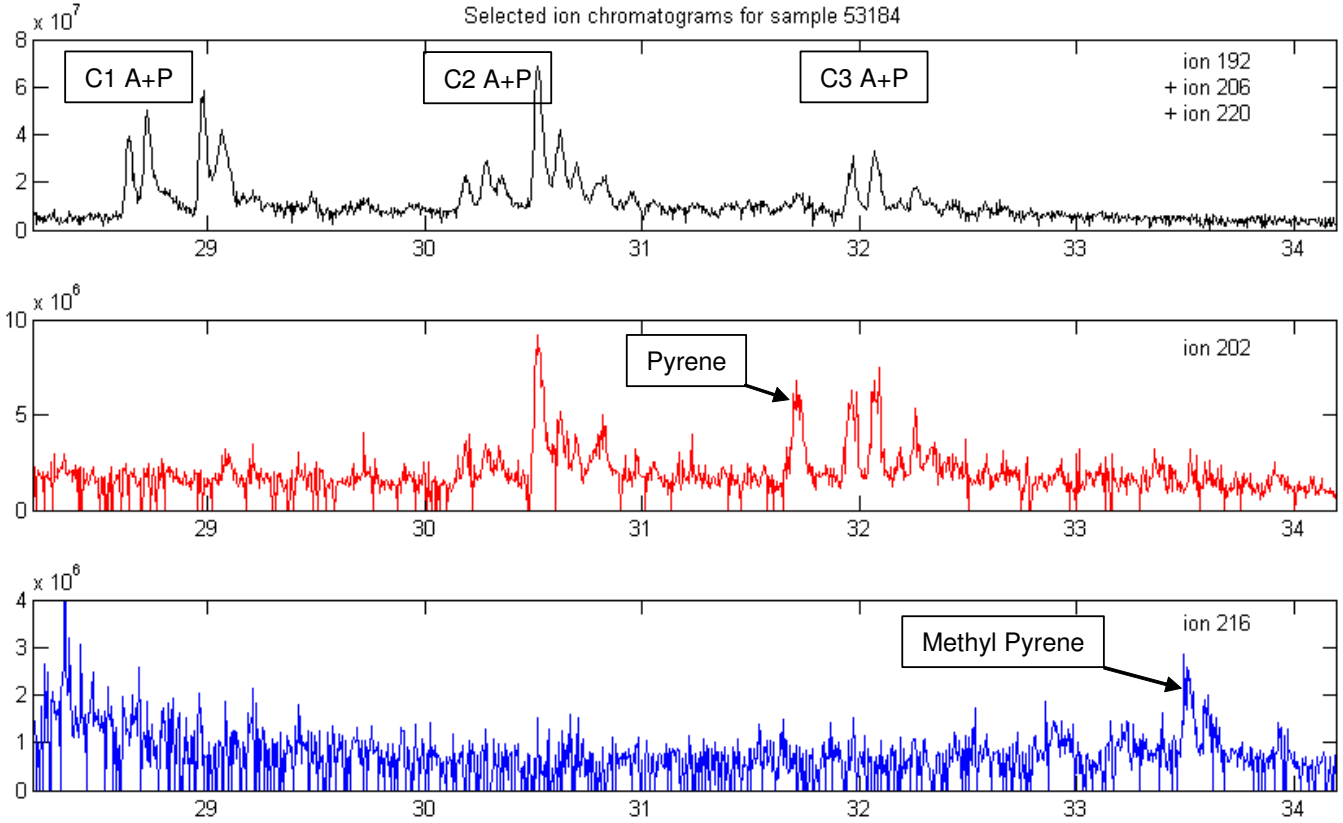

Figure 36. GC-MS data from sample 53184. Upper plot, ions for C1-C3 alkylated phenanthrene + anthracene (A+P). Middle plot, ion for pyrene (31.7 min) with smaller signals for fragments from C2-C3 alkylated phenanthrene + anthracene. Lower plot, ion for the C1 pyrenes.

In this way the hardware and methodology presented here are a realisation of the portability noted by Cortes *et al*. [62].

In comparison to GC-MS analysis (directly on a hexane soil extract) the technique offers similar or superior class selectivity when biodegradation etc has reduced an analyte class to very low concentrations against a relatively high background of weathered fuel. It appears that the GCxGC separation of the classes is superior for class quantification compared to GC-MS analysis when the analysis is carried out directly on the PHC extract. The ability of the GCxGC approach to detect pyrene and methylpyrene, at concentrations of 15 and 10 µg/kg respectively, in a field sample with ~13000 mg/kg PHCs is a good demonstration of this. The very significant cost reduction in purchasing, calibrating, operating and maintaining PFM GCxGC system compared to GC-MS should lead to GCxGC methods being used more frequently for PHC contaminated site assessment.

6 Data mining techniques for the analysis of GCxGC-FID data from the assessment of a PHC contaminated site, parts submitted in Anal. Chem., March 2012

6.1 Introduction

Statistical tools are regularly used in the analysis of environmental data such as chemical signatures or fauna and flora observations [166]. The techniques are also useful to compare multiple sites that range from being highly contaminated to undisturbed natural settings. The acquisition of a comprehensive set of GCxGC-FID data from a PHC site provided an opportunity to investigate use of statistical tools suited to the overall analysis of multiple samples. Rather than carefully reporting the many features observable in a GCxGC chromatogram the data were binned into environmentally significant groups (as done by Arey *et al*. [131,132]) in order to simplify the data analysis while preserving the separation of the important environmental groups [66,132]. Following data binning of every GCxGC-FID analysed PHC contaminated site sample, the resulting data set may be combined and analysed so that PHC compositional variations across the site can be rapidly identified. In this manner the environmental

processes governing PHC fate at the site can be determined and investigated systematically [131,132].

The process of conversion of a raw GCxGC ASCII vector file into a rectangular matrix leads to an array spaced by modulation frequency on the x-axis and the detector frequency on the y-axis. With a temperature and pressure programmed GCxGC approach this leads to the classes of compounds appearing as curved bands on the two-dimensional separation space [66,167]. Although the fitted curve in Figure 37 is easily followed with the eye, such a relationship is not as convenient to interpret as transformed data, where the structured compound series appear in linear arrangements [167]. Structured data with nonlinear alignments is also problematic when attempting to automatically group data based upon analyte class, i.e. when binning the GCxGC data into environmentally relevant categories. While it is possible to create bins that are curved shapes in the GCxGC chromatogram [131,132] this introduces significant problems. The difficulties with curved bins include the following: (1) it is a time-consuming process, (2) it requires specialist software and expert operation of that software, (3) it is difficult to implement over a long sequence when retention times might slowly drift during acquisition of a long sequence [66]. For these reasons, a straightforward automated method of aligning the data so that class patterns can be allocated to rectangular bins was developed.

6.2 Binning of GCxGC data

6.2.1 Class alignment

In order to align the data into rectangular class patterns several approaches were examined [167]. In addition to plotting ^{2}D retention in the standard format of retention

time, Harynuk *et al*. [167] manipulated data from the GCxGC analysis of FAME so that ^{2}D retention was plotted against retention factor. As part of their subsequent work, the concept of effective chain length (ECL) was used to examine retention behaviour unsaturated and branched FAMEs. The ECL was based on fitting a polynomial to a plot of the number of carbons in the chain of saturated linear FAME vs. retention time [167].

In the present work the concept of data alignment based on an ECL is used although the implementation is quite different. In this work each individual modulation slice was treated as a separate chromatographic analysis and the whole GCxGC chromatogram is transformed. The ^{2}D retention time was transformed onto a new scale by plotting relative retention compared to the acyclic aliphatics (i.e. absolute ^{2}D retention time divided by the time of the imaginary elution band fitted through the acyclic aliphatics). The fitted white line indicating the retention time of acyclic aliphatics shown in Figure 37 is based on the observed maxima of all the acyclic aliphatic components in the WC5 mixed fuel marker mix. These maxima were fitted to a cubic equation from ^{1}D retention times 10.92 minutes to 23.28 minutes and a linear equation after this. This resulted in all the acyclic aliphatic peak maxima being within 50 ms of the fitted line shown in Figure 37. The result from ^{2}D rescaling is shown in Figure 38. Of particular note is how the identifiable aromatic classes are arranged horizontally after alignment with the acyclic aliphatics. In particular naphthalene as well as the methylnaphthalenes, C2 and C3 naphthalenes all appear with a y range of 1.21 to 1.29 (Row 3, Figure 38). Such an alignment now allows these similar compounds to be placed into suitably positioned rectangular bins that have and environmental meaning and therefore may aid environmental interpretation

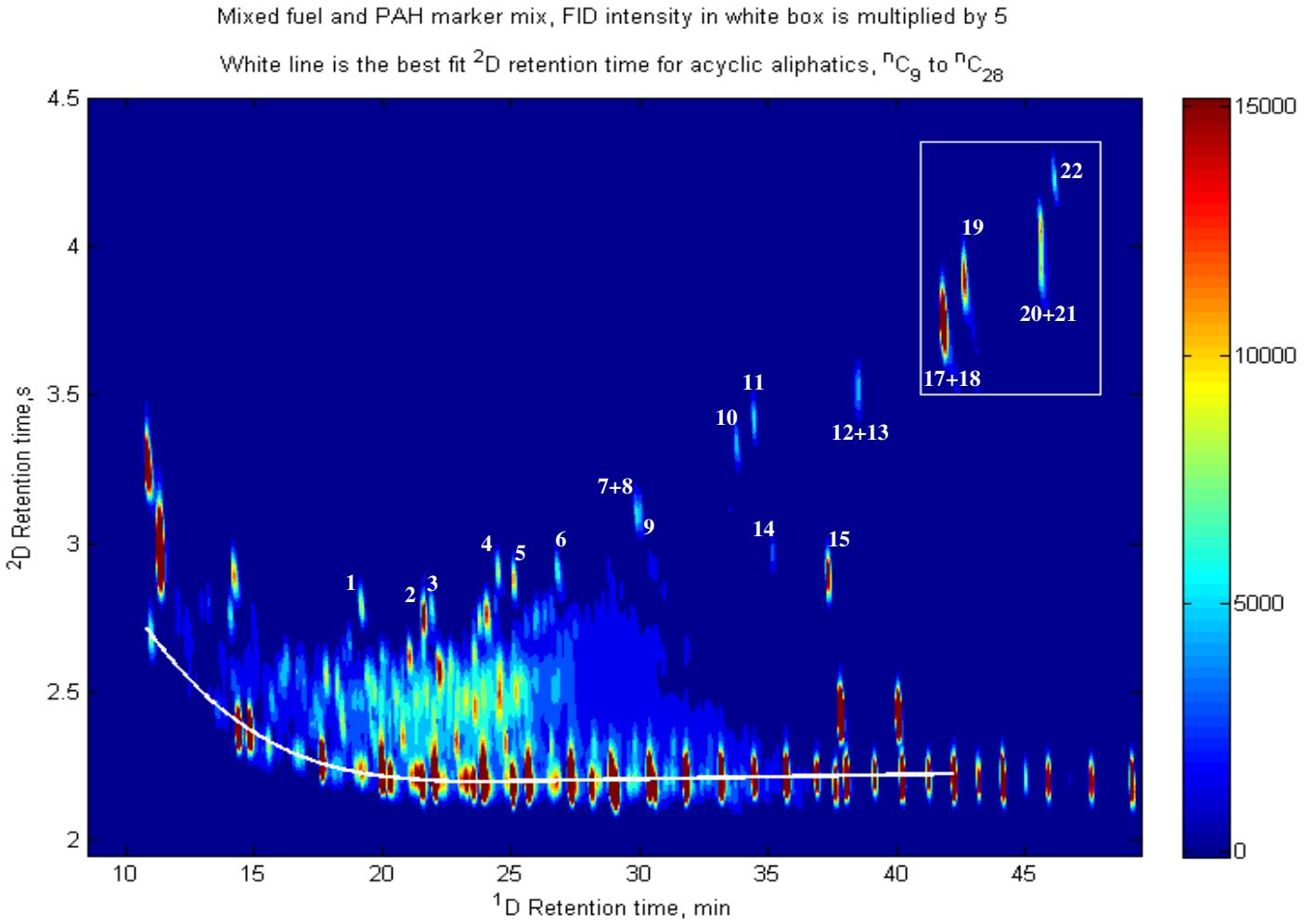

Figure 37. GCxGC-FID separation of diesel range components with PAH marker compounds added. The retention space shown in this figure ranges from *n*-C_9 to *n*-C_{36}, PHC classes range from acyclic aliphatics to Benzo(g,h,i)perylene with specific peak labels and elution times tabulated in Table 15 (page 130). White line is for the elution band drawn through the acyclic aliphatics.

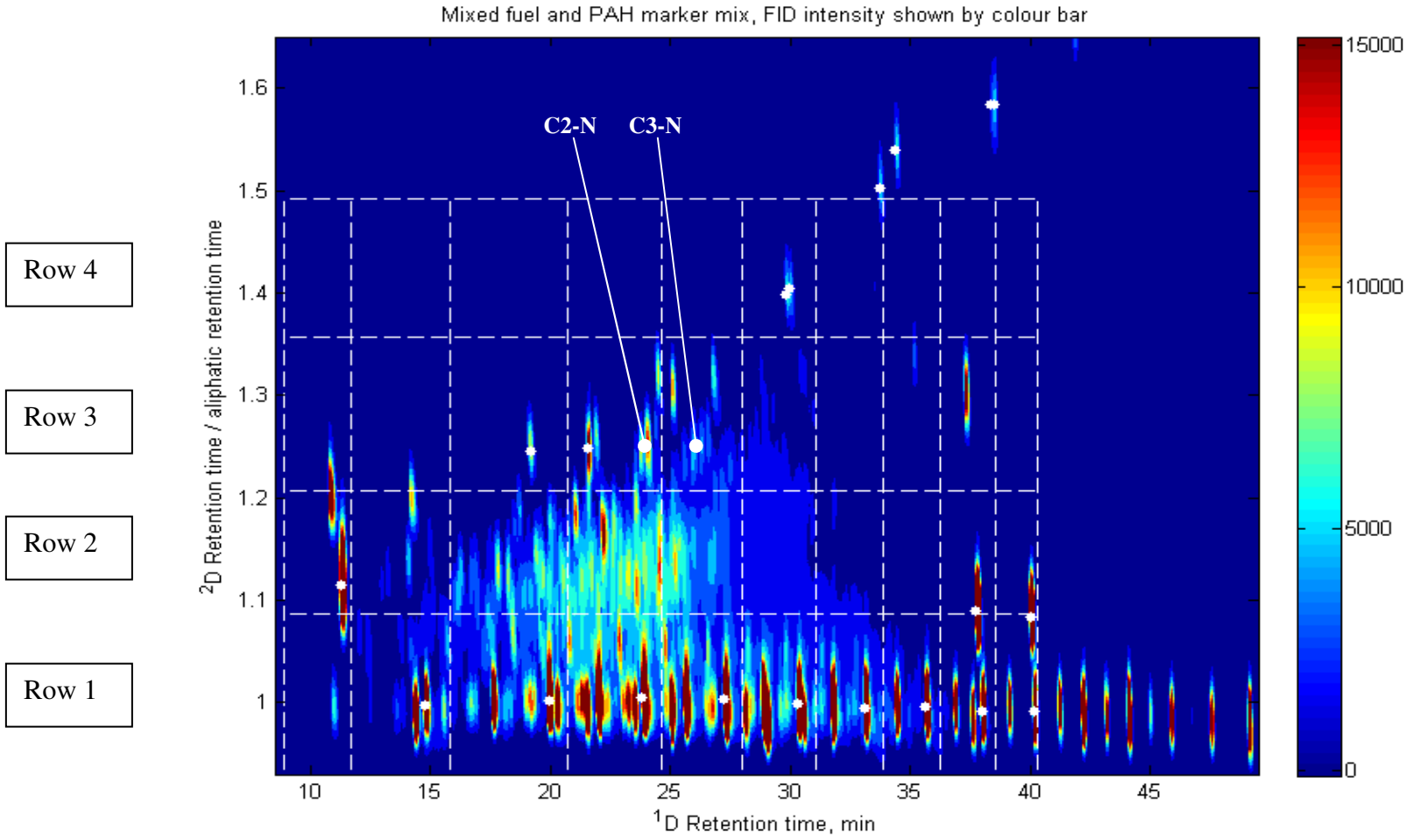

Figure 38. GCxGC data after modulation by modulation ^{2}D alignment with the average elution time of the acyclic aliphatics. Dashed white lines show the rectangular bins that the data was placed into. White dots at even *n*-alkanes *n*-C_{10} to *n*-C_{26} and selected compounds and PAHs from Table 15 (page 130). C2 and C3 naphthalenes are marked C2-N and C3-N respectively

6.2.2 Environmentally significant data-binning

Based on the binning shown with white dashed lines in Figure 38 the alkylated naphthalenes are all placed in the third row from the bottom. Several related priority PAHs (acenaphthylene, acenaphthene and fluorene) are located in this row. Each of these PAHs contains two aromatic rings with additional cyclisation within the molecule. The broad chemical assignment of the four different rows that the data is binned into in Figure 38 is, approximately,

Row 1 Acyclic aliphatics and alkyl cyclohexanes

Row 2 Alkyl benzenes and polycyclic aliphatics

Row 3 Alkyl naphthalenes and other alkylated two-aromatic ring structures

Row 4 Alkyl phenanthrenes, anthracenes and other alkylated three-aromatic ring structures

The division of the bins along the x-axis was driven principally by location of the *n*-alkanes [162,163]. Bin divisions were placed at a position mid way between *n*-alkanes with an even number of carbons and the following *n*-alkane (e.g. mid way between *n*-C_{14} and *n*-C_{15} etc). This spacing of two carbon units was chosen, in conjunction with the four levels in the y-axis, so that a sufficient number of bins were available to preserve the overall shape of the fuel envelope while keeping carbon number spacings often found in regulatory methods [96,107,108]. As a result of this the elution space is covered by 40 bins (with 24 bins containing diesel range organics).

In the work of Arey *et al*. [131,132] the spacings of data bins (called "*Two-Dimensional Finite Element Discretization of GCxGC Chromatograms*") are determined by calculating "*contours of hydrocarbon vapor pressure and aqueous solubility*" across

the raw GCxGC chromatograms. Arey *et al* has ~150 bins in the *n*-C_{11} to *n*-C_{24} range and implemented a method of partially assigning data near cell boundaries to multiple cells. In this manner spurious data analysis problems (arising from slight retention shifts of large GCxGC peaks near cell boundaries) were overcome and fractional fuel changes could be mapped for environmental samples.

The spacing used in this work is somewhat less frequent than the environmental partitioning used by Arey *et al*. [131,132] but more frequent than analysis methods developed by regulators for contaminated site assessment [96,107,108]. The data binning division used in this work also gave a modest number of bins which allows statical tools such, as MDS, to be easily applied and analyse 100 samples (including calibration standards). By having a lower number of bins the relative peak-area between bins becomes less sensitive to retention time alignment problems. In this way the relative effect from the shifting of a single component near a bin boundary from one bin to another bin in a different analysis is reduced so the additional step of partially assigning data near cell boundaries to multiple cells [131,132] was not required. The use of midpoints of the *n*-alkane ^{1}D elution times for the bin divisions also means that the abundant *n*-alkanes (in fresh SAB and diesel) are always binned correctly and not artificially split, into different bins from alignment problems and/or column overloading.

While the ^{2}D class assignments are not definitive they do allow the data to be binned into regions that will have similar environmental interpretation. In particular the first members of alkylated priority PAHs appear in appropriate bins. These are the classes that are typically targeted with isotope dilution GC-MS methods used for the analysis of a crude oil spill. These marker classes were used extensively to monitor the long-term

environmental fate of aromatics from the Exxon Valdez spill in Alaska [49,168,169]. It may be considered desirable to find GCxGC methods, separation columns and data binning methods that separate highly alkylated benzenes from polycyclic aliphatics. GCxGC methods with a polar ^{1}D column and non-polar ^{2}D column have attracted more interest in this regard [91,170] although method analysis times are in the order of 1-2 hours for analytes in the approximate range of *n*-C_9 to *n*-C_{30}. Such a method may better match data from aliphatic to aromatic separations performed with hexane on a silica stationary phase. In practice, however, all these compounds will have very low water solubility, low vapour pressure and have far lower toxicity than partially alkylated multi ring PAHs. It is also somewhat unclear as to how well the highly alkylated benzenes and polycyclic aliphatics, eluting from the ^{1}D column after ~*n*-C_{20}, remain separated. As such the separation methods and subsequent binning of these compounds (the highly alkylated benzenes and polycyclic aliphatics) into the second row from the bottom in Figure 38 is satisfactory when developing an understanding of a large site with many samples.

In order to counter GCxGC retention drift across the sequence the maximum of the internal standard 1-bromoeicosane was aligned to the observed maximum of 1-bromoeicosane in the mixed fuel + PAH retention marker mixture. The bounds for the binning were developed with the retention marker mixture (Figure 38) the analyte groups are aligned into correct bins with this process. By carrying out a simple, discrete integer, shift in the x and y directions of the data it is not necessary to partition any modulation at a bin boundary into two different bins. This would, however, be required if the cyclooctane (cC_8) internal standard was used to warp or stretch the data based on two reliably identified features in the GCxGC chromatogram. Observations of the maxima for

the d_{10}-Anthracene and cC_8 internal standards show that this shifting alignment gives stable retention locations across the analysis sequence. The greatest discrepancy is in the ^1D retention of cC_8 which varies by a maximum of to two modulations from the expected position. Additionally cC_8 varies significantly more than *n*-alkanes from *n*-C_{11} onwards. This is due to some migration of cC_8 down the ^1D separation column during the initial, isothermal oven portion.

Before further analysis was carried out the bins without PHC compounds in their retention space were removed from the analysis. Additionally the bins that contained internal standards were also removed from the analysis. This was done as the internal standards in these bins accounts for a highly variable proportion of the bin response (as the fuel concentration is between 0 and 12800 mg/kg and the fuel components in the sample can be from fresh SAB or highly evaporated and biodegraded SAB). This variability in the fuel signal to the internal standard signal makes it particularly difficult to accurately and precisely subtract away the internal standard signals across all site samples. Prior GCxGC-FID analysis with these internal standards confirmed that the internal standards are outside, or at the margins of, the SAB and diesel fuel envelope [97,155,162,163,171]. This removal of the internal standard elution windows therefore only excludes a small amount of the overall elution space of the fuel signal. It should also be noted that the signals from the internal standards have already been examined to demonstrate that the analytical method applied to each sample has worked well across all classes of compound in the internal standard mix (volatile, semi-volatile, aromatic and aliphatic). Following this internal standard removal the remaining bins were scaled so that the total sum of the remaining bins was one (i.e. bin value now represents a fraction

of the total PHCs in the remaining envelope). The effect of this is shown in Figure 39. The GCxGC data for resolved components in sample 53106 is plotted in log2 scale to highlight the compound class range for the site being studied. The binning of this sample data, ready for MDS analysis, is shown in the lower part of Figure 39.

Using this alignment approach, samples with high concentrations of analytes that are eluted in the *n*-C_9 ~ *n*-C_{10} region will suffer from the greatest problems with bin assignments. This is essentially restricted to the fresh SAB calibration samples and any sample containing SAB that has undergone minimal evaporation (and therefore has a signature similar to these standards). As the analysis sequence contained numerous repeats of the SAB calibration standards from 3000 mg/kg to 12000 mg/kg the repeatability of these standards with this binning approach will be a worst case for this approach as a whole.

6.3 Preliminary analysis of binned data

A subset of the samples analysed are presented in Figure 40 and Figure 41 in binned format. The action of evaporation skews the fuel components remaining in a soil sample towards less volatile components [131,132]. This can be appreciated in Figure 40 where the bins with the greatest amount appear towards the right hand side of the plot. In these samples the recovery of high levels of *n*-alkanes and naphthalene + alkyl naphthalenes rules out any significant biodegradation of aliphatics or aromatics. Also of note in the binned data plots, shown in Figure 40, is the relatively consistent colour grading of the bins from the lower acyclic aliphatic bins to the higher, more aromatic or cyclised aliphatic bins.

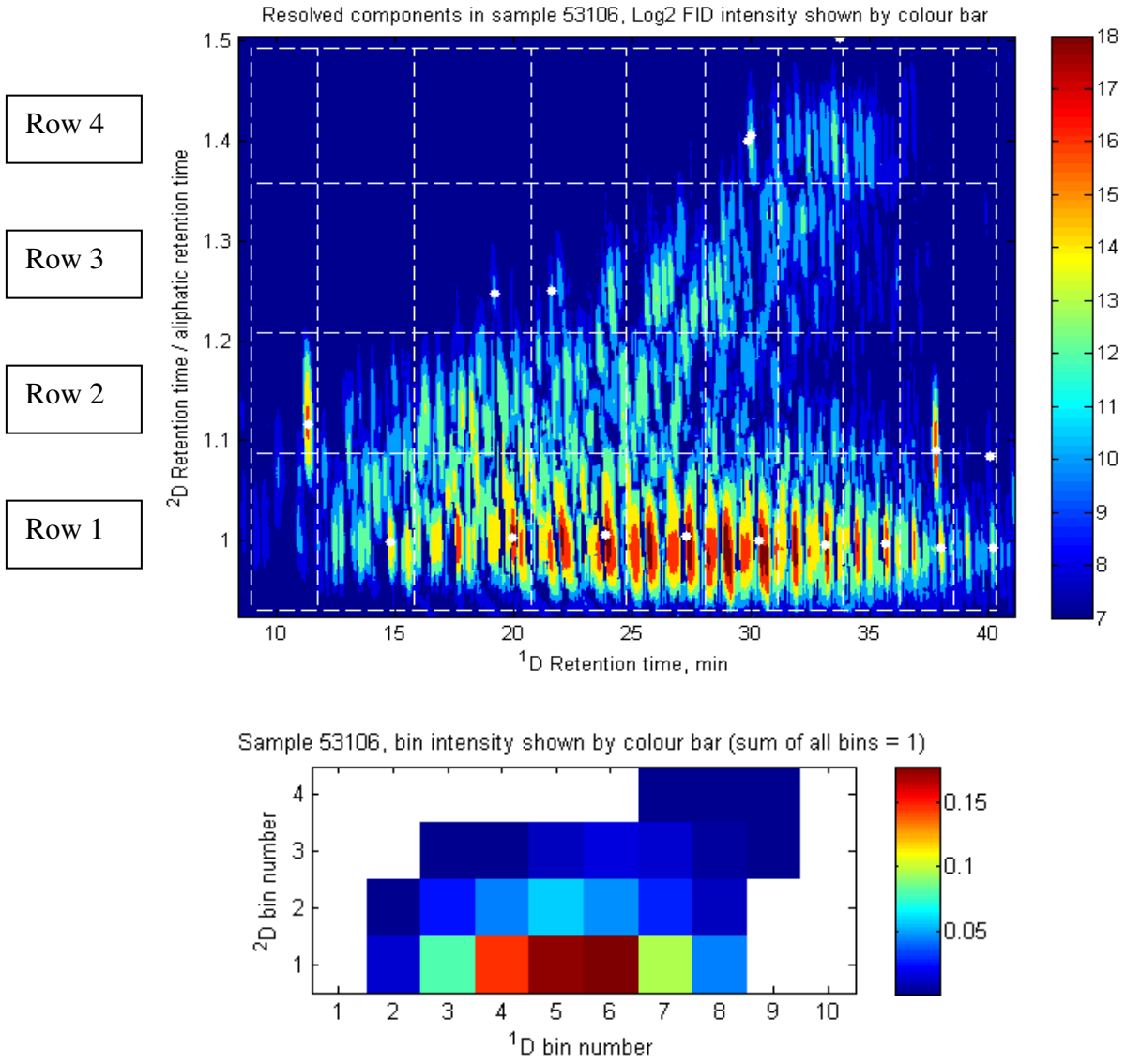

Figure 39. Top Resolved TPH components in sample 53106. The use of a log2 scale more effectively shows the responses for the very low concentration components (however peak width appears larger in this display). Bottom. Binned data for sample 53106 with all empty regions and internal standard regions set to 0 (and displayed as a white squares).

Adding in ^{2}D bins for four-ring (and higher-ring) PAH components was not carried out for the Macquarie Island samples as the concentration of PHCs in these regions is exceptionally low. It is only possible to identify a few of these compounds, at concentrations ≤15 µg/kg in the site samples with the highest fuel concentrations (i.e. >5000 mg/kg TPH).

Other samples, plotted as binned data in Figure 41, show the changes to the fuel signature from biodegradation and from aqueous aromatic transport and subsequent re-sorption onto the soil surfaces. Samples 53076 and 53262 show increasing biodegradation with loss of *n*-alkanes and aliphatics in the lowest row compared to polycyclic aliphatics and highly alkylated benzenes in the second row. This is indicative of biodegradation, a conclusion supported when individual biomarkers are examined in the raw (i.e. un-binned) GCxGC-FID data and the GC-FID data [157,172].

Samples 53187 and 53115 (both in Figure 41) have high levels of PHCs in bin (3,2), the bin containing the majority of the soluble aromatics [133] from the SAB that was spilt at the site. Aqueous transport and subsequent sorption in the particular soil samples give the elevated aromatic content. Note that the second intense region (7,2) in sample 53115 is characteristic of a very old, highly biodegraded, fuel remnant from an earlier fuel spill [172]. This has been mixed with significant amounts of the water soluble aromatic components. The very low levels aliphatics (with very low solubility [133]) are an indication of minimal NAPL transport of the more recently spilt SAB.

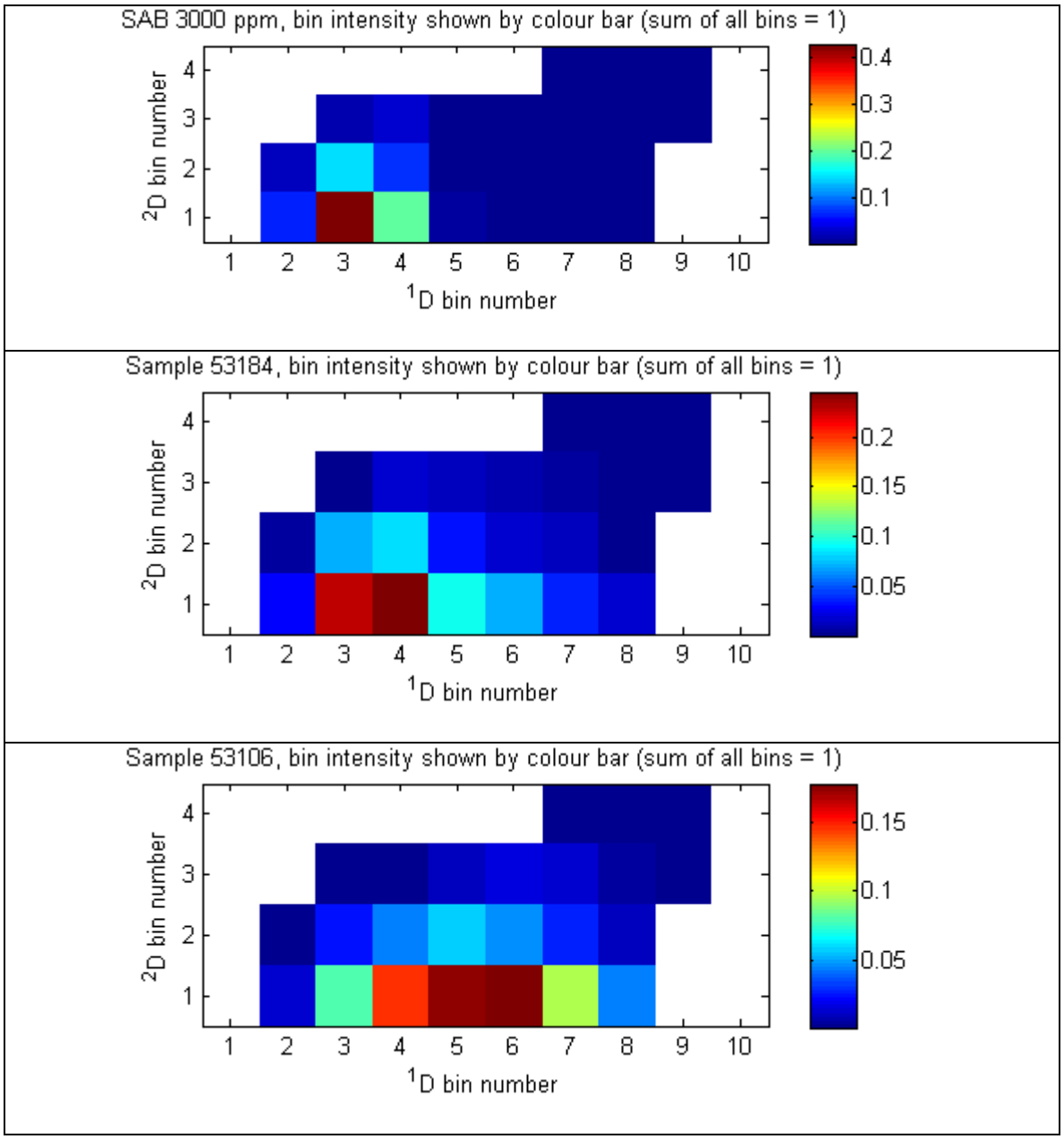

Figure 40. Binned data for an SAB standard and samples 53184 and 53106 which shown progressively greater levels of evaporation

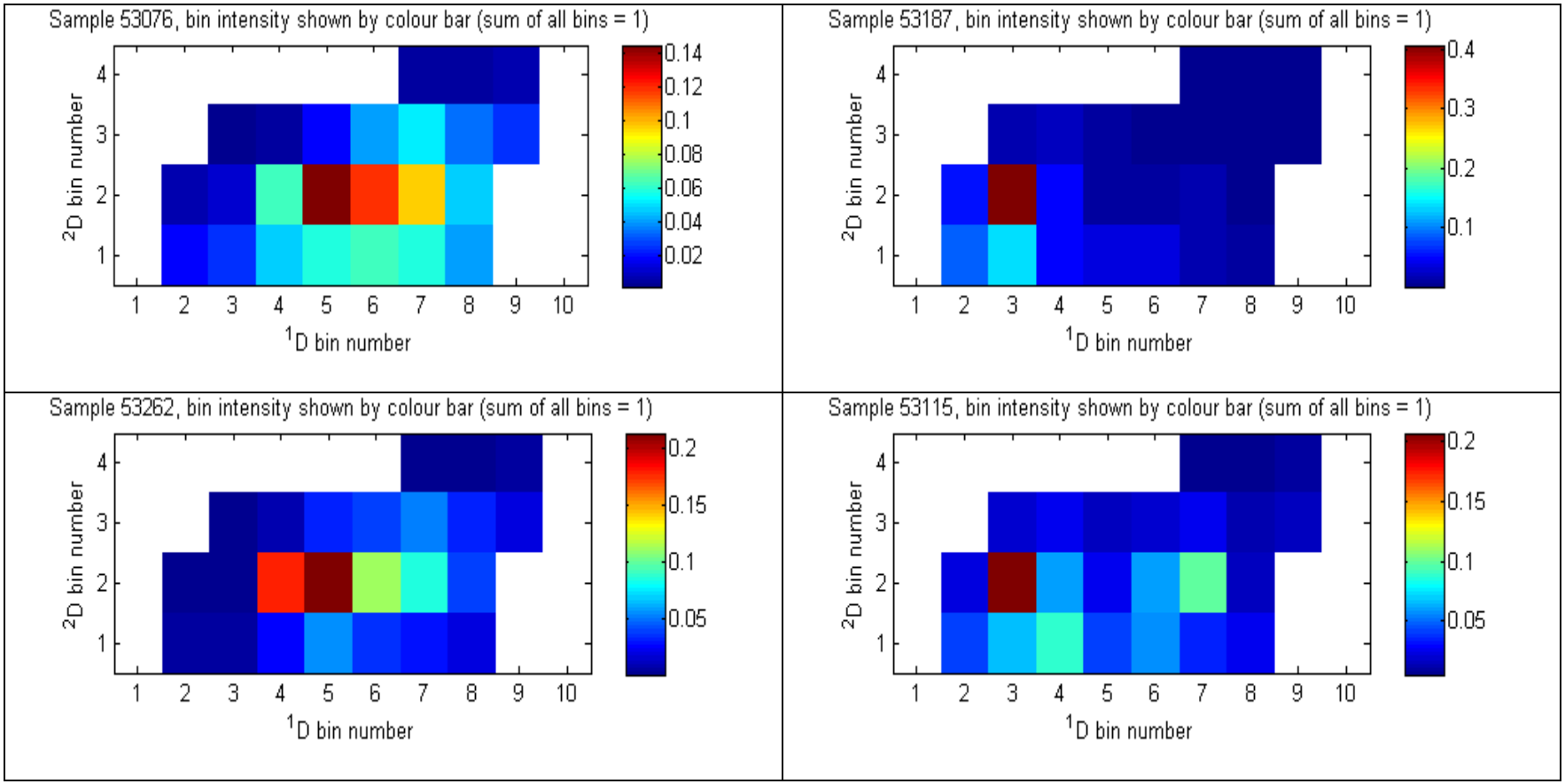

Figure 41. Binned data for biodegraded fuel signatures (left) and fuels with an elevated level of soluble aromatics (right).

6.4 MDS Analysis of binned data

MDS is a widely applied method of visualising similarities, groupings and dissimilarities in a multidimensional dataset derived from a series of objects or samples [173]. In order to implement MDS an input matrix with dissimilarities (or a measure of distances in the multidimensional space) between pairs of samples is first generated for all sample pairs. While numerous options exist for the determination of dissimilarities [173] the methods used in the this chapter use either the Euclidean distance (the "Torgerson-Gower" method) or a summation of differences across each dimension (the "Manhatten" method equivalent to "city block method"). Following the generation of a suitable dissimilarity matrix the number of dimensions for the MDS data analysis is chosen. While the number of dimensions for the MDS analysis need only be less than dimensions in the initial data set the practice of using MDS to represent data as a two dimensional plot is widespread and is especially useful when showing similarities in easily interpreted (and printed) figures Once the number of dimensions for the MDS analysis is chosen new co-ordinates for sample plotting are determined within the new dimensional space such that the dissimilarity matrix for the new plotting is as close as possible to the dissimilarity matrix within the initial data set. Outputs from MDS scaling cluster samples with similar variable values together (using inputs from all the variables measured) while placing anomalous samples away from that cluster. By applying MDS techniques to the binned GCxGC-FID data from 88 samples and 12 standards from the Macquarie Island Fuel Farm PHC contaminated site, a clear indication of on-site processes is obtained.

Having developed a protocol for binning the contaminated site GCxGC-FID data into suitable, environmentally based bins it is possible to examine the site as whole with multidimensional statistical methods. MDS plots from this are shown in Figure 42-Figure 44. The MDS figures differ in which standards and samples are included and the MDS weighting method applied to the data. In all cases there is a clear trend from the modern SAB (standards and the higher site samples) to the old degraded fuel background. The grouping of the standards shown in Figure 42 is excellent given the two SAB batches and three different concentrations used for these standards. The standards were analysed throughout the long GCxGC sequence so the scatter also includes drift not fully corrected for with the alignment approach used. The stress value for the figures is 0.083, 0.083 and 0.104, values which are generally viewed as excellent to good in terms of how well the plotting represents the overall data set [166,173]. When the values for stress are considered in conjunction with the relatively large dataset (88 samples each of which is split into 25 bins) and the plotting onto just 2 dimensions the plotting can be considered very robust [173] and very much lower than a stress likely to be produced by a random dataset of similar size [174]. The stress result of 0.083 for both the MDS plots shown in Figure 42 and Figure 43 indicate that the inclusion or standards and samples with very low PHC levels is not introducing problems with the MDS analysis and also confirms the underlying data quality.

The inclusion of random repeat sample analysis and the subsequent close plotting of these pairs on the MDS plots also confirms GCxGC approach and data processing repeatability. In all three figures the samples with major soluble aromatic enhancement (sample 53187, which was coincidently a random repeat analysis and sample 53115

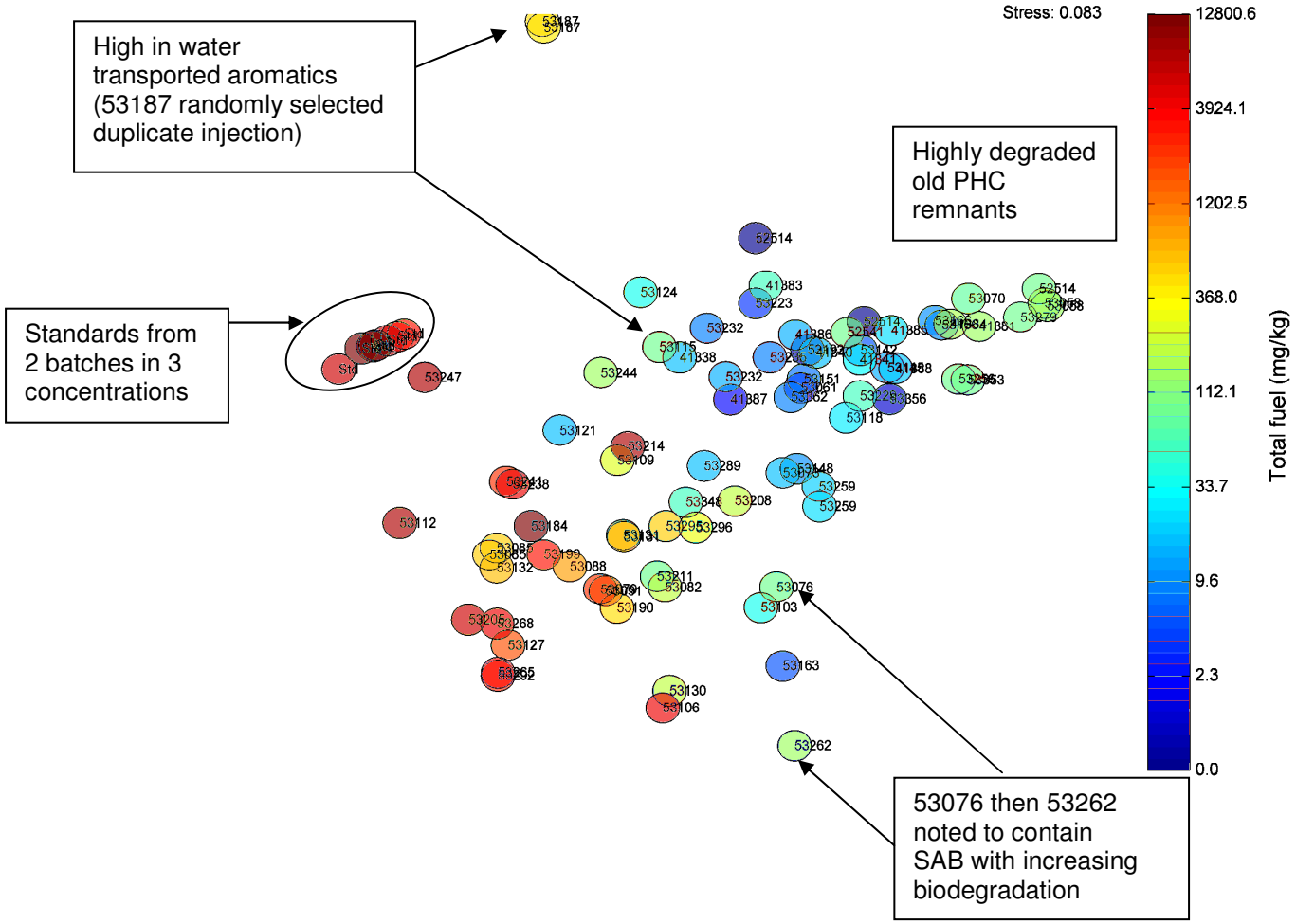

Figure 42: Classic multidimensional scaling with Torgerson-Gower ('gower' in 'R') of all site samples, repeats and SAB standards.

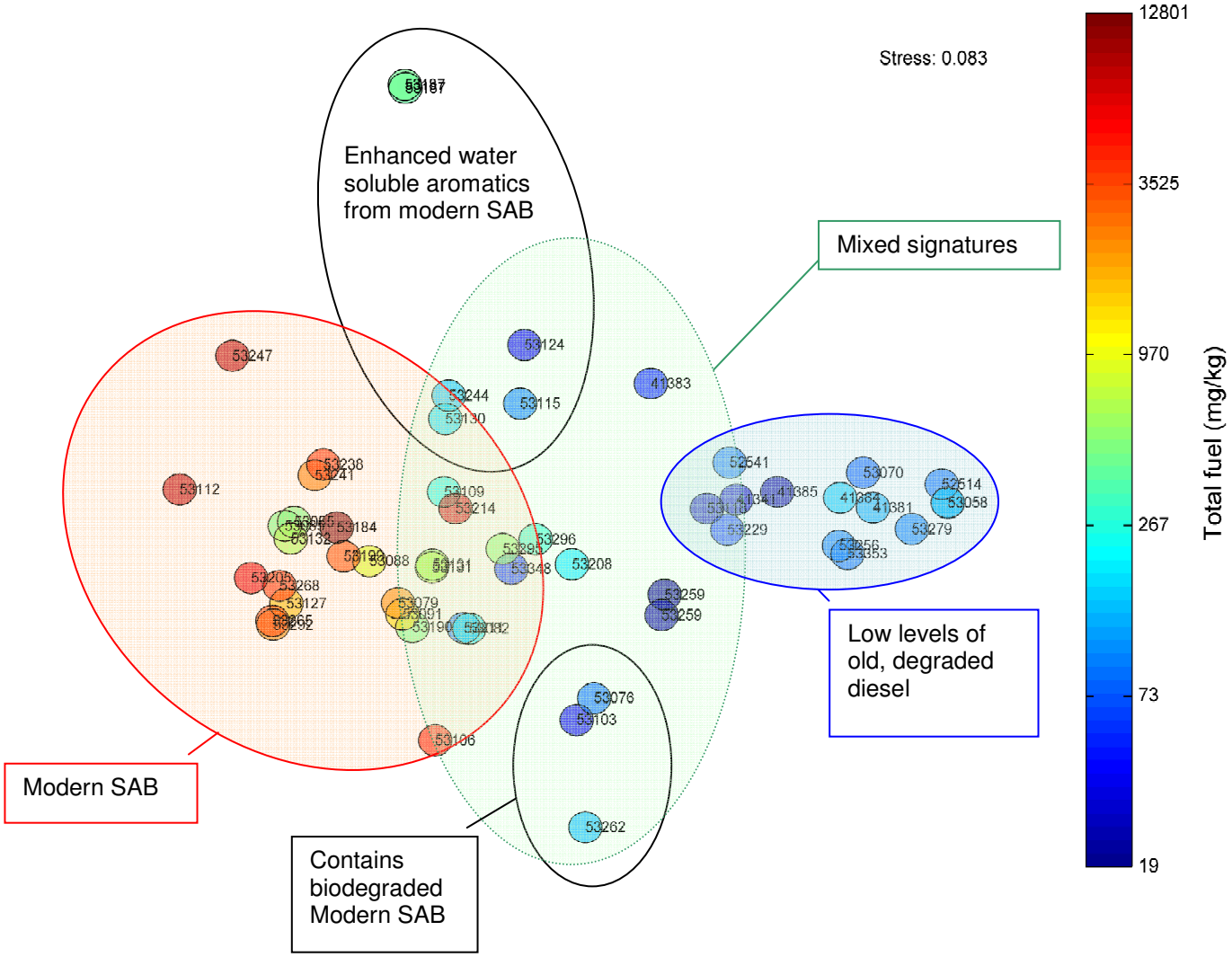

Figure 43. Classic multidimensional scaling with Torgerson-Gower ('gower' in 'R') of all site samples with PHC concentrations 20 mg/kg or higher

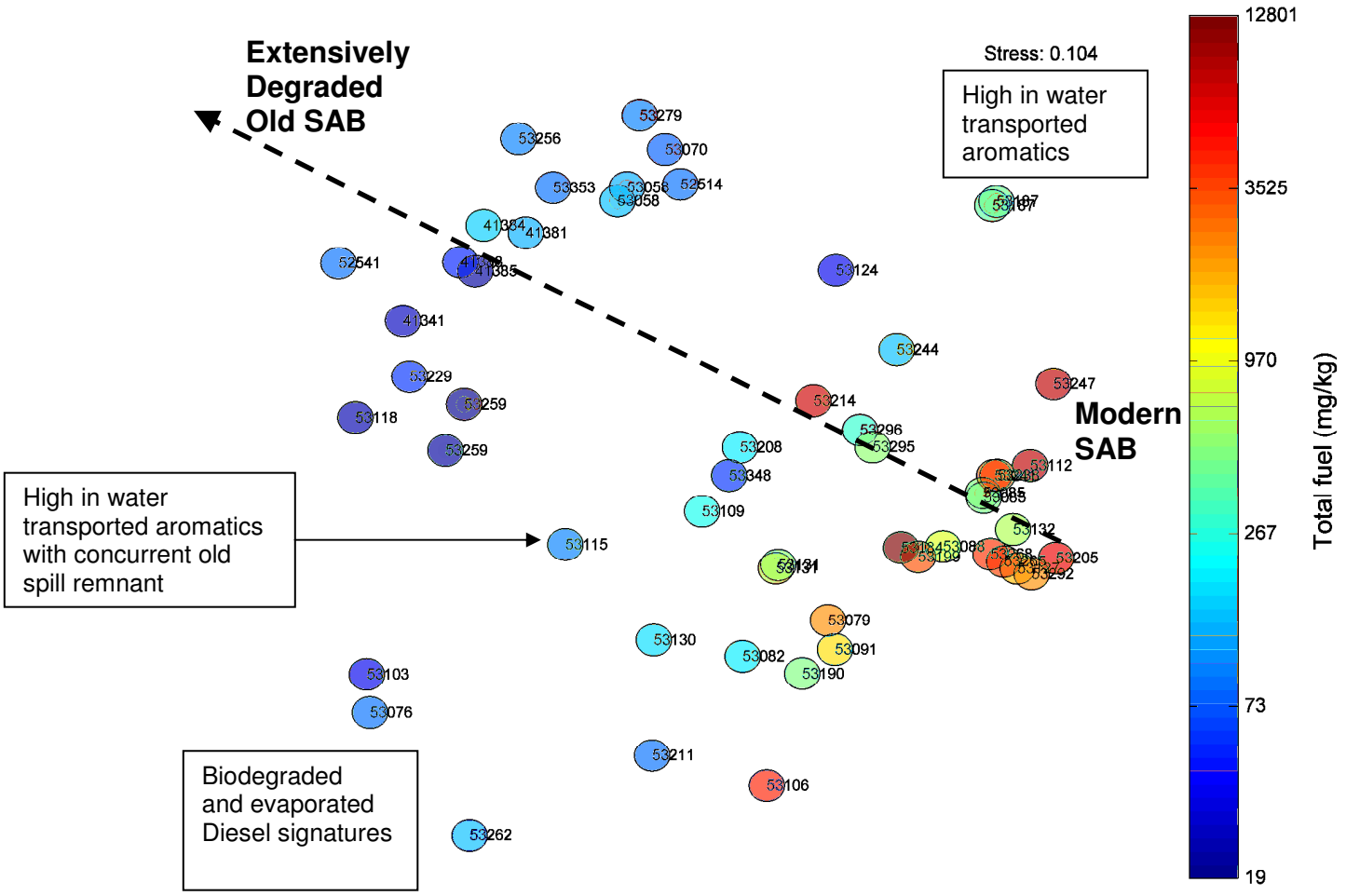

Figure 44. Non-metric multidimensional scaling ('Manhattan' option in 'R') of all site samples with PHC concentrations 20 mg/kg or higher

containing an old, degraded PHC remnant) fall well away from other samples. Additionally the samples with high PHC content (all derived from the more recent SAB spill) consistently grade from least evaporated (53247 and SAB standards) to most-evaporated (53106). The overall site interpretation is best shown in Figure 43.

Of particular note is that all the samples clustered as "enhanced water soluble aromatics from modern SAB" in Figure 43 (upper ellipse) show elevated soluble aromatics as well varying amounts of old, degraded fuel remnants in the raw GCxGC-FID data. The particular samples 53187 and 53115 (see Figure 41 for the binned GCxGC-FID data for these samples) appear in this group. The samples in this ellipse were all collected from the ground water outflow side of the fuel farm site. Samples 53115 and 53130 were excavated from a depth where moisture content rose sharply and remained high (indicating that a water table was at the same depth as these samples as documented in Table 14, page 127). Samples 53124, 53187 and 53244 were all excavated from highly permeable ground layers noted as 'gravel', 'water seep' and 'sand with cobbles' respectively in the field notes and observations recorded during sample collection. This cluster of aromatic enriched samples in Figure 43 is therefore found solely in Fuel Farm soil samples with soil porosity or water content consistent with water transport of aromatics (from the up gradient PHC spill).

The samples with a fuel signature that are comparable to "modern SAB" also cluster well and are grouped within the red ellipse in Figure 43. Sample 53247 (upper left of "modern SAB" the ellipse in Figure 43) shows a PHC distribution very similar to modern SAB. Samples 53184 and 53106, which show progressively greater levels of evaporation compared to modern SAB (as shown in Figure 40) are found at the centre

and lower right of the "modern SAB" ellipse respectively which is consistent with the progressively increasing composition change. The biodegraded samples 53076 and 53262 (Figure 41) are also clustered and contained within the lower black ellipse. Increasing biodegradation in sample 53262 corresponds to this sample being placed furthest away from modern SAB and from other degraded samples. The group of samples within the blue ellipse (Figure 43) all have TPH values <150 mg/kg and very show extensive composition changes and few GCxGC-FID identifiable compounds. The remaining mixed signatures section (centre ellipse) includes moderately degraded samples (such as the samples in Table 13 page 120) that still contain some GCxGC-FID identifiable compounds.

An alternative non-metric multidimensional scaling (using the 'Manhattan' option in R [175]) of data is shown in Figure 44. As the old degraded fuel signature is spread over numerous bins around bin (7,2) but the modern SAB is reliably centred on the early aliphatic bins this scaling method separates out the samples with degraded fuel components. Conversely the samples with modern SAB tend to be more tightly clustered with the scaling used in Figure 44. The important site features are still identified in this plot showing the robustness of the overall approach and the ability of MDS methods to group data in ways that allow new insight to be developed. The different data scaling methods will be better suited to different aspects of data mining depending upon what feature is being investigated. The spreading out of the old, degraded fuel residues shows that systematic variations exist across these samples.

The combinations available for different GCxGC data binning, different plotting and scaling methods as well as the options for adding in site data to sample clustering

(like soil sampling depth) are extensive and beyond the scope of this thesis. The fundamental point is that a relatively simple, environmentally based, data binning and plotting methodology quickly allows unusual samples to be identified as well as general trends across all samples considered.

6.5 Conclusions

Samples with a PHC composition highly altered from the composition of fresh SAB are easily identified. These are placed into biodegraded, evaporated and water transported groups. Significantly this is the first time that a GCxGC-FID site assessment identified PHCs in soil samples containing enhanced aromatics from aqueous phase transport. As such both the binning and MDS analysis methodology for GCxGC-FID data is shown to be appropriate and useful in quickly deducing new information about PHC plume dynamics. The approach also highlights the ability of GCxGC-FID methods to obtain environmentally important site information with minimal specialist examination of the GCxGC chromatograms. The identification of aqueous aromatic transport and enrichment (by subsequent re-sorption onto soil) demonstrates that prioritising the PHC class separation and a reduced analysis time during method development is a successful strategy for environmental analysis. This is important since PHC contaminated site assessment requires exactly this applied environmental information. Therefore this work documents that site assessment for regulatory and scientific research purposes can effectively be accomplished with very fast and cost effective GCxGC-FID methods with minimal ^{1}D separation of components.

Fresh SAB standards cluster together well in the MDS plots confirming the underlying quality of the acquired data. This clustering includes all likely sources of

laboratory and GCxGC-FID based scatter, namely sequence drift, standard concentration change and SAB batch changes between several different SAB standards that were used. The SAB recovered from site soil extracts shows, in all cases, minor to extensive gas phase component loss. Old fuel remnants that have been highly biodegraded have been identified and cluster as a group (especially with the Classic multidimensional scaling methods implemented here). Within group variations of the old highly weathered fuel remnants exist and these variations are better shown with alternative, non-metric multidimensional scaling, should samples of this type need further differentiation.

At sites that are dominated with higher concentration, relatively fresh SAB fuel signatures, a revised environmentally based binning many well be worthwhile. Implementing bins that are clustered more tightly at the volatile end of the ^{1}D separation may be appropriate – an approach taken in the groupings of PHC analysis methods [96,107,108]. This could be especially important for volatile rich PHC spills such as a Jet-A1 200L drum rupture occurring during AAD helicopter operations (2009).

The entire data analysis method (raw GCxGC data importing, baseline correction, binning and MDS scaling) is carried out via Matlab with automated programs and auditable input parameter files. In this way every step in the process, including the final MDS plotting of all site samples is well documented and traceable. Implementing a change to any of the steps in the overall data analysis method immediately leads to new MDS plots that reliable incorporate the methodology change across the entire sample set. This reliability and traceability is an essential part of any analytical method but especially important for contaminated sites being cleaned-up to meet regulatory approval. As such

the GCxGC-FID data and data analysis tools presented here are ideally packaged to allow a more through investigation of best practice for GCxGC data mining methodologies.

7 General Conclusions

This work represents significant progress in the technique of pneumatic modulation GCxGC and in the application of this technique to an important task: fuel spill assessment in a sensitive environmental setting.

The PFM geometry and time varying flows have been extensively studied with numerical solutions to the flows deduced and presented. This development allowed the construction and successful operation of a 'symmetrical' PFM modulator where the chromatographic flow is maintained at a near constant level. With such a device, and concurrent flow model, it is been demonstrated that new device geometries and method operation parameters can be quickly created and operate successfully.

Flow settings in both separation dimensions in pneumatically modulated GCxGC devices were also extensively studied with both numerical models and laboratory experimentation informed by these models. The significant increase in flow ratio from approximately 20:1 (in early literature devices [53,54,176]) to values ≥40:1 has allowed excellent GCxGC separations to be achieved with modulation times ranging up to 9 seconds. Critically the component of band broadening and GCxGC cross peak skewing in the resulting GCxGC chromatograms has been estimated and thoroughly described. From this ^{1}D and ^{2}D flows and other hardware and operation parameters can be chosen so that this unavoidable source of additional peak broadening is not an unknown limiting factor in any separation being attempted.

The studying of PHC contaminated soil extracts, partly at Macquarie Island in the Southern Ocean and partly at the University of Tasmania laboratories, goes a long way to realising the portability of the technique noted by Cortes *et al.* [62]. Of critical importance is the fact that this 'real world' application required the separation of all 16 US EPA priority PAHs as well as fuel components from *n*-C_9 to *n*-C_{40} with robust hardware capable of hundreds of injections without specialised operator maintenance. This driver led to the development (after extensive laboratory trails) of two extremely robust differential flow modulators with all external components made from stainless steel. The fragile restrictor tubing is contained entirely within this outer tubing. In this way all the method requirements and operation parameters could be met and the site samples analysed successfully.

The use of the differential flow modulators for site sample assessment resulted in a simplification of modulator operation (when compared to the pulsed flow methods) as time varying ^{1}D backflows are not a feature of this modulator. Essentially this device, once correctly constructed and installed, offers smoother flows through the separation columns and, if available, would be the expected choice of an analyst with chromatographic experience. The trade off for this is that the device is harder to build initially as it contains a greater number of fittings. Flow balancing between the flow paths is difficult to achieve during construction so the PFM device is the more attractive to build from an engineering perspective.

Further research and development is needed in the fabrication of the pneumatic modulation devices, especially the differential flow modulators which are attractive from a chromatography perspective. The extension of this is the need for the production of

commercial software that assists in the development of workable column and tubing selections, ^{1}D and ^{2}D flows plus appropriate instrument pressures during temperature and flow programmed GCxGC methods.

With the analysis of the Macquarie Island sample set various data manipulation methods were developed as applications within Matlab. The options for baseline correction, which are all automated packages, can quickly transform GCxGC-FID data with high, varying background FID intensity into data files with a baseline noise very close to the baseline noise of the FID itself (i.e. instrument drift and bias removed and only random FID fluctuations remaining). Exceptionally good limits of detection can be achieved by having GCxGC-FID acquisition methods with a region in each modulation without eluting analytes. In this manner ± 3 mg/kg, as the 99.9% confidence interval, for the analysis of diesel range organics was obtained in a hexane extract without any extract concentration or other manipulation (10 g soil extracted into 10 mL hexane solvent). The Matlab method for pneumatic modulation GCxGC-FID peak deconvolution allows individual peaks to be extracted from the data. This can be accomplished despite data bilinearity being lost due to temperature and flow programming in the GCxGC-FID acquisition method.

The more general site assessment methodology of environmentally appropriate data binning and subsequent analysis of the entire sample set has also been proven to be extremely advantageous. This entire process has been carried out with documented and automated Matlab programs including an overall site analysis presented with, for example, a MDS plot. This can quickly allow sample patterns to be recognised and then site regions, with important site processes, identified. In this way soil samples showing an

enhanced concentration of water transported aromatics were identified. A more through investigation of this approach is a worthwhile area of future research. It is an especially attractive option for sites being investigated with a number of methods and with regulatory involvement during clean-up operations. The rigour of carrying out all data analysis steps with automated methods and maintaining documented, traceable links from raw acquisition data to site interpretation plots should be especially attractive in projects where justification of important decisions will be required.

References

[1] J. Blomberg, P.J. Schoenmakers, U.A.T. Brinkman, Journal of Chromatography A 972 (2002) 137.

[2] M. Taki, T. Asahara, Y. Mandai, T. Uno, M. Nagai, Energy & Fuels 23 (2009) 5003.

[3] F.D. Hostettler, Y. Wang, Y.S. Huang, W.H. Cao, B.A. Bekins, C.E. Rostad, C.F. Kulpa, A. Laursen, Environmental Forensics 8 (2007) 139.

[4] C. von Muhlen, C.A. Zini, E.B. Caramao, P.J. Marriott, Journal of Chromatography A 1105 (2006) 39.

[5] Z. Wang, S.A. Stout, Oil spill environmental forensics, Elsevier, Burlington, MA., 2007.

[6] L.E. Twerdok, Drug and Chemical Toxicology 22 (1999) 275.

[7] D.A. Edwards, M.D. Andriot, M.A. Amoruso, A.C. Tummey, C.J. Bevan, A. Tveit, L.A. Hayes, S.H. Youngren, D.V. Nakles, Development of Fraction Specific Reference Doses (RfDs) and Reference Concentrations (RfCs) for Total Petroleum Hydrocarbons (TPH), Amherst Scientific Publishers, Amherst, 1997.

[8] J.B. Gustafson, J.G. Tell, D. Orem, Selection of Representative TPH Fractions Based on Fate and Transport Considerations, Amherst Scientific Publishers, Amherst, 1997.

[9] T.L. Potter, K.E. Simmons, Composition of Petroleum Mixtures, Amherst Scientific Publishers, Amherst, 1998.

[10] D.J. Vorhees, W.H. Weisman, J.B. Gustafson, Human Health Risk-Based Evaluation of Petroleum Release Sites: Implementing the Working Group Approach, Amherst Scientific Publishers, Amherst, 1999.

[11] W. Weisman, Analysis of Petroleum Hydrocarbons in Environmental Media, Amherst Scientific Publishers, Amherst, 1998.

[12] C. De Sousa, Journal of Environmental Management 62 (2001) 131.

[13] S.M. Rodrigues, M.E. Pereira, E.F. da Silva, A.S. Hursthouse, A.C. Duarte, Environment International 35 (2009) 202.

[14] A.E. Latawiec, P. Simmons, B.J. Reid, Environment International 36 (2010) 383.

[15] NEPC, Guideline on the Investigation Levels for Soil and Groundwater, Schedule B(1), 1999.

[16] NEPC, Guideline on Health-Based Investigation Levels, Schedule B(7a), 1999.

[17] A.E. Bence, K.A. Kvenvolden, M.C. Kennicutt, Organic Geochemistry 24 (1996) 7.

[18] P.D. Boehm, G.S. Douglas, W.A. Burns, P.J. Mankiewicz, D.S. Page, A.E. Bence, Marine Pollution Bulletin 34 (1997) 599.

[19] J.R. Bragg, R.C. Prince, E.J. Harner, R.M. Atlas, Nature 368 (1994) 413.

[20] S. Harvey, I. Elashvili, J.J. Valdes, D. Kamely, A.M. Chakrabarty, Bio-Technology 8 (1990) 228.

[21] R.A. Heintz, J.W. Short, S.D. Rice, Environmental Toxicology and Chemistry 18 (1999) 494.

[22] J.E. Lindstrom, R.C. Prince, J.C. Clark, M.J. Grossman, T.R. Yeager, J.F. Braddock, E.J. Brown, Applied and Environmental Microbiology 57 (1991) 2514.

[23] D.S. Page, P.D. Boehm, G.S. Douglas, A.E. Bence, C. Environment, IDENTIFICATION OF HYDROCARBON SOURCES IN THE BENTHIC SEDIMENTS OF PRINCE-WILLIAM-SOUND AND THE GULF OF ALASKA FOLLOWING THE EXXON-VALDEZ OIL-SPILL, Environment Canada, Ottawa, 1993.

[24] C.H. Peterson, S.D. Rice, J.W. Short, D. Esler, J.L. Bodkin, B.E. Ballachey, D.B. Irons, Science 302 (2003) 2082.

[25] J.F. Piatt, C.J. Lensink, W. Butler, M. Kendziorek, D.R. Nysewander, Auk 107 (1990) 387.

[26] J.W. Short, T.J. Jackson, M.L. Larsen, T.L. Wade, in S.D. Rice, R.B. Spies, D.A. Wolfe, B.A. Wright (Editors), Proceedings of the Exxon Valdez Oil Spill Symposium, Amer Fisheries Soc, Bethesda, 1996, p. 140.

[27] H.M.R.a.A.D. NOAA, Report No. HMRAD 92-11 (1992).

[28] J.H. Reynolds, N. Braman, Marine Pollution Bulletin 58 (2009) 1496.

[29] P.D. Boehm, D.S. Page, J.S. Brown, J.M. Neff, J.R. Bragg, R.M. Atlas, Environmental Science & Technology 42 (2008) 9210.

[30] H.L. Li, M.C. Boufadel, Nature Geoscience 3 (2010) 96.

[31] J.W. Short, R.A. Heintz, Environmental Science & Technology 31 (1997) 2375.
[32] D.S. Page, P.D. Boehm, G.S. Douglas, A.E. Bence, in P.G. Wells, J.N. Butler, J.S. Hughes (Editors), Exxon Valdez Oil Spill: Fate and Effects in Alaskan Waters, American Society Testing and Materials, W Conshohocken, 1995, p. 41.
[33] F.D. Hostettler, K.A. Kvenvolden, Organic Geochemistry 21 (1994) 927.
[34] H.U. Deepthike, R. Tecon, G. van Kooten, J.R. van der Meer, H. Harms, M. Wells, J. Short, Environmental Science & Technology 43 (2009) 5864.
[35] H.U. Deepthike, R. Tecon, G.K. Van Kooten, J.R. van der Meer, H. Harms, M. Wells, J. Short, Environmental Science & Technology 44 (2010) 2212.
[36] D.S. Page, P.D. Boehm, J.M. Neff, Environmental Science & Technology 44 (2010) 2210.
[37] P.D. Boehm, D.S. Page, E.S. Gilfillan, A.E. Bence, W.A. Burns, P.J. Mankiewicz, Environmental Science & Technology 32 (1998) 567.
[38] J.C. Giddings, Analytical Chemistry 32 (1960) 1707.
[39] H.W. Habgood, W.E. Harris, Analytical Chemistry 32 (1960) 1206.
[40] P.H. Stirling, H. Ho, Industrial and Engineering Chemistry 52 (1960) A61.
[41] W.J.A. Vandenheuvel, C.C. Sweeley, E.C. Horning, Journal of the American Chemical Society 82 (1960) 3481.
[42] T.J. Klayder, Journal of the Association of Official Agricultural Chemists 47 (1964) 1146.
[43] J.M. Brooks, M.C. Kennicutt, T.L. Wade, A.D. Hart, G.J. Denoux, T.J. McDonald, Environmental Science & Technology 24 (1990) 1079.
[44] M.M. Krahn, G.M. Ylitalo, J. Buzitis, S.L. Chan, U. Varanasi, T.L. Wade, T.J. Jackson, J.M. Brooks, D.A. Wolfe, C.A. Manen, Environmental Science & Technology 27 (1993) 699.
[45] J.G. Dojahn, W.E. Wentworth, S.N. Deming, S.D. Stearns, Journal of Chromatography A 917 (2001) 187.
[46] M. Jalali-Heravi, M.H. Fatemi, Journal of Chromatography A 825 (1998) 161.
[47] A.D. Jorgensen, K.C. Picel, V.C. Stamoudis, Analytical Chemistry 62 (1990) 683.
[48] A.R. Katritzky, E.S. Ignatchenko, R.A. Barcock, V.S. Lobanov, M. Karelson, Analytical Chemistry 66 (1994) 1799.
[49] D.S. Page, P.D. Boehm, W.A. Stubblefield, K.R. Parker, E.S. Gilfillan, J.M. Neff, A.W. Maki, Environmental Toxicology and Chemistry 21 (2002) 1438.
[50] E. Skoczynska, P. Korytar, J. De Boer, Environmental Science & Technology 42 (2008) 6611.
[51] Z.Y. Liu, J.B. Phillips, Journal of Chromatographic Science 29 (1991) 227.
[52] C.J. Venkatramani, J.B. Phillips, Journal of Microcolumn Separations 5 (1993) 511.
[53] P.A. Bueno, J.V. Seeley, Journal of Chromatography A 1027 (2004) 3.
[54] J.V. Seeley, N.J. Micyus, J.D. McCurry, S.K. Seeley, American Laboratory 38 (2006) 24.
[55] W. Bertsch, Hrc-Journal of High Resolution Chromatography 22 (1999) 647.
[56] M. Adahchour, J. Beens, U.A.T. Brinkman, Journal of Chromatography A 1186 (2008) 67.
[57] M. Adahchour, J. Beens, R.J.J. Vreuls, U.A.T. Brinkman, Trac-Trends in Analytical Chemistry 25 (2006) 821.
[58] M. Adahchour, J. Beens, R.J.J. Vreuls, U.A.T. Brinkman, Trac-Trends in Analytical Chemistry 25 (2006) 726.
[59] M. Adahchour, J. Beens, R.J.J. Vreuls, U.A.T. Brinkman, Trac-Trends in Analytical Chemistry 25 (2006) 540.
[60] M. Adahchour, J. Beens, R.J.J. Vreuls, U.A.T. Brinkman, Trac-Trends in Analytical Chemistry 25 (2006) 438.
[61] W. Bertsch, Hrc-Journal of High Resolution Chromatography 23 (2000) 167.
[62] H.J. Cortes, B. Winniford, J. Luong, M. Pursch, Journal of Separation Science 32 (2009) 883.
[63] J. Dalluge, J. Beens, U.A.T. Brinkman, Journal of Chromatography A 1000 (2003) 69.
[64] R.B. Gaines, G.S. Frysinger, Journal of Separation Science 27 (2004) 380.
[65] K.M. Pierce, J.C. Hoggard, R.E. Mohler, R.E. Synovec, Journal of Chromatography A 1184 (2008) 341.
[66] L. Ramos, Comprehensive Two Dimensional Gas Chromatography, Elsevier, 2009.
[67] R.B. Gaines, G.S. Frysinger, Journal of Chromatography A 1045 (2004) 263.
[68] H.J. de Geus, J. de Boer, J.B. Phillips, E.B. Ledford, U.A.T. Brinkman, Hrc-Journal of High Resolution Chromatography 21 (1998) 411.

[69] R.M. Kinghorn, P.J. Marriott, P.A. Dawes, Hrc-Journal of High Resolution Chromatography 23 (2000) 245.
[70] G.M. Gross, B.J. Prazen, J.W. Grate, R.E. Synovec, Analytical Chemistry 76 (2004) 3517.
[71] P. Marriott, R. Kinghorn, Trac-Trends in Analytical Chemistry 18 (1999) 114.
[72] P.J. Marriott, R.M. Kinghorn, R. Ong, P. Morrison, P. Haglund, M. Harju, Hrc-Journal of High Resolution Chromatography 23 (2000) 253.
[73] F. Begnaud, C. Debonneville, J.P. Probst, A. Chaintreau, P.D. Morrison, J.L. Adcock, P.J. Marriott, Journal of Separation Science 32 (2009) 3144.
[74] R.M. Kinghorn, P.J. Marriott, Hrc-Journal of High Resolution Chromatography 22 (1999) 235.
[75] M. Kallio, T. Hyotylainen, Journal of Chromatography A 1148 (2007) 228.
[76] M. Kallio, T. Hyotylainen, M. Jussila, K. Hartonen, S. Palonen, M. Shimmo, M.L. Riekkola, Analytical and Bioanalytical Chemistry 375 (2003) 725.
[77] R.B. Gaines, G.S. Frysinger, M.S. Hendrick-Smith, J.D. Stuart, Environmental Science & Technology 33 (1999) 2106.
[78] C.A. Bruckner, B.J. Prazen, R.E. Synovec, Analytical Chemistry 70 (1998) 2796.
[79] J.V. Seeley, F. Kramp, C.J. Hicks, Analytical Chemistry 72 (2000) 4346.
[80] J.V. Seeley, Journal of Chromatography A 962 (2002) 21.
[81] D.R. Stoll, Analytical and Bioanalytical Chemistry 397 (2010) 979.
[82] A. Roy, M.D. Miller, D.M. Meunier, A.W. Degroot, W.L. Winniford, F.A. Van Damme, R.J. Pell, J.W. Lyons, Macromolecules 43 (2010) 3710.
[83] V.R. Reid, R.E. Synovec, Talanta 76 (2008) 703.
[84] R.E. Mohler, B.J. Prazen, R.E. Synovec, Analytica Chimica Acta 555 (2006) 68.
[85] R.E. Mohler, K.M. Dombek, J.C. Hoggard, K.M. Pierce, E.T. Young, R.E. Synovec, Analyst 132 (2007) 756.
[86] R.E. Mohler, B.P. Tu, K.M. Dombek, J.C. Hoggard, E.T. Young, R.E. Synovec, Journal of Chromatography A 1186 (2008) 401.
[87] J.C. Hoggard, J.H. Wahl, R.E. Synovec, G.M. Mong, C.G. Fraga, Analytical Chemistry 82 (2010) 689.
[88] A.E. Sinha, K.J. Johnson, B.J. Prazen, S.V. Lucas, C.G. Fraga, R.E. Synovec, Journal of Chromatography A 983 (2003) 195.
[89] V.R. Reid, M. Stadermann, O. Bakajin, R.E. Synovec, Talanta 77 (2009) 1420.
[90] M. Poliak, M. Kochman, A. Amirav, Journal of Chromatography A 1186 (2008) 189.
[91] M. Adahchour, J. Beens, R.J.J. Vreuls, A.M. Batenburg, U.A.T. Brinkman, Journal of Chromatography A 1054 (2004) 47.
[92] K.E. Peters, C.C. Walters, J.M. Moldowan, The Biomarker Guide, Prentice Hall, Englewood Cliffs, NJ, 1993.
[93] TPHCWG, Analysis of petroleum hydrocarbons in environmental media Amherst Scientific Publishers, Amherst, Mass., 1998.
[94] TPHCWG, Characterisation of C_6 to C_{35} petroleum hydrocarbons in environmental samples, Amherst Scientific Publishers, Amherst, Mass., 1998.
[95] Chiron, http://chiron.no/pdf/Chiron_Biomarker _catalogue_2008.pdf (2008).
[96] TPHCWG, in Characterization of C6 to C35 petroleum hydrocarbons in environmental samples, Amherst Scientific Publishers, Amherst, 1998.
[97] J.L. Rayner, I. Snape, J.L. Walworth, P.M. Harvey, S.H. Ferguson, Cold Regions Science and Technology 48 (2007) 139.
[98] AAD, in, Australian Antarctic Division internal report, Field Work Plan 2006_07 Macquarie Island Main Power House and Fuel Farm spill remediation, 2006.
[99] M.I. AAD 2008 Annual Report: Fuel Spill Risk and Remediation Program, Tasmania., in, Department of the Environment, Water, Heritage and the Arts: Australian Antarctic Division, 2008.
[100] Agilent 6890 Operating manual. Volume 1, Agilent Technologies, Inc. 2850 Centerville Road Wilmington, DE 19808-1610, 2000.
[101] Agilent 6890 Operating manual. Volume 3. Detectors, Agilent Technologies, Inc. 2850 Centerville Road Wilmington, DE 19808-1610, 2000.
[102] SGE, in, http://www.sge.com/uploads/92/f5/92f587fa57be5ff4054982b3f18519ad/PD-0002-C.pdf Publication No. PD-0002-C Rev:03 03/01, 2001.

[103] SGE, in, http://www.sge.com/products/gc--lc-supplies/gc-supplies/gc-tubing/fused-silica-100-methyl-deactivated3

[104] Restek, in Siltek sulfinert deactivated stainless steel tubing, 2009.
[105] M. Poliak, M. Kochman, A. Arnirav, Journal of Chromatography A 1186 (2008) 189.
[106] HIRP, AAD internal reports (2008-2010).
[107] TNRCC, Draft TNRCC method 1006 (2000).
[108] TNRCC, TNRCC method 1005 Revision 3 (2001).
[109] M. Junge, S. Bieri, H. Huegel, P.J. Marriott, Analytical Chemistry 79 (2007) 4448.
[110] R. Shellie, P.J. Marriott, Analytical Chemistry 74 (2002) 5426.
[111] J.V. Seeley, S.K. Seeley, E.K. Libby, J.D. McCurry, Journal of Chromatographic Science 45 (2007) 650.
[112] J.V. Seeley, S.K. Seeley, E.K. Libby, Z.S. Breitbach, D.W. Armstrong, Analytical and Bioanalytical Chemistry 390 (2008) 323.
[113] J.V. Seeley, E.M. Libby, S.K. Seeley, J.D. McCurry, Journal of Separation Science 31 (2008) 3337.
[114] J.V. Seeley, E.M. Libby, K.A.H. Edwards, S.K. Seeley, Journal of Chromatography A 1216 (2009) 1650.
[115] M. Poliak, A.B. Fialkov, A. Amirav, Journal of Chromatography A 1210 (2008) 108.
[116] P.Q. Tranchida, A. Giannino, M. Mondello, D. Sciarrone, P. Dugo, G. Dugo, L. Mondello, Journal of Separation Science 31 (2008) 1797.
[117] E. Kaal, S. de Koning, S. Brudin, H.G. Janssen, Journal of Chromatography A 1201 (2008) 169.
[118] J. Beens, H.G. Janssen, M. Adahchour, U.A.T. Brinkman, Journal of Chromatography A 1086 (2005) 141.
[119] P.Q. Tranchida, A. Casilli, P. Dugo, G. Dugo, L. Mondello, Analytical Chemistry 79 (2007) 2266.
[120] R. Shellie, P. Marriott, P. Morrison, L. Mondello, Journal of Separation Science 27 (2004) 504.
[121] R. Ong, R. Shellie, P. Marriott, Journal of Separation Science 24 (2001) 367.
[122] C.F. Poole, The Essence of Chromatography, 2003.
[123] T. Skov, J.C. Hoggard, R. Bro, R.E. Synovec, Journal of Chromatography A 1216 (2009) 4020.
[124] A.L. Lee, K.D. Bartle, A.C. Lewis, Analytical Chemistry 73 (2001) 1330.
[125] V.B. Di Marco, G.G. Bombi, Journal of Chromatography A 931 (2001) 1.
[126] J.L. Adcock, M. Adams, B.S. Mitrevski, P.J. Marriott, Analytical Chemistry 81 (2009) 6797.
[127] J.B. Phillips, J. Beens, Journal of Chromatography A 856 (1999) 331.
[128] J. Beens, R. Tijssen, J. Blomberg, Journal of Chromatography A 822 (1998) 233.
[129] P.Q. Tranchida, G. Purcaro, P. Dugo, G. Dugo, P. Dawes, L. Mondello, in 7th GCxGC Symposium, Riva del Garda, 2010.
[130] H. Van De Weghe, G. Vanermen, J. Gemoets, R. Lookman, D. Bertels, Journal of Chromatography A 1137 (2006) 91.
[131] J.S. Arey, R.K. Nelson, D.L. Plata, C.M. Reddy, Environmental Science & Technology 41 (2007) 5747.
[132] J.S. Arey, R.K. Nelson, C.M. Reddy, Environmental Science & Technology 41 (2007) 5738.
[133] TPHCWG, Selection of Representative TPH Fractions Based on Fate and Transport Considerations, Amherst Scientific Publishers, Amherst, Mass., 1997.
[134] NEPC, National Environmental Protection (Assessment of Site Contamination) Measure, National Environmental Protection Council Service Corporation, Adelaide, 1999.
[135] NEPC, Review of the National Environmental Protection (Assessment of Site Contamination) Measure: Issues Paper., National Environmental Protection Council Service Corporation, Adelaide, 2005.
[136] NEPC, National Environmental Protection (Assessment of Site Contamination) Measure Review: Review Report., National Environmental Protection Council Service Corporation, Adelaide, 2006.
[137] S.o. Alaska, in, State of Alaska, Department of Environmental Conservation, 1993.
[138] Z.D. Wang, S.A. Stout, M. Fingas, Environmental Forensics 7 (2006) 105.
[139] M. Blumer, J. Sass, Science 176 (1972) 1120.
[140] M.R. Schure, Analytical Chemistry 71 (1999) 1645.
[141] W. Khummueng, J. Harynuk, P.J. Marriott, Analytical Chemistry 78 (2006) 4578.
[142] J.J. Harynuk, A.H. Kwong, P.J. Marriott, Journal of Chromatography A 1200 (2008) 17.

[143] D.S. Page, E.S. Gilfillan, P.D. Boehm, W.A. Stubblefield, K.R. Parker, J.M. Neff, A.W. Maki, Environmental Toxicology and Chemistry 22 (2003) 2540.
[144] S.K. Seeley, S.V. Bandurski, R.G. Brown, J.D. McCurry, J.V. Seeley, Journal of Chromatographic Science 45 (2007) 657.
[145] J.K. Volkman, R. Alexander, R.I. Kagi, S.J. Rowland, P.N. Sheppard, Organic geochemistry 6 (1984) 619.
[146] J.K. Volkman, in Typical effects of biodegradation on crude oil, CSIRO Report, 1984.
[147] C. McIntyre, P.M. Harvey, S.H. Ferguson, A.M. Wressnig, H. Volk, S.C. George, I. Snape, Environmental Science & Technology 41 (2007) 2452.
[148] R. Xu, J.P. Obbard, Journal of Environmental Quality 32 (2003) 1234.
[149] E. Vasileva-Tonkova, V. Gesheva, Zeitschrift Fur Naturforschung C-a Journal of Biosciences 59 (2004) 140.
[150] Y.S. Oh, D.S. Sim, S.J. Kim, Marine Pollution Bulletin 42 (2001) 1367.
[151] M.H. Huesemann, T.S. Hausmann, T.J. Fortman, Biodegradation 15 (2004) 261.
[152] S.M. Powell, J.P. Bowman, S.H. Ferguson, I. Snape, J.S. Stark, S.D. Siciliano, M.J. Riddle, in 2nd SCAR Open Science Conference "Antarctica in the Earth System", Hobart, 2006, p. 237.
[153] J. Van de Steene, H. Verplancke, European Journal of Soil Science 57 (2006) 106.
[154] M.H. Borresen, A.G. Rike, Cold Regions Science and Technology 48 (2007) 129.
[155] S.M. Powell, P.M. Harvey, J.S. Stark, I. Snape, M.J. Riddle, Marine Pollution Bulletin 54 (2007) 434.
[156] G. Ratcliffe, in, Australian Antarctic Division, Kingston, Tasmania, Australia, Personal Communication, 2010.
[157] R.M. Atlas, Microbiological Reviews 45 (1981) 180.
[158] Chiron_AS, in www.chiron.no (Editor), The collection of reference standards - 2008, 2008.
[159] Z.D. Wang, M. Fingas, K. Li, Journal of Chromatographic Science 32 (1994) 361.
[160] Z.D. Wang, M. Fingas, K. Li, Journal of Chromatographic Science 32 (1994) 367.
[161] T.C. Raymond, I. Snape, J.L. Rayner, C.K. King, S.H. Ferguson, G. Hince, P. Harvey, in, Field Work Plan 2007/08: Remediation of the Main Power House and Fuel Farm at Macquarie Island Station Australian Antarctic Division, Hobart, 2007, p. 34.
[162] I. Snape, S.H. Ferguson, P.M. Harvey, M.J. Riddle, Chemosphere 63 (2006) 89.
[163] I. Snape, P.M. Harvey, S.H. Ferguson, J.L. Rayner, A.T. Revill, Chemosphere 61 (2005) 1485.
[164] J.S. Arey, R.K. Nelson, L. Xu, C.M. Reddy, Analytical Chemistry 79 (2007) 4736.
[165] J.S. Arey, R.K. Nelson, L. Xu, C.M. Reddy, Analytical Chemistry 77 (2005) 7172.
[166] K.R. Clarke, R.M. Warwick, Change in marine communities: an approach to statistical analysis and interpretation, Primer-E Ltd, Plymouth, 2001.
[167] J. Harynuk, B. Vlaeminck, P. Zaher, P.J. Marriott, Analytical and Bioanalytical Chemistry 386 (2006) 602.
[168] P.D. Boehm, D.S. Page, G.S. Douglas, W.A. Burns, A.E. Bence, P.J. Mankiewicz, Abstracts of Papers of the American Chemical Society 224 (2002) 006.
[169] D.S. Page, E.S. Gilfillan, P.D. Boehm, J.M. Neff, W.A. Stubblefield, K.R. Parker, A.W. Maki, Sediment toxicity measurements in oil spill injury assessment: A study of shorelines affected by the Exxon Valdez oil spill in Prince William Sound, Alaska, Battelle Press, Columbus, 2002.
[170] T.C. Tran, G.A. Logan, E. Grosjean, D. Ryan, P.J. Marriott, Geochimica Et Cosmochimica Acta 74 (2010) 6468.
[171] J.L. Rayner, I. Snape, J.L. Walworth, P.M. Harvey, S.H. Ferguson, in A.A.D. Report (Editor), 2005, p. 74.
[172] R.M. Atlas, P.D. Boehm, J.A. Calder, Estuarine, Coastal and Shelf Science 12 (1981) 589.
[173] I. Borg, P.J.F. Groenen, Modern Multidimensional scaling: theory and applications, Springer, New York, 2005.
[174] K. Sturrock, J. Rocha, Field Methods 12 (2000) 49.
[175] R. Project, in, http://cran.r-project.org/web/packages/vegan/index.html, 2010.
[176] R.W. LaClair, P.A. Bueno, J.V. Seeley, Journal of Separation Science 27 (2004) 389.

Appendix 1. Tabulated GCxGC-FID data

The following table contains the GCxGC-FID TPH value and the percentage of fuel found in each of the GCxGC elution regions (as defined in Chapter 6). The TPH value was calculated on the basis of mg TPH per kg of dry soil (oven dried at 105 °C). The percentage of fuel found in the GCxGC bins has been rounded to 2 decimal places unless the value was less than 0.10% in which case the value is reported to 3 decimal places. Rounding errors lead to the percentages of fuel found in all the regions not summing perfectly to 100%.

Sample Barcode or name of SAB standard	TPH value by GCxGC, mg/kg		^{1}D Bin number							
			2	3	4	5	6	7	8	9
53184	12801	^{2}D Row 4						0.21%	0.14%	0.044%
		^{2}D Row 3		0.27%	1.60%	1.25%	0.96%	0.64%	0.23%	0.086%
		^{2}D Row 2	0.59%	6.93%	8.16%	3.31%	1.90%	1.33%	0.420%	
		^{2}D Row 1	2.73%	22.71%	24.51%	9.38%	7.21%	3.71%	1.69%	
53247	8042	^{2}D Row 4						0.029%	0.019%	0.007%
		^{2}D Row 3		0.47%	2.09%	0.59%	0.20%	0.17%	0.048%	0.018%
		^{2}D Row 2	1.49%	9.89%	7.64%	1.26%	0.34%	0.32%	0.050%	
		^{2}D Row 1	9.71%	38.94%	21.95%	3.06%	1.04%	0.46%	0.21%	
53112	7775	^{2}D Row 4						0.051%	0.041%	0.023%
		^{2}D Row 3		0.21%	0.70%	0.49%	0.34%	0.26%	0.12%	0.074%
		^{2}D Row 2	0.27%	5.51%	6.89%	1.78%	0.76%	0.69%	0.19%	
		^{2}D Row 1	1.90%	35.33%	34.15%	5.68%	2.62%	1.30%	0.66%	
53214	7276	^{2}D Row 4						0.11%	0.15%	0.15%
		^{2}D Row 3		0.65%	1.97%	0.84%	0.65%	2.22%	0.66%	1.03%
		^{2}D Row 2	3.64%	7.20%	7.56%	2.90%	5.86%	7.55%	1.24%	
		^{2}D Row 1	7.71%	16.23%	15.88%	6.98%	2.14%	2.40%	4.26%	

53205	5838	^{2}D Row 4						0.018%	0.022%	0.025%
		^{2}D Row 3		0.25%	3.14%	1.44%	0.23%	0.09%	0.064%	0.079%
		^{2}D Row 2	0.54%	7.90%	13.28%	3.48%	0.35%	0.13%	0.10%	
		^{2}D Row 1	2.20%	20.66%	35.17%	8.91%	1.28%	0.35%	0.30%	
53106	4443	^{2}D Row 4						0.27%	0.24%	0.097%
		^{2}D Row 3		0.09%	0.30%	1.08%	1.68%	1.32%	0.62%	0.24%
		^{2}D Row 2	0.23%	2.34%	4.44%	5.64%	4.53%	2.64%	1.11%	
		^{2}D Row 1	1.34%	8.04%	14.67%	17.33%	17.81%	9.60%	4.34%	
53238	4046	^{2}D Row 4						0.044%	0.047%	0.026%
		^{2}D Row 3		0.38%	0.98%	1.03%	0.59%	0.40%	0.17%	0.074%
		^{2}D Row 2	1.28%	14.42%	16.69%	4.70%	1.01%	0.49%	0.19%	
		^{2}D Row 1	4.63%	21.97%	20.96%	6.00%	2.41%	1.00%	0.50%	
53268	3941	^{2}D Row 4						0.086%	0.059%	0.028%
		^{2}D Row 3		0.20%	1.53%	1.44%	0.52%	0.30%	0.14%	0.067%
		^{2}D Row 2	0.51%	7.15%	12.63%	3.88%	0.68%	0.39%	0.19%	
		^{2}D Row 1	2.58%	17.77%	33.31%	11.34%	2.91%	1.50%	0.79%	
53265	3802	^{2}D Row 4						0.077%	0.062%	0.029%
		^{2}D Row 3		0.23%	0.88%	1.10%	0.56%	0.34%	0.14%	0.060%
		^{2}D Row 2	0.44%	7.72%	15.62%	4.58%	0.72%	0.38%	0.16%	
		^{2}D Row 1	1.50%	14.21%	34.89%	11.80%	2.56%	1.29%	0.66%	
53199	3237	^{2}D Row 4						0.13%	0.11%	0.072%
		^{2}D Row 3		0.30%	1.78%	1.44%	0.90%	0.70%	0.34%	0.24%
		^{2}D Row 2	0.43%	8.64%	12.93%	4.50%	1.94%	1.44%	0.57%	
		^{2}D Row 1	1.79%	17.86%	24.37%	9.59%	5.53%	2.78%	1.61%	
53241	2489	^{2}D Row 4						0.050%	0.046%	0.030%
		^{2}D Row 3		0.40%	1.32%	1.20%	0.53%	0.46%	0.18%	0.088%
		^{2}D Row 2	1.31%	12.97%	13.46%	3.39%	0.99%	0.81%	0.20%	
		^{2}D Row 1	5.65%	24.00%	23.09%	6.33%	2.19%	0.88%	0.44%	
53079	2261	^{2}D Row 4						0.16%	0.19%	0.12%

		^{2}D Row 3		0.23%	0.73%	1.34%	1.55%	1.07%	0.61%	0.35%
		^{2}D Row 2	0.39%	6.61%	10.55%	6.68%	3.38%	1.96%	0.970%	
		^{2}D Row 1	1.24%	12.26%	18.93%	12.79%	9.95%	5.14%	2.82%	
53292	2126	^{2}D Row 4						0.03%	0.023%	0.023%
		^{2}D Row 3		0.28%	1.11%	1.30%	0.38%	0.18%	0.070%	0.062%
		^{2}D Row 2	0.45%	8.41%	17.74%	4.64%	0.69%	0.38%	0.100%	
		^{2}D Row 1	1.81%	14.00%	34.05%	11.05%	2.15%	0.67%	0.39%	
53127	1634	^{2}D Row 4						0.030%	0.028%	0.020%
		^{2}D Row 3		0.25%	0.93%	1.27%	0.41%	0.18%	0.087%	0.071%
		^{2}D Row 2	0.60%	8.24%	16.14%	5.06%	0.77%	0.35%	0.150%	
		^{2}D Row 1	2.33%	15.05%	31.87%	11.99%	2.77%	0.88%	0.52%	
53091	1295	^{2}D Row 4						0.16%	0.16%	0.11%
		^{2}D Row 3		0.24%	1.52%	1.70%	1.47%	1.01%	0.58%	0.33%
		^{2}D Row 2	0.34%	6.01%	8.33%	6.13%	3.15%	1.79%	0.89%	
		^{2}D Row 1	1.43%	13.54%	17.20%	13.76%	11.06%	5.86%	3.23%	
53088	861	^{2}D Row 4						0.080%	0.074%	0.055%
		^{2}D Row 3		0.28%	0.95%	1.42%	0.73%	1.47%	0.31%	0.15%
		^{2}D Row 2	0.70%	8.48%	14.16%	5.28%	2.68%	5.33%	0.41%	
		^{2}D Row 1	2.12%	13.91%	24.50%	11.37%	3.57%	1.29%	0.66%	
53131	632	^{2}D Row 4						0.25%	0.22%	0.41%
		^{2}D Row 3		0.42%	1.18%	1.27%	1.38%	1.73%	0.60%	0.88%
		^{2}D Row 2	0.44%	6.97%	9.20%	4.61%	4.35%	7.04%	1.02%	
		^{2}D Row 1	1.45%	11.61%	19.78%	9.40%	8.36%	4.58%	2.84%	
53132	631	^{2}D Row 4						0.035%	0.032%	0.024%
		^{2}D Row 3		0.35%	1.43%	1.35%	0.37%	0.22%	0.088%	0.074%
		^{2}D Row 2	0.91%	9.76%	13.54%	3.78%	0.69%	0.52%	0.15%	
		^{2}D Row 1	3.71%	20.66%	29.79%	9.07%	2.17%	0.81%	0.47%	
53131	621	^{2}D Row 4						0.25%	0.26%	0.27%
		^{2}D Row 3		0.45%	1.25%	1.35%	1.44%	1.93%	0.67%	0.70%

		^{2}D Row 2	0.50%	7.46%	9.59%	4.69%	4.49%	6.74%	1.10%	
		^{2}D Row 1	1.47%	11.41%	19.34%	9.21%	8.15%	4.45%	2.84%	
53295	534	^{2}D Row 4						0.12%	0.14%	0.057%
		^{2}D Row 3		0.21%	0.85%	0.81%	0.66%	4.32%	0.52%	0.16%
		^{2}D Row 2	0.79%	5.01%	10.37%	2.88%	7.30%	17.83%	0.67%	
		^{2}D Row 1	1.68%	11.03%	23.85%	7.00%	2.00%	1.14%	0.60%	
53085	508	^{2}D Row 4						0.071%	0.057%	0.038%
		^{2}D Row 3		0.40%	1.14%	0.92%	0.56%	0.53%	0.18%	0.094%
		^{2}D Row 2	0.81%	11.17%	13.12%	2.98%	1.11%	1.34%	0.23%	
		^{2}D Row 1	2.97%	21.36%	30.03%	6.07%	2.79%	1.35%	0.69%	
53085	507	^{2}D Row 4						0.066%	0.055%	0.037%
		^{2}D Row 3		0.35%	0.98%	0.84%	0.52%	0.46%	0.18%	0.091%
		^{2}D Row 2	0.64%	10.09%	12.33%	2.91%	1.07%	1.35%	0.220%	
		^{2}D Row 1	3.07%	22.25%	31.18%	6.30%	2.90%	1.41%	0.72%	
53190	492	^{2}D Row 4						0.37%	0.24%	0.074%
		^{2}D Row 3		0.22%	1.40%	1.95%	1.79%	1.47%	0.45%	0.16%
		^{2}D Row 2	0.32%	4.15%	7.75%	5.16%	3.79%	3.29%	0.77%	
		^{2}D Row 1	1.27%	11.22%	19.56%	13.76%	11.69%	6.25%	2.89%	
53187	434	^{2}D Row 4						0.12%	0.093%	0.13%
		^{2}D Row 3		2.01%	1.98%	0.81%	0.60%	0.64%	0.17%	0.10%
		^{2}D Row 2	5.73%	41.04%	4.66%	1.36%	1.25%	1.62%	0.30%	
		^{2}D Row 1	8.73%	13.54%	5.13%	3.49%	3.67%	1.87%	0.99%	
53187	404	^{2}D Row 4						0.14%	0.093%	0.17%
		^{2}D Row 3		1.92%	2.04%	0.86%	0.62%	0.64%	0.17%	0.16%
		^{2}D Row 2	5.78%	40.65%	4.62%	1.36%	1.25%	1.62%	0.30%	
		^{2}D Row 1	8.78%	13.46%	5.09%	3.59%	3.77%	1.92%	1.00%	
53296	297	^{2}D Row 4						0.12%	0.11%	0.054%
		^{2}D Row 3		0.22%	0.81%	0.75%	0.75%	4.79%	0.48%	0.15%
		^{2}D Row 2	0.90%	4.71%	9.80%	2.76%	8.51%	20.03%	0.70%	

		^{2}D Row 1	1.90%	10.23%	21.77%	6.49%	2.00%	1.29%	0.65%	
53109	239	^{2}D Row 4						0.27%	0.33%	0.39%
		^{2}D Row 3		0.49%	1.32%	1.22%	2.16%	2.53%	1.66%	1.55%
		^{2}D Row 2	1.36%	11.92%	12.65%	7.56%	5.88%	4.59%	1.95%	
		^{2}D Row 1	3.46%	14.35%	12.38%	4.66%	3.12%	2.48%	1.71%	
53208	188	^{2}D Row 4						0.28%	0.21%	0.18%
		^{2}D Row 3		0.46%	2.45%	1.94%	1.68%	6.06%	0.80%	0.50%
		^{2}D Row 2	1.19%	2.89%	10.74%	5.00%	9.88%	18.59%	1.08%	
		^{2}D Row 1	1.89%	7.07%	14.47%	5.75%	3.04%	2.36%	1.50%	
53082	187	^{2}D Row 4						0.24%	0.24%	0.20%
		^{2}D Row 3		0.50%	2.08%	2.23%	1.92%	1.93%	0.82%	0.54%
		^{2}D Row 2	0.82%	6.50%	8.49%	6.82%	4.82%	5.41%	1.33%	
		^{2}D Row 1	1.60%	7.37%	12.85%	12.47%	11.29%	6.05%	3.47%	
53130	185	^{2}D Row 4						0.36%	0.48%	0.69%
		^{2}D Row 3		0.70%	1.35%	1.34%	1.64%	1.59%	1.11%	1.38%
		^{2}D Row 2	0.94%	6.56%	7.34%	4.01%	3.13%	3.42%	1.47%	
		^{2}D Row 1	2.98%	7.26%	13.63%	7.32%	23.37%	4.47%	3.48%	
41384	166	^{2}D Row 4						0.60%	0.52%	0.43%
		^{2}D Row 3		0.59%	0.51%	0.45%	2.06%	10.42%	1.34%	0.82%
		^{2}D Row 2	2.46%	1.32%	0.51%	0.67%	14.47%	39.71%	1.70%	
		^{2}D Row 1	6.25%	4.43%	0.81%	0.66%	1.99%	4.99%	2.29%	
53058	142	^{2}D Row 4						0.28%	0.24%	0.22%
		^{2}D Row 3		0.19%	0.16%	0.19%	0.91%	7.22%	1.22%	0.87%
		^{2}D Row 2	1.25%	1.12%	0.44%	0.69%	16.17%	50.93%	2.19%	
		^{2}D Row 1	2.33%	3.29%	0.80%	1.44%	3.19%	2.81%	1.86%	
53244	138	^{2}D Row 4						0.13%	0.12%	0.073%
		^{2}D Row 3		0.69%	1.84%	0.87%	0.86%	3.12%	0.41%	0.19%
		^{2}D Row 2	3.18%	15.73%	8.80%	1.75%	4.73%	8.19%	0.49%	
		^{2}D Row 1	8.84%	20.37%	12.55%	2.85%	2.06%	1.32%	0.83%	

53262	137	^{2}D Row 4						0.19%	0.31%	0.46%
		^{2}D Row 3		0.05%	0.94%	3.12%	3.94%	5.05%	3.21%	1.87%
		^{2}D Row 2	0.20%	0.22%	17.88%	21.40%	11.33%	8.55%	3.81%	
		^{2}D Row 1	0.53%	0.60%	2.69%	5.53%	3.47%	2.91%	1.74%	
53058	133	^{2}D Row 4						0.26%	0.23%	0.19%
		^{2}D Row 3		0.17%	0.12%	0.17%	0.93%	7.48%	1.17%	0.84%
		^{2}D Row 2	1.28%	1.18%	0.37%	0.62%	16.48%	51.15%	2.13%	
		^{2}D Row 1	2.42%	4.26%	0.74%	0.77%	2.68%	2.66%	1.69%	
41381	132	^{2}D Row 4						0.47%	0.37%	0.38%
		^{2}D Row 3		0.46%	0.42%	0.44%	2.02%	10.12%	1.06%	0.73%
		^{2}D Row 2	2.10%	1.00%	0.41%	0.61%	16.76%	42.33%	1.55%	
		^{2}D Row 1	4.99%	3.33%	0.52%	0.59%	2.22%	4.91%	2.20%	
53279	96	^{2}D Row 4						0.26%	0.22%	0.12%
		^{2}D Row 3		0.18%	0.01%	0.04%	1.47%	11.01%	1.07%	0.38%
		^{2}D Row 2	1.55%	1.51%	0.18%	0.28%	22.94%	44.30%	1.46%	
		^{2}D Row 1	3.18%	4.54%	0.39%	0.29%	1.45%	2.06%	1.11%	
53115	95	^{2}D Row 4						0.48%	0.54%	0.81%
		^{2}D Row 3		1.96%	2.49%	1.45%	1.80%	2.52%	1.22%	1.50%
		^{2}D Row 2	2.34%	20.71%	6.14%	2.66%	6.17%	9.76%	1.46%	
		^{2}D Row 1	4.03%	6.75%	8.96%	4.26%	5.81%	3.61%	2.58%	
53256	95	^{2}D Row 4						0.41%	0.53%	0.26%
		^{2}D Row 3		0.12%	0.03%	0.19%	2.46%	13.60%	1.92%	0.80%
		^{2}D Row 2	2.16%	1.03%	2.45%	1.48%	20.30%	36.37%	2.04%	
		^{2}D Row 1	3.21%	3.81%	0.46%	0.47%	1.75%	2.56%	1.57%	
53211	89	^{2}D Row 4						0.48%	0.34%	0.39%
		^{2}D Row 3		1.05%	5.22%	4.00%	2.65%	2.14%	0.76%	0.90%
		^{2}D Row 2	1.37%	2.47%	13.71%	7.58%	4.87%	4.68%	1.07%	
		^{2}D Row 1	4.18%	6.83%	14.77%	8.30%	5.14%	4.30%	2.81%	
53353	88	^{2}D Row 4						0.32%	0.29%	0.22%

		^{2}D Row 3		0.24%	0.18%	0.38%	2.26%	11.97%	1.70%	0.86%
		^{2}D Row 2	1.42%	1.03%	0.89%	2.00%	21.71%	36.82%	2.34%	
		^{2}D Row 1	2.55%	2.43%	0.57%	1.34%	2.81%	3.51%	2.16%	
53076	87	^{2}D Row 4						0.43%	0.50%	0.66%
		^{2}D Row 3		0.19%	0.46%	1.95%	4.13%	5.21%	3.53%	2.48%
		^{2}D Row 2	0.66%	1.29%	6.34%	14.45%	11.80%	9.73%	4.71%	
		^{2}D Row 1	1.88%	2.62%	4.86%	5.84%	6.26%	5.96%	4.07%	
52541	85	^{2}D Row 4						0.64%	0.55%	0.68%
		^{2}D Row 3		2.90%	1.22%	0.82%	3.43%	6.85%	0.99%	1.42%
		^{2}D Row 2	2.98%	3.58%	1.18%	0.65%	10.37%	27.97%	1.37%	
		^{2}D Row 1	9.95%	6.32%	1.29%	0.85%	1.31%	8.69%	4.00%	
52514	85	^{2}D Row 4						0.26%	0.16%	0.13%
		^{2}D Row 3		0.24%	0.16%	0.17%	1.00%	7.25%	0.77%	0.29%
		^{2}D Row 2	1.39%	2.62%	0.57%	0.37%	16.29%	50.98%	1.55%	
		^{2}D Row 1	3.67%	5.18%	0.89%	0.42%	2.26%	2.37%	1.01%	
53070	75	^{2}D Row 4						0.22%	0.15%	0.14%
		^{2}D Row 3		0.18%	0.13%	0.17%	1.22%	5.31%	0.86%	0.45%
		^{2}D Row 2	2.83%	1.41%	0.73%	1.16%	21.04%	40.69%	1.59%	
		^{2}D Row 1	9.39%	3.99%	0.49%	0.56%	3.70%	2.48%	1.11%	
53348	58	^{2}D Row 4						0.25%	0.24%	0.18%
		^{2}D Row 3		0.33%	0.44%	0.63%	1.36%	3.71%	0.66%	0.40%
		^{2}D Row 2	1.48%	2.92%	5.07%	3.50%	6.67%	13.64%	1.04%	
		^{2}D Row 1	4.41%	9.21%	17.57%	11.26%	6.61%	5.48%	2.94%	
53229	55	^{2}D Row 4						0.56%	0.74%	0.86%
		^{2}D Row 3		0.68%	0.65%	0.84%	2.23%	7.92%	2.40%	1.99%
		^{2}D Row 2	1.96%	2.83%	2.64%	2.57%	12.41%	28.44%	2.73%	
		^{2}D Row 1	5.02%	3.98%	2.97%	3.33%	4.72%	4.61%	2.94%	
41383	54	^{2}D Row 4						0.59%	0.50%	0.53%
		^{2}D Row 3		0.76%	0.61%	0.59%	2.39%	5.69%	1.09%	1.13%

		^{2}D Row 2	5.73%	7.03%	1.26%	0.81%	7.51%	19.61%	1.30%	
		^{2}D Row 1	16.88%	13.42%	1.32%	0.73%	2.80%	5.15%	2.55%	
53124	39	^{2}D Row 4						0.17%	0.13%	0.16%
		^{2}D Row 3		0.72%	0.53%	0.42%	0.97%	2.30%	0.31%	0.32%
		^{2}D Row 2	3.52%	13.18%	4.23%	1.04%	5.48%	14.19%	0.57%	
		^{2}D Row 1	11.95%	23.94%	7.39%	2.02%	2.74%	2.46%	1.29%	
53103	38	^{2}D Row 4						0.44%	0.50%	0.81%
		^{2}D Row 3		0.21%	0.59%	2.30%	3.07%	3.45%	2.65%	4.30%
		^{2}D Row 2	2.23%	2.66%	10.64%	17.19%	7.61%	8.40%	4.18%	
		^{2}D Row 1	5.91%	4.47%	2.62%	4.04%	3.00%	4.51%	4.20%	
41341	29	^{2}D Row 4						0.60%	0.58%	0.69%
		^{2}D Row 3		0.80%	0.80%	0.66%	2.23%	7.81%	1.82%	2.10%
		^{2}D Row 2	3.48%	2.19%	1.72%	2.11%	9.96%	29.85%	3.05%	
		^{2}D Row 1	8.37%	5.96%	2.19%	1.96%	2.89%	4.37%	3.80%	
53118	26	^{2}D Row 4						0.75%	0.69%	1.44%
		^{2}D Row 3		0.95%	1.15%	1.11%	2.63%	5.92%	1.32%	2.06%
		^{2}D Row 2	1.79%	1.80%	2.61%	1.86%	8.64%	27.00%	1.69%	
		^{2}D Row 1	6.35%	4.11%	3.00%	2.09%	11.11%	6.66%	3.27%	
41385	24	^{2}D Row 4						0.55%	0.53%	0.48%
		^{2}D Row 3		0.71%	0.59%	0.58%	2.22%	8.46%	1.15%	0.94%
		^{2}D Row 2	3.17%	2.39%	0.98%	0.96%	12.59%	33.08%	1.61%	
		^{2}D Row 1	10.69%	4.49%	1.55%	1.20%	2.47%	5.73%	2.89%	
53259	22	^{2}D Row 4						0.54%	0.60%	0.49%
		^{2}D Row 3		0.37%	0.93%	1.49%	3.78%	8.47%	2.18%	1.36%
		^{2}D Row 2	2.37%	2.45%	12.77%	5.40%	16.43%	16.36%	2.34%	
		^{2}D Row 1	5.80%	3.12%	1.77%	1.62%	2.65%	4.04%	2.68%	
53259	19	^{2}D Row 4						0.49%	0.58%	0.46%
		^{2}D Row 3		0.20%	0.29%	0.85%	3.49%	8.10%	2.20%	1.33%
		^{2}D Row 2	2.38%	2.40%	12.13%	4.83%	16.79%	17.89%	2.390%	

		^{2}D Row 1	6.09%	5.40%	1.76%	1.12%	2.31%	3.88%	2.65%	
41388	19	^{2}D Row 4						0.68%	0.59%	0.57%
		^{2}D Row 3		1.95%	0.92%	0.65%	2.71%	7.15%	1.38%	1.19%
		^{2}D Row 2	2.31%	2.56%	1.04%	0.73%	18.52%	30.30%	1.78%	
		^{2}D Row 1	6.96%	3.45%	1.05%	0.79%	2.94%	6.64%	3.15%	
41340	18	^{2}D Row 4						0.70%	0.55%	0.67%
		^{2}D Row 3		0.88%	0.88%	1.03%	2.71%	5.02%	1.22%	1.80%
		^{2}D Row 2	3.19%	2.62%	1.61%	2.20%	8.82%	25.56%	2.41%	
		^{2}D Row 1	10.24%	10.34%	2.31%	2.06%	3.21%	5.68%	4.30%	
53121	17	^{2}D Row 4						0.44%	0.50%	0.40%
		^{2}D Row 3		1.32%	1.32%	1.01%	1.67%	1.09%	0.60%	0.70%
		^{2}D Row 2	2.42%	10.30%	7.56%	2.20%	1.58%	2.03%	0.70%	
		^{2}D Row 1	8.76%	22.29%	17.30%	4.44%	3.74%	5.03%	2.58%	
53073	17	^{2}D Row 4						0.51%	0.66%	0.93%
		^{2}D Row 3		0.40%	0.43%	0.89%	3.29%	5.63%	3.73%	2.93%
		^{2}D Row 2	1.99%	1.07%	2.77%	4.80%	8.43%	13.66%	5.71%	
		^{2}D Row 1	5.53%	2.88%	3.76%	4.90%	7.87%	9.94%	7.29%	
53289	17	^{2}D Row 4						0.52%	0.78%	0.89%
		^{2}D Row 3		1.47%	1.20%	1.07%	2.02%	3.69%	1.86%	1.91%
		^{2}D Row 2	2.35%	5.17%	8.71%	3.67%	5.04%	10.33%	2.33%	
		^{2}D Row 1	7.10%	6.69%	10.32%	4.49%	8.04%	7.07%	3.29%	
41338	16	^{2}D Row 4						0.75%	1.00%	1.02%
		^{2}D Row 3		1.04%	1.00%	1.19%	2.40%	3.22%	1.83%	2.94%
		^{2}D Row 2	4.53%	6.91%	2.29%	1.75%	4.29%	9.45%	2.72%	
		^{2}D Row 1	12.89%	15.93%	6.69%	3.50%	3.54%	4.49%	4.62%	
53232	15	^{2}D Row 4						2.53%	1.08%	1.03%
		^{2}D Row 3		0.72%	0.86%	1.02%	3.19%	5.80%	1.87%	1.84%
		^{2}D Row 2	2.58%	5.14%	2.50%	2.10%	4.42%	11.28%	2.26%	
		^{2}D Row 1	9.19%	9.69%	4.78%	3.82%	4.88%	13.82%	3.62%	

53145	14	^{2}D Row 4						0.67%	0.58%	0.64%
		^{2}D Row 3		1.12%	0.95%	0.73%	2.61%	5.39%	1.06%	1.10%
		^{2}D Row 2	1.82%	2.06%	0.99%	0.79%	18.09%	30.10%	1.47%	
		^{2}D Row 1	7.65%	5.12%	1.66%	1.12%	3.28%	7.80%	3.23%	
41386	14	^{2}D Row 4						1.19%	0.92%	0.97%
		^{2}D Row 3		1.37%	1.28%	1.24%	3.83%	5.80%	1.43%	1.77%
		^{2}D Row 2	4.04%	1.72%	0.98%	1.27%	10.70%	18.91%	1.41%	
		^{2}D Row 1	14.16%	8.00%	1.37%	1.47%	2.95%	9.06%	4.16%	
53166	11	^{2}D Row 4						0.48%	0.52%	0.49%
		^{2}D Row 3		0.66%	0.62%	0.46%	1.99%	8.54%	1.08%	0.86%
		^{2}D Row 2	2.00%	3.08%	1.47%	0.78%	13.71%	40.02%	1.59%	
		^{2}D Row 1	5.68%	4.01%	1.50%	0.72%	2.00%	5.27%	2.49%	
53166	11	^{2}D Row 4						0.50%	0.57%	0.46%
		^{2}D Row 3		0.97%	0.64%	0.53%	1.87%	8.31%	1.05%	0.78%
		^{2}D Row 2	2.04%	3.36%	1.52%	0.77%	12.96%	39.32%	1.61%	
		^{2}D Row 1	6.03%	4.52%	1.45%	0.74%	2.01%	5.51%	2.48%	
53148	11	^{2}D Row 4						0.60%	0.57%	0.72%
		^{2}D Row 3		0.78%	0.90%	0.78%	2.31%	4.02%	1.78%	1.97%
		^{2}D Row 2	1.27%	1.10%	2.32%	2.58%	10.21%	17.49%	3.50%	
		^{2}D Row 1	5.11%	1.84%	6.24%	7.35%	8.22%	10.89%	7.46%	
53362	9	^{2}D Row 4						0.46%	0.38%	0.48%
		^{2}D Row 3		0.76%	0.50%	0.67%	3.46%	6.92%	1.80%	1.51%
		^{2}D Row 2	3.01%	3.21%	1.31%	3.27%	12.34%	18.30%	3.07%	
		^{2}D Row 1	8.94%	6.94%	3.69%	3.33%	4.17%	7.24%	4.26%	
53232	9	^{2}D Row 4						2.60%	1.27%	1.20%
		^{2}D Row 3		0.84%	0.03%	0.24%	2.35%	6.09%	2.16%	2.25%
		^{2}D Row 2	3.33%	5.79%	1.05%	0.63%	3.15%	11.79%	2.54%	
		^{2}D Row 1	10.69%	15.23%	4.22%	2.62%	3.67%	12.46%	3.82%	
53235	8	^{2}D Row 4						1.87%	1.12%	1.05%

		^{2}D Row 3		0.58%	0.03%	0.20%	2.21%	7.28%	2.11%	2.01%
		^{2}D Row 2	3.45%	4.42%	0.76%	0.81%	8.54%	18.69%	2.55%	
		^{2}D Row 1	10.38%	11.96%	2.80%	2.53%	3.88%	6.87%	3.90%	
53151	8	^{2}D Row 4						0.78%	0.70%	0.94%
		^{2}D Row 3		1.00%	0.77%	0.74%	2.84%	4.72%	1.87%	2.48%
		^{2}D Row 2	2.71%	3.80%	2.51%	2.09%	11.76%	20.46%	2.82%	
		^{2}D Row 1	10.39%	6.27%	2.17%	1.66%	3.07%	8.11%	5.33%	
53142	5	^{2}D Row 4						0.68%	0.75%	0.65%
		^{2}D Row 3		1.52%	0.87%	0.82%	2.79%	7.18%	1.20%	1.15%
		^{2}D Row 2	2.75%	2.99%	1.96%	1.04%	9.82%	30.34%	1.52%	
		^{2}D Row 1	9.23%	4.61%	3.25%	1.59%	1.91%	7.67%	3.72%	
53163	5	^{2}D Row 4						0.81%	1.38%	3.62%
		^{2}D Row 3		1.43%	1.09%	0.98%	2.69%	5.28%	1.74%	2.47%
		^{2}D Row 2	2.59%	5.13%	2.02%	1.24%	3.43%	9.16%	1.86%	
		^{2}D Row 1	9.89%	6.84%	1.61%	1.17%	23.64%	5.94%	3.98%	
53223	4	^{2}D Row 4						0.93%	1.10%	1.35%
		^{2}D Row 3		2.18%	1.62%	1.48%	3.86%	4.58%	2.26%	3.41%
		^{2}D Row 2	4.86%	3.26%	2.37%	2.34%	5.03%	11.99%	3.28%	
		^{2}D Row 1	15.61%	3.64%	1.74%	2.23%	2.63%	10.21%	8.06%	
41387	2	^{2}D Row 4						0.94%	0.84%	1.15%
		^{2}D Row 3		3.34%	1.84%	1.73%	4.13%	3.64%	2.07%	3.15%
		^{2}D Row 2	3.62%	3.99%	4.39%	5.78%	6.69%	8.43%	2.87%	
		^{2}D Row 1	11.48%	7.16%	2.81%	3.27%	3.31%	8.20%	5.15%	
53061	2	^{2}D Row 4						0.47%	0.39%	0.78%
		^{2}D Row 3		0.53%	0.41%	0.73%	3.21%	4.31%	1.66%	2.32%
		^{2}D Row 2	3.94%	2.10%	2.20%	4.61%	11.16%	19.29%	2.78%	
		^{2}D Row 1	12.22%	5.61%	2.07%	2.59%	3.99%	6.64%	6.01%	
Calibration standard SAB	12000	^{2}D Row 4						0.007%	0.005%	0.003%
		^{2}D Row 3		1.16%	2.52%	0.11%	0.070%	0.052%	0.019%	0.008%

12000 ppm		^{2}D Row 2	1.68%	10.83%	6.96%	0.41%	0.12%	0.082%	0.023%	
		^{2}D Row 1	5.89%	46.82%	21.71%	0.76%	0.42%	0.22%	0.12%	
Calibration standard SAB 12000 ppm	12000	^{2}D Row 4						0.007%	0.005%	0.005%
		^{2}D Row 3		1.28%	2.57%	0.10%	0.066%	0.049%	0.018%	0.010%
		^{2}D Row 2	1.82%	11.67%	6.71%	0.41%	0.12%	0.08%	0.022%	
		^{2}D Row 1	6.46%	45.70%	21.28%	0.80%	0.45%	0.24%	0.13%	
Calibration standard SAB 12000 ppm	12000	^{2}D Row 4						0.005%	0.004%	0.003%
		^{2}D Row 3		1.31%	2.49%	0.09%	0.061%	0.046%	0.018%	0.008%
		^{2}D Row 2	1.79%	12.28%	6.95%	0.42%	0.12%	0.087%	0.023%	
		^{2}D Row 1	6.36%	45.27%	21.13%	0.76%	0.42%	0.22%	0.12%	
Calibration standard SAB 6000 ppm	6000	^{2}D Row 4						0.008%	0.006%	0.003%
		^{2}D Row 3		0.89%	2.09%	0.12%	0.075%	0.051%	0.019%	0.009%
		^{2}D Row 2	1.37%	8.39%	6.56%	0.44%	0.11%	0.066%	0.023%	
		^{2}D Row 1	5.02%	48.32%	24.85%	0.78%	0.43%	0.23%	0.12%	
Calibration standard SAB 6000 ppm	6000	^{2}D Row 4						0.006%	0.005%	0.004%
		^{2}D Row 3		1.40%	2.60%	0.10%	0.065%	0.047%	0.019%	0.009%
		^{2}D Row 2	1.91%	13.78%	7.18%	0.43%	0.12%	0.073%	0.024%	
		^{2}D Row 1	6.37%	43.90%	20.42%	0.78%	0.42%	0.23%	0.12%	
Calibration standard SAB 3000 ppm	3000	^{2}D Row 4						0.012%	0.008%	0.004%
		^{2}D Row 3		1.48%	2.95%	0.13%	0.098%	0.18%	0.029%	0.013%
		^{2}D Row 2	2.33%	14.60%	7.22%	0.40%	0.32%	0.42%	0.035%	
		^{2}D Row 1	6.06%	42.58%	19.57%	0.75%	0.44%	0.25%	0.14%	
Calibration standard SAB 3000 ppm	3000	^{2}D Row 4						0.010%	0.007%	0.008%
		^{2}D Row 3		1.51%	2.68%	0.11%	0.083%	0.14%	0.027%	0.016%
		^{2}D Row 2	2.14%	15.69%	7.58%	0.43%	0.29%	0.53%	0.038%	
		^{2}D Row 1	6.06%	41.71%	19.33%	0.78%	0.43%	0.26%	0.14%	

Appendix 2. Manuscript published in Analytical Chemistry

The following pages contain a copy of the manuscript "Data reduction in comprehensive two-dimensional gas chromatography for rapid and repeatable automated data analysis". This manuscript includes work from Chapter 5 and Chapter 6 of this thesis and has been published in Analytical Chemistry, volume 84, issue 15, pages 6501-6507.

*Appendix 3. Manuscript published in LC*GC Europe.*

The following pages contain a copy of the manuscript "GCxGC with Fluidic Modulation for Enantioselective Essential Oil Analysis". This manuscript has been published in LC*GC Europe, October 2011, pages 548-555.